UNIVERSIDADE ESTADUAL DE CAMPINAS
FACULDADE DE ENGENHARIA MECÂNICA
E INSTITUTO DE GEOCIÊNCIAS

MASOUD MALEKI

INTEGRATION OF 3D AND 4D SEISMIC IMPEDANCE INTO THE SIMULATION MODEL TO IMPROVE RESERVOIR CHARACTERIZATION

INTEGRAÇÃO DA IMPEDÂNCIA SÍSMICA 3D E 4D AO MODELO DE SIMULAÇÃO PARA MELHORAR A CARACTERIZAÇÃO DO RESERVATÓRIO

CAMPINAS
2018

MASOUD MALEKI

INTEGRATION OF 3D AND 4D SEISMIC IMPEDANCE INTO THE SIMULATION MODEL TO IMPROVE RESERVOIR CHARACTERIZATION

INTEGRAÇÃO DA IMPEDÂNCIA SÍSMICA 3D E 4D AO MODELO DE SIMULAÇÃO PARA MELHORAR A CARACTERIZAÇÃO DO RESERVATÓRIO

Thesis presented to the Mechanical Engineering Faculty and Geosciences Institute of the University of Campinas in partial fulfillment of the requirements for the degree of Doctor of Philosophy in Petroleum Sciences and Engineering in the area of Reservoirs and Management.

Tese de Doutorado apresentada à Faculdade de Engenharia Mecânica e Instituto de Geociências da Universidade Estadual de Campinas como parte dos requisitos exigidos para a obtenção do título de Doutor em Ciências e Engenharia de Petróleo na área de Reservatórios e Gestão.

Orientador: Prof. Dr. Denis José Schiozer

Coorientador: Dra. Alessandra Davólio Gomes

Este exemplar corresponde à versão final da Dissertação defendida pelo aluno Masoud Maleki e orientada pelo Prof. Dr. Denis José Schiozer.

_____

Assinatura do Orientador

CAMPINAS

[2018]

Agência(s) de fomento e nº(s) de processo(s): FUNCAMP, 24365/2012
ORCID: https://orcid.org/0000-0001-7332-9454

Ficha catalográfica
Universidade Estadual de Campinas
Biblioteca da Área de Engenharia e Arquitetura
Luciana Pietrosanto Milla - CRB 8/8129

M293i

Maleki, Masoud, 1987-
Integration of 3D and 4D seismic impedance into the simulation model to improve reservoir characterization / Masoud Maleki. – Campinas, SP : [s.n.], 2018.

Orientador: Denis José Schiozer.
Coorientador: Alessandra Davólio Gomes.
Tese (doutorado) – Universidade Estadual de Campinas, Faculdade de Engenharia Mecânica.

1. Reservatório de petróleo. 2. Engenharia de petróleo. 3. Reservatórios (Simulação). 4. Geofísica. 5. Prospecção sísmica. I. Schiozer, Denis José, 1963-. II. Davólio, Alessandra Gomes. III. Universidade Estadual de Campinas. Faculdade de Engenharia Mecânica. IV. Título.

Informações para Biblioteca Digital

Título em outro idioma: Integração da impedância sísmica 3D e 4D ao modelo de simulação para melhorar a caracterização do reservatório
Palavras-chave em inglês:
Petroleum reservoir
Petroleum engineering
Reservoirs (Simulation)
Geophysics
Seismic prospecting
Área de concentração: Reservatórios e Gestão
Titulação: Doutor em Ciências e Engenharia de Petróleo
Banca examinadora:
Denis José Schiozer [Orientador]
Alexandre Campane Vidal
Emilson Pereira Leite
Marcos Hexsel Grochau
Alvaro Favinha Martini
Data de defesa: 20-02-2018
Programa de Pós-Graduação: Ciências e Engenharia de Petróleo

UNIVERSIDADE ESTADUAL DE CAMPINAS
FACULDADE DE ENGENHARIA MECÂNICA
E INSTITUTO DE GEOCIÊNCIAS

PHD THESIS

INTEGRATION OF 3D AND 4D SEISMIC IMPEDANCE INTO THE SIMULATION MODEL TO IMPROVE RESERVOIR CHARACTERIZATION

Autor: Masoud Maleki
Orientador: Prof. Dr. Denis José Schiozer
Coorientador: Dra. Alessandra Davólio Gomes

A Banca Examinadora composta pelos membros abaixo aprovou esta Dissertação:

Prof. Dr. Denis José Schiozer, Presidente
DEP / FEM / UNICAMP

Prof. Dr. Alexandre Campane Vidal
DGRN / IG / UNICAMP

Prof. Dr. Emilson Pereira Leite
DGRN / IG / UNICAMP

Dr. Marcos Hexsel Grochau
PETROBRAS

Dr. Alvaro Favinha Martini
PETROBRAS

A Ata da defesa com as respectivas assinaturas dos membros encontra-se no processo de vida acadêmica do aluno.

Campinas, 20 de fevereiro de 2018.

DEDICATION

This thesis is dedicated to the memory of my beloved sister, ***Mahtab Maleki****, who passed away 10 years ago when she was preparing for her post-graduation studies. I wish if she was still alive to share these special moments together. Dear Mahtab, our dreams came true!*

I also dedicate this scientific contribution to my patient parents as I had promised to make them proud by the achievement of this monumental academic goal and hope that I have proudly fulfilled that promise. Dear ***Tahereh*** *and* ***Gol Hossein****, I carry your hearts with me in all four corners of the world!*

Eventually, my lovely sister, Dr. Mahboubeh Maleki, I always appreciate your sacrifices and unconditional love. Dear ***Mahboubeh****, without you this journey would not have started!*

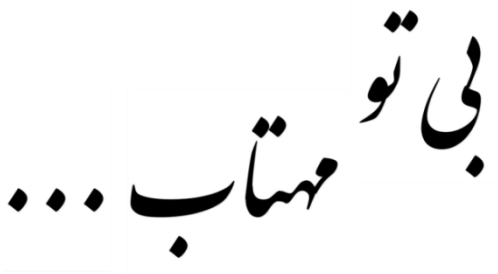

ACKNOWLEDGEMENTS

I would like to thank my advisor Prof. Denis José Schiozer for providing the opportunity for me to be a member of UNISIM research group, and for all of his supports and guidance during my research.

I would like to extend my gratitude to Dr. Alessandra Davolio (my co-advisor), for her immense attention and supports.

I want to thank Prof. Peter Hubral for his spiritual supports within my research life, and Prof. Martin Tygel and Prof. Leiv Jacob Gelius and for their patronages during my studies at LGA research group and University of Oslo.

I also thank my colleagues at Unicamp, UNISIM group, CEPETRO, and research teams of Shell and BG for their support and assistance, and CGG, Schlumberger and CMG for software licenses.

To all my friends in Iran, Norway, Canada and Brazil, I thank their friendship and all the special moments shared together.

I acknowledge Statoil (operator of the Norne Field) and its license partners ENI and Petoro for the release of the Norne data. Further, the author acknowledges the Center for Integrated Operations at NTNU for cooperation and coordination of the Norne Cases. The view expressed in this thesis are the views of the author and do not necessarily reflect the views of Statoil and the Norne license partners.

This work was carried out in association with the ongoing project registered as ‘‘BG-07: Reduction of Uncertainties through the Incorporation of 4D Seismic Data in the Modeling of the Reservoir” (UNICAMP/BG Brazil/ANP) funded by BG E&P Brazil Ltda (a subsidiary of Shell) under the ANP R&D levy as ‘Investment Commitment to Research and Development’.

RESUMO

O objetivo principal da simulação numérica de reservatórios é prever a produção e planejar o desenvolvimento de campos de petróleo, mantendo modelos de reservatórios confiáveis que respeitem os dados estáticos e dinâmicos disponíveis. A sísmica 4D (S4D) desempenha papel importante no monitoramento de reservatórios, fornecendo dados que descrevem o comportamento dinâmico das propriedades do reservatório durante a produção. Aplicações recentes mostraram que a S4D possibilita reduzir a incerteza na distribuição de heterogeneidades, melhorando o conhecimento da estrutura geológica e permitindo que o reservatório seja gerenciado de forma mais eficaz. Dados de S4D podem ser integrados com dados de simulação do fluxo do reservatório, qualitativamente (como na interpretação de causas prováveis de anomalias devido a mudanças na saturação e pressão dos poros) ou quantitativamente (adicionando atributos derivados da sísmica dentro da função objetivo de um processo de ajuste de histórico). Dados sísmicos 3D são associados aos parâmetros estáticos do reservatório e podem fornecer conhecimento da estrutura e litologia do reservatório. Assim, a integração entre o modelo de simulação de fluxo e os dados sísmicos observados (domínios de engenharia e sísmica) deve respeitar a interpretação dinâmica, estrutural e estratigráfica do reservatório através da modelagem direta e inversa e subsequente comparação entre as observações previstas e reais. Este trabalho destina-se a desenvolver metodologias para usar dados sísmicos 3D e 4D, para mitigar as incertezas no modelo de simulação numérica de reservatórios. Deste modo, este trabalho propõe uma metodologia de estudos para integrar impedância sísmica invertida (3D e 4D) com dados de engenharia, dando ênfase na interface entre modelos estáticos e dinâmicos, para proporcionar um modelo de reservatório mais confiável. A metodologia é aplicada a um reservatório de arenito com geologia estrutural complexa, o benchmark do campo de Norne (Noruega). A primeira parte do trabalho apresenta uma inversão do levantamento sísmico 3D base (adquirido em 2001) discutindo o uso de diferentes números e localização de poços para determinar as características estáticas do reservatório. Demonstrou-se que a inversão 3D fornece melhores resultados se os dados de entrada, neste caso os dados de poço, respeitarem a complexa geologia estrutural do reservatório de Norne. Destacamos as vantagens da interpretação sísmica 4D em forma de impedância, obtida através de inversão sísmica 4D,através da comparação das anomalias de impedância sísmica com as diferenças de amplitude sísmica para alguns exemplos no campo de Norne. A inversão 4D atenua as anomalias que não são

causadas pelas atividades produtivas do campo. Em seguida, interpretamos as variações de impedância entre os levantamentos sísmicos base (2001) e monitor (2006) para todo o campo para identificar anomalias de impedância 4D (sinais de aumento e diminuição de impedância) e desacoplar os efeitos das variações de fluido e pressão (devido à atividade de produção) suportado por dados de engenharia do reservatório. Assim, uma interpretação sísmica 4D qualitativa precisa foi alcançada através dos resultados da inversão permitindo entender os efeitos da atividade de produção, que é outra contribuição importante a ser destacada. A natureza multidisciplinar da modelagem do reservatório exige uma abordagem mais quantitativa para integrar os dados sísmicos 4D na metodologia de ajuste de histórico. A avaliação quantitativa da consistência entre a simulação do fluxo do reservatório e os parâmetros elásticos necessita de um modelo petro-elástico (PEM) para fornecer uma comparação lógica entre domínios. No entanto, o PEM pode ser bastante incerto. Assim, atualizamos o modelo do reservatório usando a integração quantitativa da impedância sísmica invertida (3D e 4D) dentro do modelo de simulação de fluxo do reservatório, levando em consideração que o desajuste de dados sísmicos pode ser associado à um modelo de simulação incerto, ou à um PEM incerto. O caso estudado mostrou um desajuste considerável entre dados simulados e observados de pressão de fundo dos poços. Portanto, propomos duas etapas para resolver a ambiguidade na geração de um modelo de simulação de reservatório confiável tendo um PEM incerto. Em primeiro lugar, melhoramos a confiabilidade do modelo de reservatório usando a integração quantitativa da impedância sísmica observada em 3D e 4D, juntamente com os dados do histórico dos poços. Em seguida, calibramos os parâmetros no modelo petro-elástico, referente aos dados observados 4D e ao histórico de produção para garantir valores realistas às mudanças nos parâmetros elásticos *in situ* devido à atividade de produção. Este estudo apresenta a integração dos domínios de engenharia e sísmica, em um fluxo de trabalho iterativo, em um campo real para fechar o ciclo entre os dois domínios, permitindo atualizar o modelo de reservatório e validar o modelo petro-elástico. A principal contribuição deste trabalho é destacar a incorporação dos dados estáticos e dinâmicos do reservatório para diagnosticar a confiabilidade da simulação de fluxo do reservatório para um caso complexo, considerando as incertezas inerentes a esses dados e melhorando a compreensão do comportamento do reservatório.

Palavras Chave: Sísmica 4D, Inversão sísmica 4D, Simulação de numérica de reservatório, Monitoramento de reservatórios, Ajuste de histórico com sísmica, Campo de Norne.

ABSTRACT

The ultimate goal of reservoir simulation in reservoir surveillance technology is to estimate long-term production forecasting and to plan further development of petroleum fields by maintaining reliable reservoir models that honor available static and dynamic data. Moreover, time-lapse seismic (or 4DS) has played a preeminent role in the reservoir surveillance technology by providing new data describing the dynamic behavior of reservoir properties during production. Recent applications have shown that 4DS yields a reduction in the uncertainty in reservoir properties allowing the improvement of the knowledge of the geological framework and a more effective reservoir management. 4DS response can be integrated with reservoir flow simulation either qualitatively (such as interpreting likely causes of 4D anomalies due to changes in saturation and pore pressure) or quantitatively (by adding seismic derived attributes inside the objective function of a history matching process). Alternatively, 3D seismic data is associated to the static reservoir parameters which can provide reservoir framework knowledge. Thus, closing the loop between the flow simulation model and the observed seismic data (engineering and seismic domains) must honor static, dynamic, structural and stratigraphic interpretation of reservoirs through forward and inverse modeling and consequent comparison between predicted and actual observations. This work aims using 3D and 4D seismic data to mitigate uncertainties in numerical reservoir simulation model, proposing a circular workflow of inverted seismic impedance (3D and 4D) and engineering studies, with emphasis on the interface between static and dynamic models. The methodology is applied to a complex structural geology, sandstone reservoir, the Norne Field benchmark case (Norway). The first part of the work presents a 3D seismic inversion of the baseline seismic survey (2001) discussing different numbers and locations of wells to characterize the static reservoir framework. It was shown that the 3D inversion provides better results if the input data, in this case the well-logs data, respect the complex structural geology of Norne reservoir. Meanwhile, we highlight the advantages of time-lapse seismic interpretation in form of inverted impedance by running 4D seismic inversion and comparing derived seismic impedance anomalies within the standard seismic amplitude differences for some examples in the Norne Field. The 4D inversion mitigates the anomalies that are not caused by production activity. Then, we interpret impedance variations between the base (2001) and monitor (2006) seismic surveys for entire field to identify 4D impedance anomalies (hardening and softening signals) and decouple the effects of fluid and pressure

variations (due to the production activity), supported by reservoir engineering data. Thus, an accurate qualitative 4D seismic interpretation are provided by inversion results to be able to understand the effects of production activity, which is another important contribution to be highlighted. However, the multidisciplinary nature of reservoir modeling demands more quantitative approach to integrate 4D seismic data into the history matching workflows. Nevertheless, quantitative evaluation of consistency between reservoir flow simulation and elastic parameters relies on calibrated petro-elastic modelling (PEM) to provide the logical cross-domain comparison. However the petro-elastic model can be very uncertain. Thereby, we update the reservoir model using quantitative integration of seismic inverted impedance (3D and 4D) within reservoir flow simulation model, taking into account that the seismic data mismatch can be associated to an uncertain simulation model as well as to an uncertain PEM. The case studied presented a considerable initial mismatch between simulated and measured bottom-hole pressure (BHP). We therefore propose two steps in order to resolve ambiguity in generating validated reservoir flow simulation and PEM. First, we improve the reliability of reservoir model using quantitative integration of 3D and 4D observed seismic impedance together with well history data. Eventually, we calibrate the parameters in petro-elastic model, referring to 4D observed and production history data to ensure realistic values for changes in in-situ elastic parameters due to the production activity. This study presents the integration of engineering and seismic domains, in an iterative workflow, on a real field to close the loop and subsequently to update reservoir flow simulation and validate the petro-elastic model. The main contributions of this work is to highlight the incorporation of available static and dynamic reservoir data to diagnose the reservoir flow simulation reliability for a complex case, considering the uncertainties inherent to these data and improve the reservoir behavior understanding.

Keywords: 4D seismic, 4D seismic inversion, Reservoir flow simulation, Reservoir monitoring, Seismic history matching, Norne Field.

LIST OF FIGURES

Figure 1.1. Integration of different elements of reservoir management. 24

Figure 1.2. Integration between 4D seismic and simulation data in form of impedance domain. 27

Figure 1.3. Structure of work according to the main area of concentration of each article. 30

Figure 2.1. Workflow scheme of the 3D model-based seismic inversion (modified from Russell, 1998). 40

Figure 2.2. Top reservoir map showing Norne horst block with the four segments (modified from Osdal et al., 2006). 41

Figure 2.3. Database of the Norne benchmark including post-stack seismic data of 2001 and location of the nine well-logs. 42

Figure 2.4. Well to seismic calibration of deviated wells (a) D-4H and (b) E-3H. 43

Figure 2.5. Interpretation of the main reservoir horizons. 44

Figure 2.6. Profile of initial impedance models derived from (a) nine-wells, (b) two-wells. .. 45

Figure 2.7. Profile plot of the inversion analysis for (a) nine-wells and (b) two-wells. 46

Figure 2.8. Profile of inverted impedance results for segment E derived from (a) nine-wells and (b) two-wells. The detached zones highlight improvement of vertical resolution throughout 9-well constrained post-stack inversion. 47

Figure 2.9. Profile of inverted impedance results for segment C derived from (a) nine-wells and (b) two-wells. The detached zones highlight improvement of vertical resolution throughout 9-well constrained post-stack inversion. 48

Figure 2.10. Profile of inverted impedance results from the 9-well constrained post-stack inversion. Note the significant decreases in impedance for regions between the Garn and Ile formations and below the top of Ile Formation. 49

Figure 2.11. (a) Cross plot of P-impedance versus V_P/V_S for well C-3H. (b) Cross-section of interpreted zones (A and B) in the well C-3H. (c) Profile of inverted impedance results from the 9-well constrained post-stack inversion at location of well C-3H. Note the significant decreases in impedance for detached region (uppermost part of Garn formation) compared to upper formation. 50

Figure 3.1. (a) Location of Norne Field in the Norwegian Sea. (b) Stratigraphy of the Norne Field. 54

Figure 3.2. Impedance logs of wells 10-2, 10-4, B-4H, C-1H, C-3H, D-1H, D-4H, E-3H and F-1H) in the reservoir zones of Norne Field. 55

Figure 3.3. Segments of the Norne Field and locations of the 9 wells. 55

Figure 3.4. Injected water and gas rates of well C-1H (top) and C-2H (bottom). 56

Figure 3.5. Impact of fluid saturation and pore pressure changes on impedance and V_P to V_S ratio. 57

Figure 3.6. Workflow scheme of the 4D seismic interpretation. 58

Figure 3.7. A cross-section of differences between the initial models for the base and monitor surveys through segment C showing, in green, negative impedance changes (decreasing impedance from 2001 to 2006) around the injectors C-1H and C-2H in the inserted ellipses. 59

Figure 3.8. (a) Results of fitting curves to each 9 wells (alpha factor). A value of -0.848 was chosen to represent the alpha factor of entire field in this case. (b) Frequency spectrum of coloured inversion operator filter in this case. 60

Figure 3.9. (a) Segments of the Norne Field and locations of the southern flank of segment C (marked by orange color). A profile of: (b) difference volume of near stack, (c) difference volume of far stack, (d) difference volume of full stack, (e) 4D coloured seismic inversion results, (f) 4D model-based seismic inversion results 61

Figure 3.10. Well history data of producer B-2H (produced water rate). 62

Figure 3.11. A profile of: (a) 4D impedance changes (model-based inversion) between the 2001 and 2003, (b) 4D impedance changes (model-based inversion) between the 2003 and 2006. Red dots denote perforation of wells C-2H and C-1H. 63

Figure 3.12. 4D impedance maps (model-based inversion) between the 2001 and 2006 through (a) anomaly CS-1, (b) anomaly CS-3 65

Figure 4.1. (a) Location of the Norne Field in the Norwegian Sea (modified from Huang et al., 2013). (b) Stratigraphy of the Norne Field. 72

Figure 4.2. Segments of the Norne Field in the top reservoir map and locations of the nine wells. The field is confined by major tectonic faults and compartmentalized by a series of minor faults. 73

Figure 4.3. Workflow scheme of the 4D seismic inversion. 75

Figure 4.4. SW–NE section through the monitor seismic survey (2006). The Garn Formation represents the top of Norne reservoir and Aare Formation is the base. 76

Figure 4.5. A cross-section of differences between the initial models for the base and monitor surveys through segment E showing, in green, negative impedance changes (decreasing impedance from 2001 to 2006) below the top of the Ile Formation in the inserted ellipses. 77

Figure 4.6. Normalized RMS map of 4D inverted impedance differences over the Norne reservoir interval between the 2001 base and 2006 monitor surveys. 79

Figure 4.7. 4D acoustic impedance maps between the 2001 and 2006 surveys for (a) below the top of the Ile Formation and (b) above the top of the Tilje Formation. 80

Figure 4.8. Profiles of the inverted impedance difference and simulation model for segment E. (a) Cross-section of the inverted impedance difference around injectors F-3H and F-1H (black dots denote completion of injectors). Anomalies SE-1, SE-2 and SE-3 highlight regions where softening (decrease in impedance) is most evident. (b) Crosssection of the simulation model showing pore-pressure changes around injectors F-3H and F-1H. (c) Cross-section of the inverted impedance difference in the southern flank of segment E. The black dotted region shows the location of the hardening signal (increase in impedance) and probable water flooding. (d) A cross-section of the simulation model showing water-saturation changes in the southern flank of segment E. 81

Figure 4.9. 4D acoustic impedance maps between the 2001 and 2006 surveys for (a) below the top of the Ile formation and (b) the bottom of the Ile Formation. Anomaly SD-1 delineates regions around the F-2H injector between the major faults (black dotted lines), while anomaly SD-2 shows the hardening signal (increase in impedance) in the SW and SE regions of segment D. 83

Figure 4.10. Profiles of the inverted impedance difference and simulation model for segment D. (a) A cross-section of the inverted impedance difference showing decreased impedance around injector F-2H (black dots denote the completion of F-2H). (b) A cross-section of the simulation model showing increased pore pressure around injector F-2H. (c) A cross-section of the inverted impedance difference in the southern flank of segment D. The black dotted region shows the location of the hardening signal and the potentially water-flooded area. (d) A cross-section of the simulation model showing the water-saturation changes in the southern flank of segment D. 84

Figure 4.11. Water rate for well D-4AH. Green points are the history data and the red line shows the simulation results. 85

Figure 4.12. 4D acoustic impedance maps between the 2001 and 2006 surveys for (a) below the top of the Garn Formation and (b) below the top of the Ile Formation. 86

Figure 4.13. Profiles of the inverted impedance difference and simulation model for segment C. (a) A cross-section of the inverted impedance difference showing a strong hardening signal around the injector C-2H (black dots denote the completion of C-2H). (b) A cross-section of the simulation model showing no pore-pressure change around anomaly SC-1. (c) A cross-section of the simulation model showing a significant increase in water saturation around anomaly SC-1. (d) A cross-section of the inverted impedance difference showing anomalies SC-2 (softening signal) and SC-3 (hardening signal) around the injector C-4AH (black dots denote the completion of C-4AH). (e) A cross-section of the simulation model showing a gentle increase in pore pressure around anomaly SC-2. (f) A cross-section of the simulation model showing the significant increase in water saturation around anomaly SC-3. 87

Figure 4.14. 4D acoustic impedance maps between the 2001 and 2006 surveys for (a) below the top of the Garn Formation and (b) around the bottom of the Tilje Formation. In

(a), the areas surrounding injector F-4H and producer E-4AH show decreases in acoustic impedance, while a significant softening anomaly that spreads across the entire segment G (anomaly SG 3) can be seen in (b).....89

Figure 4.15. Profile of the inverted impedance difference and simulation model for segment G. (a) A cross-section of the inverted impedance difference showing the softening anomalies of SG-1, SG-2 and SG-3 (black dots denote the completion of F-4H). (b) A cross-section of the simulation model showing higher increases in pore pressure around anomalies SG-1 and SG-2 compared to the smaller changes in the middle region 90

Figure 5.1. Location and segments of the Norne Field in the Norwegian Sea.....99

Figure 5.2. Workflow scheme of updating the reservoir flow simulation model. The seismic side of the flowchart provides observed static (3D) and dynamic (4D) seismic impedance models, while the engineering side contains the initial reservoir flow simulation model.....107

Figure 5.3. Location of the producers and injectors in the top reservoir map of segments E and D. Blue dots denote well-head position of injectors, while red dots represent well-head positions of producers.....109

Figure 5.4. Observed seismic impedance in the simulation scale over the Norne reservoir for (a) baseline survey of 2001 (3D) and (b) impedance variations from 2001 to 2006 monitor survey (4D).....110

Figure 5.5. Profile of the preliminary comparison between (a) synthetic 3D impedance (derived by initial simulation model) and (b) observed 3D impedance (derived by inversion results).....111

Figure 5.6. Maps of the evolution of matching between the observed and synthetic 3D impedance models throughout our workflow in step 1. Maps of (a) initial synthetic 3D impedance, (b) updated synthetic 3D impedance and (c) observed 3D impedance for the deeper layers of Ile-2 (layer K-08), Tofte-2 (layer K-14) and Tofte-1 (layer K-18) formations (from top to bottom). 112

Figure 5.7. Maps of the evolution of matching between the synthetic and observed 4D impedance models (2006 minus 2001) throughout our workflow in steps 1 and 2. Black dots denote well-head position of injectors. (a) Map of initial synthetic impedance variations for the deeper zone of Tofte-2 Formation (layer K-14). (b) Map of updated synthetic impedance variations in the first step of updating for the deeper zone of Tofte-2 Formation (layer K-14). (c) Map of updated synthetic impedance variations in the second step of updating for the deeper zone of Tofte-2 Formation (layer K-14). (d) Map of observed impedance variations for the deeper zone of Tofte-2 Formation (layer K-14). 114

Figure 5.8. Maps of the evolution of matching between the synthetic and observed 4D impedance models (2006 minus 2001) throughout our workflow in steps 1 and 2. Back dot denote well-head position of producer E-3AH. (a) Map of initial synthetic impedance variations for the upper zone of Garn Formation (layer K-01). (b) Map of updated synthetic impedance variations in the first step of updating for the upper

zone of Garn Formation (layer K-01). (c) Map of updated synthetic impedance variations in the second step of updating for the upper zone of Garn Formation (layer K-01). (d) Map of observed impedance for the upper zone of Garn Formation (layer K-01). 116

Figure 5.9. The BHP rates through the different updating steps. Red points represent the BHP history data, while blue lines, black dotted and green lines show the BHP of initial, first step updated and second step updated simulation models, respectively. The blue, black and green dots represent the value of NQDS for the initial, first step updated and second step updated simulation models, respectively. 117

Figure 5.10. Maps of the evolution of matching between the synthetic and observed 4D impedance models (2006 minus 2001) throughout our workflow in step 3. (a) Map of updated synthetic impedance variations in the second step of updating for the deeper zone of Tofte-2 Formation (layer K-14). (b) Map of updated synthetic impedance variations in the pressure dependency modification for the deeper zone of Ile-1 Formation (layer K-11). (c) Map of observed impedance for the deeper zone of Ile-1 Formation (layer K-11). (d) Map of water saturation changes considering updated simulation model for the deeper zone of Ile-1 Formation (layer K-11). (e) Map of pore-pressure changes considering updated simulation model for the deeper zone of Ile-1 Formation (layer K-11). 119

Figure 5.11. NQDS of fluid rates for producers B-4BH, E-2H and E-3AH through the different updating steps. The blue, black and green dots represent the value of NQDS for the initial, first step updated and second step updated simulation models, respectively. 120

Figure 5.12. A profile of the evolution of matching between the synthetic and observed 4D impedance models throughout our workflow in step 3. (a) 4D impedance response of simulation model during the second step of updating. (b) 4D impedance response of simulation model during the calibration of PEM pressure dependency. (c) observed 4D impedance model (derived by inversion results). (d) pore-pressure changes considering second step updated simulation model. (e) water saturation changes considering second step updated simulation model. The ellipses show the regions of matching improvements with observed 4D impedance model during the modifications of pressure sensitivity of PEM in the third stage of updating methodology..... 121

Figure A.1. Inversion analysis plot for the well B-4H including different statistical wavelets. Red traces denote synthetic inverted seismic trace, while black traces represent actual seismic trace. 138

Figure A.2. Detailed information of the statistical wavelet M-3; including location of the in-line 1076 and nine wells (left), and phase and amplitude spectrums of the extracted wavelet (right). 139

Figure A.3. Inversion analysis plot for the well B-4H including different scenarios of inversion parameters. 139

Figure B.1. Produced water rate of well E-3CH..... 141

Figure B.2. Produced water rate of well E-1H. 142
Figure B.3. Produced water rate of well B-3H. 142
Figure B.4. Injected water rate of well C-2H. 143
Figure B.5. Produced water rate of well B-2H. 143
Figure B.6. Injected water and gas rates of well C-4AH. 144

LIST OF TABLES

Table 2.1. Model-based inversion parameters. 45

Table 3.1. Description of each set of anomalies (Article-2). 65

Table 4.1. Description of each set of anomalies (Article-3). 92

Tabe 5.1. Early-Middle Jurassic stratigraphy of the Norne Field and reservoir zonation from the simulation model. 101

Table 5.2. Main PEM parameters used in Article-4. 103

Table 5.3. Parameters for over and underburden in the PEM. 104

Table 5.4. Modified pressure dependency of PEM in the Norne reservoir segments of E and D. 120

Table A.1. Description of each scenario of inversion parameters (Article-1). 140

NOMENCLATURE

Abbreviations and acronyms		*Units*
3D	Three-dimensional	
4D	Time-lapse	
4DS	Time-lapse seismic	
Amp	Amplitude	
AVO	Amplitude v. Offset	
BHP	Bottom-hole pressure	kPa
CMG	Computer Modeling Group	
ECLIPSE	Volatile-oil simulation software (Schlumberger)	
Fm.	Formation	
GOR	Gas-Oil-ratio	
H	integration operator	
IMEX	Black-oil simulation software (CMG)	
IP	P-wave impedance	$(m\ s^{-1})*(g\ cm^{-3})$
K	Bulk modulus	GPa
Kdry	Effective bulk modulus of dry rock	GPa
kx	Horizontal permeability	mD
kz	Vertical permeability	mD
M	Initial impedance guess	
NE	Northeast	
NQDS	Normalized Quadratic Distance with Signal	
NRMS	Normalized Root Mean Square	
NtG	Net-to-gross	
OWC	Oil-water contact	m
$P_{eff\ initial}$	Reservoir pre-production effective pressure	kPa
$P_{eff\ mon}$	effective pressure at the monitor survey time	kPa
QC	Quality control	
Qgi	Gas injection rate	m3/day
Qo	Oil rate	m3/day
Qw	Water rate	m3/day
Qwi	Water injection rate	m3/day
r	Reflectivity	

RMS	Root Mean Square	
SE	Southeast	
Sg	Gas saturation	fraction
So	Oil saturation	fraction
SW	Southwest	
S_w	Water saturation	fraction
T	Seismic trace	
TWT	Two-Way-Time	ms
V_P	P-wave velocity	$m\ s^{-1}$
V_P/V_S	P- to S-wave velocity ratio	
V_S	S-wave velocity	$m\ s^{-1}$
W	Wavelet	
ΔP	Pore-pressure changes	bar
ΔS_w	Water saturation changes	fraction
Ø	Porosity	$m^3\ m^{-3}$
ρ	Density	$kg\ m^{-3}$
μ	Shear modulus	GPa
*	Convolution	

CONTENTS

1. INTRODUCTION 23

1.1. Motivation 29

1.2. Objective 29

1.3. Description of the thesis 30

1.3.1. Article-1: "Reservoir characterization using model based post-stack inversion: a case study in Norne field to show the impact of the number of wells in inversion" 30

1.3.2. Article-2: "Qualitative time-lapse seismic interpretation of the Norne Field to assess the challenges of 4D seismic attributes" 31

1.3.3. Article-3: "Using simulation and production data to resolve ambiguity in interpreting 4D seismic inverted impedance in the Norne Field" 32

1.3.4. Article-4: "Quantitative integration of 3D and 4D seismic inverted impedance into reservoir simulation model updating in the Norne Field" 33

2. ARTICLE-1: *Reservoir characterization using model based post-stack inversion: a case study in Norne field to show the impact of the number of wells in inversion* 36

2.1. Introduction 37

2.2. Methodology 38

2.3. Norne Field and dataset 41

2.4. Application 42

2.5. Results and discussion 45

2.6. Conclusions 49

3. ARTICLE-2: *Qualitative time-lapse seismic interpretation of the Norne Field to assess the challenges of 4D seismic attributes* 51

3.1. Introduction 52

3.2. Nonre Field and benchmark dataset 54

3.3. Comparison of 4D seismic attributes 56

3.4. Results and discussion 61

3.5. Conclusions 66

4. ARTICLE-3: ***Using simulation and production data to resolve ambiguity in interpreting 4D seismic inverted impedance in the Norne Field*** **..... 67**

4.1. Introduction 68

4.2. Norne Field 71

4.3. Norne benchmark dataset 71

4.4. Time-lapse inversion and interpretation 73

4.5. Results and discussion 78

4.5.1. Segment E 78

4.5.2. Segment D 82

4.5.3. Segment C 85

4.5.4. Segment G 88

4.6. Conclusions 90

5. ARTICLE-4: ***Quantitative integration of 3D and 4D seismic inverted impedance into reservoir simulation model updating in the Norne Field*** **..... 93**

5.1. Introduction 94

5.2. Norne Field 99

5.3. Dataset preparation 100

5.4. Reservoir model updating workflow 104

5.5. Results and discussion 108

5.6. Conclusions 122

6. CONCLUSIONS 124

6.1. Future research directions 127

REFERENCES 129

APPENDIX A - Complementary results of Article-1 137

APPENDIX B - Complementary results of Article-3 141

1. INTRODUCTION

The ultimate goal of geoscientists and reservoir engineers is to build reliable reservoir models, which provide a better understanding of field planning and management. This motivated the development of integration between multiple elements of management, including people (geophysicist, geologist and engineers), data, and wide ranges of well-known techniques (such as time-lapse seismic data, reservoir flow simulation and history matching). The essential elements of a reservoir management are shown in Figure 1.1. Reservoir management requires simulation models to improve understanding of complex flow behavior in reservoirs, and to provide a long term perspective on the future performance of the reservoir (Hoffman and Caers, 2007; Lucia, 2007). However, the reliability of the predictions of simulation models as a stand-alone procedure depends on knowledge about rock and fluid properties such as the distribution of heterogeneities, relative permeability, faults location and transmissivity, and the production mechanism that control the reservoir performance.

Nowadays, among the different technologies that contribute to reservoir management, the role of seismic is critical at different stages of life of the field cycle due to its unique character to capture the fluid flow behavior during production (Johnston, 2013). Time-lapse seismic data (or 4DS) reduces the attached uncertainty in distribution of heterogeneities, in which allowing the improvement of the knowledge of geological framework and a more effective reservoir management. In fact, 4DS can be used to follow the evolution of the reservoir properties over time while continuing hydrocarbon production. It provides new data describing the dynamic behavior of the reservoir fluids in between the wells, often providing a surprise relative to preconceived views of reservoir flow, or even stratigraphy. For that reason, it is nowadays a well-established and mature technology. Hydrocarbon production induces fluid substitution and pressure variations which are likely to modify the amplitudes and travel-times of seismic signals recorded during monitor seismic surveys (4D signals). Fine analyses of these changes can provide valuable information about the reservoir characterization, time evolution of the reservoir and guide the optimal positioning of future wells to improve hydrocarbon production and enhance oil recovery operations.

Time-lapse seismic data have been tried in several fields to date, and proven to be a powerful technique to optimize field and enhanced oil recovery operations (Landrø et al., 1999; Koster et al., 2000; Strønen and Digranes, 2000; Johnston, 2013) by imaging production induced changes within the reservoir and providing invaluable information about reservoir heterogeneity (Greaves and Fulp, 1987; Tura and Lumley, 1999; Koster et al., 2000; Landro, 2001; Tura et al., 2005).

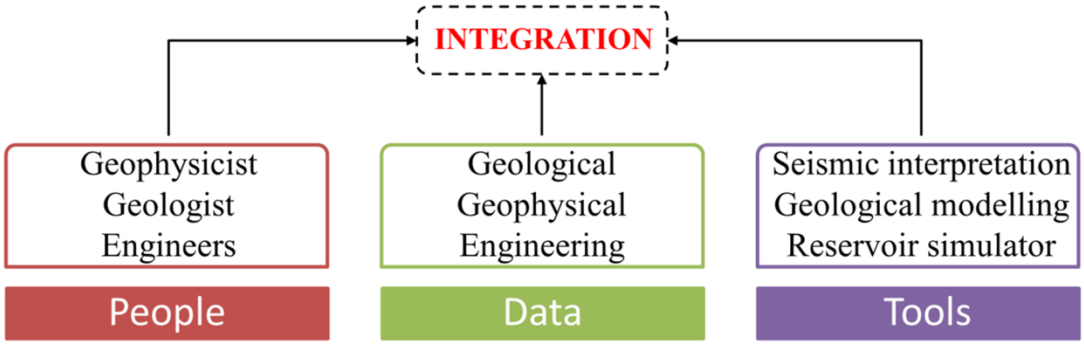

Figure 1.1. Integration of different elements of reservoir management.

Meanwhile, the possibilities for integration of 4D seismic attribute data into the reservoir simulation updating process should be considered as it can be integrated in form of seismic amplitude, acoustic impedance or any other seismic-derived attribute. Time-lapse seismic attribute must reflect a good understanding of the character of the seismic prior to its integration in the simulation model in order to be most effective and less erroneous. It seems that, inverted impedances provide better results than the seismic amplitudes for 4D interpretation, allowing detection of subtle changes in repeatedly acquired seismic data (Ayzenberg et al., 2013). Furthermore, inverted impedance converts the seismic reflectivity into volumetric impedance data that are more suited to cross-domain comparison (Tian et al., 2014). For instance, the advantage of 4D seismic impedance attribute to capture the effect of pressure and saturation variations (with reasonable degree of success) has been highlighted in the Draugen Field (Guderian et al., 2003), UKCS turbidite reservoir (Stephen et al., 2006) and Girassol Field (Roggero et al., 2007).

Additionally, techniques for inverting for 4D changes are now readily available. Abubakar et al., (2001), Sarkar et al., (2003) and Calvert (2005) presented 4D inversion as two separate 3D inversions. They inverted the base and monitor surveys separately, and computed the impedance variation by straightforward subtraction of the inverted acoustic

impedances. Gluck et al., (2000), Lorenzen (2000) and Lafet et al., (2005) jointly inverted base and monitor surveys using a time-aligned base seismic survey with the subsequent monitor survey. This approach uses a single initial model to invert the base and monitor seismic data to quantitatively estimate representative changes of impedance. Williamson et al. (2007) integrated elements of image warping with impedance inversion to model both time-shifts and amplitude changes when formulating the 4D inversion. In this inversion, the authors assume that production-induced changes in the reservoir primarily affect the P-wave velocity, and cause observable time-shifts and amplitude changes between the monitor and base seismic data. Buland and El Ouair (2006) used the direct inversion of the amplitude differences between the time-aligned base and monitor seismic surveys when obtaining the impedance variations. Tian (2014) coupled the baseline and monitor seismic data in a Bayesian scheme in which the modelling errors are propagated from baseline to monitor to ensure their consistency.

Another aspect to highlight is how to incorporate the 4D seismic data within reservoir flow simulation. 4D seismic response can be integrated either qualitatively (such as interpreting likely causes of 4D anomalies due to changes in saturation and pore pressure) or quantitatively (by adding seismic derived attributes inside in the objective function of a history matching process). Most 4D seismic interpretation remains qualitative in the literature (Johnston, 2013) and it was recently discussed in Byerley et al. (2016) by utilizing time lapse seismic data (impedance domain) to identify areas where water was replacing oil for the Forties Field. However, the multidisciplinary nature of reservoir modeling demands more quantitative approach to integrate 4D seismic data. Amini (2014) used simulation model to generate synthetic time-lapse seismic data during different stages of production which in turn were compared to measured time-lapse data. More recently, 4D seismic has been used quantitatively in reservoir simulation model updating processes as a constraint into history matching, by defining a procedure to match not only the well production data but also 4D seismic attributes (Gosselin et al., 2003; Lygren et al., 2005; Skjervheim et al., 2007; Stephen et al., 2008; Peters et al., 2010). For instance, Roggero et al., (2012) proposed an assisted history matching technique to update reservoir models with 4D seismic data in a quantitative way, in which represented a significant improvement in the reservoir modeling process. However, the updates derived by 4D seismic data

integration may not make geological sense as characterizing the static reservoir framework demands reliable geological knowledge before proceeding with the history matching workflow. Alternatively, the geological framework and property distributions of the reservoir can be defined by the 3D seismic data as it is associated to the static reservoir framework (Tian et al., 2014). Consequently, instead of having only history production data at well locations (few points in the reservoir), spatial variations of static and dynamic properties derived by 3D and 4D seismic data also become accessible to update reservoir simulation parameters iteratively, in order to match both the observed seismic and production data and measures the quality of the matching. Under this type of analysis, seismic and reservoir engineering studies are linked in a circular work-flow to provide better production forecast, with the emphasis being placed on the interface between static and dynamic models, seismic and rock physics.

Nevertheless, quantitative evaluation of consistency between seismic data and reservoir flow simulation relies on petro-elastic modelling (PEM) which links the reservoir simulation to elastic parameters and provides the logical cross-domain comparison. The parameters in PEM should be calibrated according to the specific field of study to ensure realistic values for changes in in-situ elastic parameters due to production activity. The main inputs to PEM are mineral and fluid properties, dry rock model, and a pressure sensitivity model for velocities. Calibrated parameters of rock frame and fluid properties are computed by well-logs data, while related calibration to pressure sensitivity are evaluated by repeated well logging and core measurements. However, there are difficulties in calibrating the pressure sensitivity of the PEM with lab measurements (Osdal et al., 2006) and in case of absent of repeated well logging or not enough core measurements, 4D seismic data can be useful to evaluate the pressure sensitivity of PEM

Thereby, the main contributions of this thesis are: (1) improvement of reservoir characterization and monitoring using 3D and 4D seismic inversion procedures, and time-lapse seismic interpretation (to identify the production effects); (2) updating of reservoir models using quantitative integration of seismic inverted impedance (3D and 4D) within reservoir flow simulation model, in a circular workflow, to improve history matching and close the loop between engineering and seismic domains. Figure 1.2 illustrates the integration of two datasets (engineering and seismic domains) in the impedance domain

which is the procedure here followed. We propose two main steps in order to resolve ambiguity in calibrating reservoir flow simulation model with an uncertain PEM: first, we improve the reliability of reservoir model using quantitative integration of 3D and 4D observed seismic impedance and relying on well history (BHP); then, we calibrate the pressure dependency in the petro-elastic model to ensure realistic values for changes in in-situ elastic parameters due to the production activity and proper match with 4D inverted impedance.

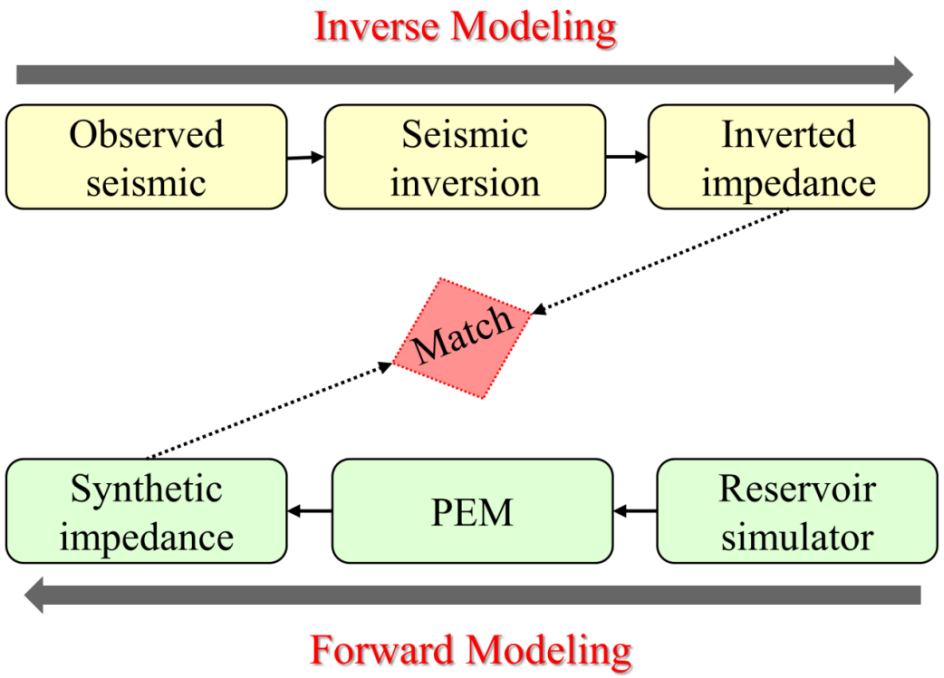

Figure 1.2. Integration between 4D seismic and simulation data in form of impedance domain.

The methodology is evaluated in a complex, faulted, sandstone reservoir, the Norne Field, where a significant reservoir model improvements were obtained. The Norne reservoir is situated in a flat horst structure (9 x 3 km) with a trend of NE-SW, in the Norwegian Sea. The petroleum system that comprises the reservoir sandstones of the Norne Field are post-rift sediments deposited during the continued northward drift of mid-Norway after the pronounced rifting of the northern North Sea during the Triassic (Swiecicki et al., 1998). Rifting of the area occurred in Permian and Late Jurassic - Early Cretaceous. Normal faults with north-northeast to south-southwest trends are common from the first rifting period. Footwall uplift and erosion of the higher structures appeared in the second rifting. In between the rifting periods there was limited tectonic activity, subsidence and

transgression was dominating. As time goes the reservoir has been buried deeper, increasing the diagenetic processes. Furthermore, the field consist of four segments, divided into two compartments. Norne C-, D- and E-segment which are the Norne Main Structure, and Norne G-segment which is the Northeast segment. Alternatively, the hydrocarbons are proven in the rocks of Lower and Middle Jurassic age. The Norne Main Structure is relatively flat with a gas filled in the Garn Formation and Oil is mainly found in the Ile, Tofte and upper zones of Tilje Formations. Tilje Formation is composed of interbedded sandstones, shales and siltstones, often heterolithic, and an unconformity separates it from the overlying Tofte Formation due to tectonic uplift and subsequent erosion (Swiecicki et al., 1998). The Ile and Tofte formations are contained with fine to medium sandstones interbedded with thinly laminated siltstones, shales and some carbonate-cemented which are separated from Garn Formation (with coarser sandstones) due to the effective Not-1 sealing layer, which breaking the communication between the reservoirs above and below it. Approximately 80% of the initial oil is located in the Norne Main structure. Additionally, the reservoir depth is about 2500-2700 meters below the sea surface. Meanwhile, Due to increased erosion to the North reservoir thickness varies over the entire field and from top of Aare to top of Garn it goes from 260m in the southern parts to 120m in the northern part. The average porosity is in the range of 25-30%, while permeability varies from 20 to 2500 mD, net-to-gross values range from 0.7-1 and water saturation 12-43% for the hydrocarbon zones.

The Norne benchmark case proposes to use real field data for research (Rwechungura et al., 2010). The database was organized by the Center of Integrated Operations in the Petroleum Industry (IO Center), the Norwegian University of Science and Technology (NTNU) and Norne Field Operations (Statoil, ENI and Petoro). There are several researches that highlights the beneficial of 4D seismic data for better reservoir behavior understanding in the Norne Filed: Osdal and Alsos (2002); Osdal (2004); El Ouair et al., (2005); Lygren et al., (2005); Osdal et al., 2006; Boutte (2007); Cheng and Osdal (2008); Dadashpour et al., (2009); Huang et al. (2011); Aschjem (2013); Huang et al., (2013); Yan (2014) and Santos et al., (2016). However, this study addresses in more details the evaluation of consistency between the reservoir simulation model and seismic data of Norne Feld, guided by 3D and 4D seismic impedance, to provide geologically consistent

reservoir models that could match the production data, the static data, and the available geological knowledge.

Eventually, this thesis is structured in four scientific articles (Figure 1.3), the first of which describes the 3D inversion of the baseline seismic survey to characterize the static reservoir framework. The second article discusses the advantages of 4D seismic interpretation in terms of seismic impedance variations compared to seismic amplitude. The third article then proposes a 4D inversion procedure to interpret qualitatively the observed 4D inversion anomalies and decouple the effects of fluid and pressure variations, supported by reservoir engineering data. Thus, in the fourth and last article, the results of articles 1 and 3 are quantitatively incorporated into reservoir simulation model updating process, in an iterative loop, that matches the production data and maintains reliable reservoir model which honors all static and dynamic data.

1.1. Motivation

The reliability of the predictions of simulation models as a stand-alone procedure depends on knowledge of rock and fluid properties such as the distribution of heterogeneities, relative permeability, faults location and transmissivity and the production mechanism that control the reservoir performance. Moreover, seismic data has proven to enhance the interpretive capability of reservoir properties for engineers. Thus, the motivation of this work is to generate methodologies to build more reliable reservoir models by improving the integration between reservoir flow simulation and inverted seismic impedance to reduce the attached uncertainty in distribution of heterogeneities and, consequently, improve the knowledge of the static and dynamic reservoir properties in order to manage the reservoir more effectively.

1.2. Objective

The objective of this work is to develop a workflow in an engineering-consistent manner for a structurally complex geological area that uses seismic data as input, to address the issue of maintaining reliable reservoir model. The central ingredient in this scheme is to generate a quantitative integration of inverted seismic data that allows a robust reservoir simulation model updating process, in agreement with information from seismic data when performing a history matching.

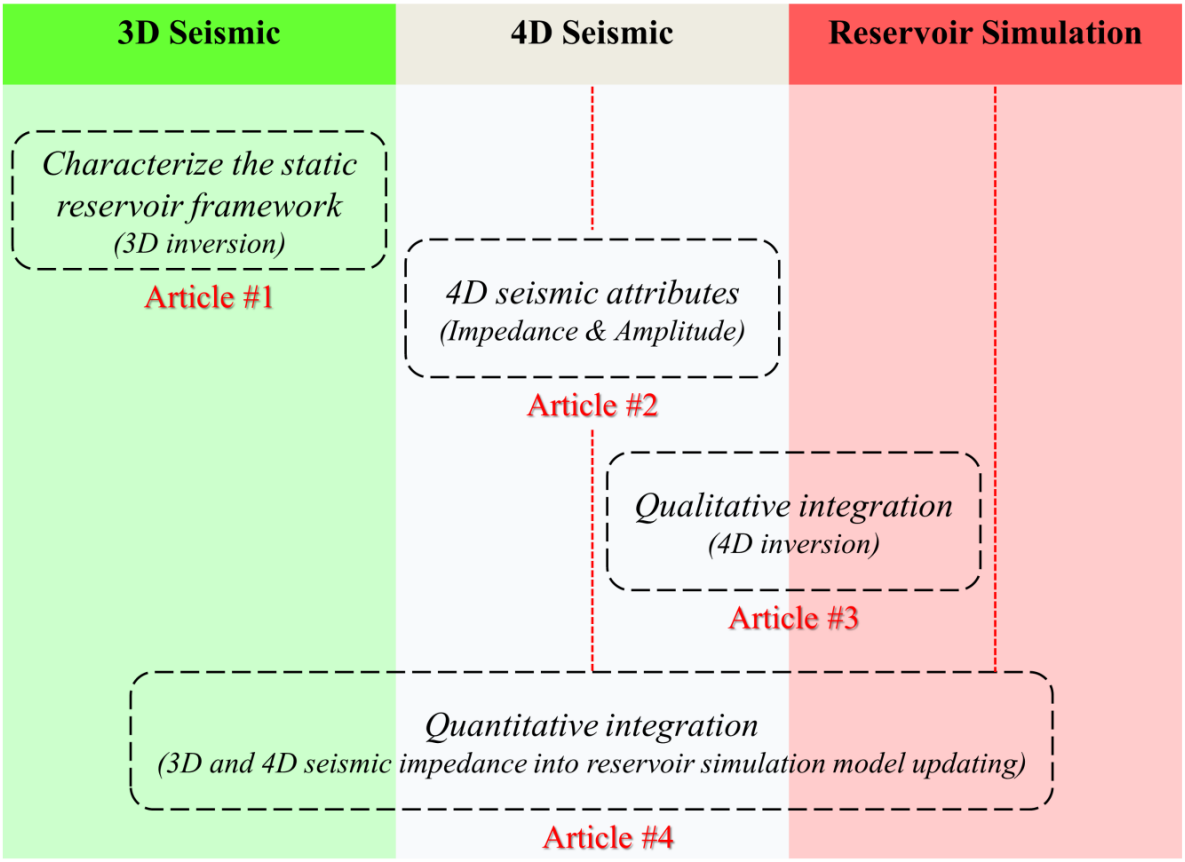

Figure 1.3. Structure of work according to the main area of concentration of each article.

1.3. Description of the thesis

This section presents summary parts of each article, highlighting the main contributions and their link in order to reach the goal of the thesis. The thesis also comprises two appendixes with complementary analyses and results of the articles; the relations between the articles and the appendixes are described in this section as well. The articles in full extension are presented in the following chapters.

1.3.1. Article-1: "*Reservoir characterization using model based post-stack inversion: a case study in Norne field to show the impact of the number of wells in inversion*"

Masoud Maleki, Alessandra Davolio, Denis José Schiozer

Paper IBP1957-16 presented at the Rio Oil and Gas Conference & Exhibition, 24–27 October 2016, Rio de Janeiro.

The first article of this study presents the influence of well constraint (namely different number and location of wells) considered in the 3D model-based seismic inversion (Russell, 1998), which are fundamental to the accuracy of the results and lead to mismatches between the geological interpretation results from the impedance inversion and the spatial distribution of the actual reservoir. In model-based inversion, the initial model is needed as a background of observed seismic data due to the lack of low frequencies in the seismic data. This model represents a low frequency P-wave impedance volume, generated from well-logs data in order to guide the seismic inversion. Thus, the quality of the model-based inversion is partly related to the initial model, which is built by the well-logs data and it is considered to be representative of the actual geological model. The main goal of this article is to evaluate the impact of well constraint in a model-based post-stack inversion applied to the Norne Field; hence, it investigates the reservoir characterization using more robust acoustic impedance interpretation within advantages of maximizing the vertical resolution.

The main contribution of this article to the thesis is to analyze the 3D post-stack, model-based inversion of the Norne Field base survey from 2001. However, the main objective of this study is to provide critical information for 4D seismic inversion (articles 2 and 3) as the initial monitor model is constructed based on the initial base model properties, and consequently, the error in the baseline inversion can propagate into the 4D seismic inversion, which may introduce additional uncertainty. Meanwhile, the first step of reservoir simulation model updating (article 4) requires reliable 3D seismic inverted impedance.

Appendix A presents some complementary results regarding to the inversion analysis constraint by 9 wells in order to estimate the best source wavelet and inversion parameters for all 9 wells.

1.3.2. Article-2: "*Qualitative time-lapse seismic interpretation of the Norne Field to assess the challenges of 4D seismic attributes*"

Masoud Maleki, Alessandra Davolio, Denis José Schiozer

Submitted to The Leading Edge journal,

Presented at the IEEE/OES Acoustics in Underwater Geosciences, 25–27 July 2017, Rio de Janeiro.

This article proposes the advantage of time-lapse seismic interpretation in terms of seismic impedance variations compared to the standard seismic amplitude differences. When time-lapse seismic data is properly interpreted, it can provide valuable information of production activities and their associated saturations and pressure changes. However, opposed to seismic amplitude variations, which are sensitive to layer interface properties, inversion replaces the seismic signal by a blocky impedance response to increase the vertical resolution, and also improves interdisciplinary communication. Thus, this study focuses on comparing the amplitude and impedance changes to evaluate the impact of different seismic attributes in time-lapse seismic interpretation and shed light on the 4D seismic anomalies in the Norne Field. Accordingly, difference volumes of amplitude through the subtraction of the base (2001) and monitor (2006) seismic surveys for middle, far and full stacks data are generated. Meanwhile, two approaches of 4D seismic inversion (model-based and coloured inversion) are performed to evaluate the comparison between different time-lapse seismic attributes. Furthermore, the observed 4D anomalies of amplitude and the both estimated acoustic impedance changes (4D model-based and coloured inversion) are compared to interpret the reliable anomalies.

The main contribution of this work is to better understand the most common time-lapse seismic attributes and highlights the robustness and confidence of 4D seismic impedance data to improve the vertical resolution by eliminating the anomalies that are not caused by production activities.

1.3.3. Article-3: "*Using simulation and production data to resolve ambiguity in interpreting 4D seismic inverted impedance in the Norne Field*"

Masoud Maleki, Alessandra Davolio, Denis José Schiozer

Journal of Petroleum Geoscience, October 2017,

https://doi.org/10.1144/petgeo2017-032

This article presents the efficiency of 4D seismic inversion anomalies to decouple, as much as possible, the effects of fluid and pressure variations caused by production activity. Seismic impedance derived from 4D inversion provides explicit information on changes in pressure and saturation within the reservoir as the impedance changes are saturation–pressure interdependent. However, identifying the causes of 4D acoustic

impedances changes is often a challenge; hence, this is a good example of why integrating different data types is important to decouple these competing time-lapse effects and reduce the uncertainties inherent in 4D reservoir seismic interpretation. This study focuses on analyzing and discussing the impedance anomalies derived from 4D inversion and estimated changes in time-lapse impedance within the entire Norne Field, including all reservoir segments. We inverted the base (2001) and monitor (2006) seismic surveys to access the time-lapse anomalies (softening and hardening signals). To thoroughly investigate inversion anomalies, we compared selected 4D inversion scenarios against well-history and engineering data to identify anomalies caused by production-related changes and the injected fluids. Furthermore, we analyze these scenarios and compare anomalies with the available flow simulation model to suggest specific regions of the field where updates to the simulation model might be appropriate. Our study indicates that joint interpretation of time-lapse seismic inversion with the flow-simulation model results builds confidence in identifying the production effects in the Norne benchmark case, and provides valuable input for reservoir characterization and monitoring.

The main contribution of this article to the thesis is to integrate qualitatively the inverted 4D seismic data into the reservoir simulation model to show how it is possible both to identify likely causes of 4D anomalies (separate the effects of changes in saturation and pore pressure) and to highlight parts of the flow model for further inspection. Moreover, an accurate reservoir simulation model updating (article 4) seeks validate 4D seismic inverted impedance.

There are some complementary results regarding this paper in Appendix B, which include the well-history data of principal producer and injector wells for interpreting the anomalies derived by 4D seismic inversion in the Norne Field.

1.3.4. Article-4: "*Quantitative integration of 3D and 4D seismic inverted impedance into reservoir simulation model updating in the Norne Field*"

Masoud Maleki, Alessandra Davolio, Denis José Schiozer

Submitted to Geophysical Prospecting journal.

Although the qualitative interpretation of time-lapse seismic data proposed in article-3 yielded improvements in reservoir characterization, the multidisciplinary nature of

reservoir modeling demands a more quantitative approach to use 4D seismic data as a constraint in history matching. In fact, calibrated reservoir model with well historical data and observed seismic should provide better production forecast. This work proposes an updating procedure to evaluate consistency of reservoir simulation model and inverted seismic impedance, assisted by production history data, in order to close the loop between reservoir engineering and seismic domains.

The main contribution of this work is to adjust reservoir simulation response using seismic impedance data (provided by 3D and 4D seismic inversion) in order to mitigate uncertainties in numerical reservoir simulation model of the Norne Field. Additionally, this article addresses in details the quantitative evaluation of consistency between the reservoir simulation model and seismic data to provide geologically consistent reservoir models that could match the production data, the static data, and the available geological knowledge. To thoroughly investigate, we convert the inversion results of base (2001) and monitor (2006) seismic surveys to the simulation scale in order to access the observed impedance models (3D and 4D). Alternatively, synthetic impedance models (3D and 4D) are calculated using the initial reservoir flow simulation model and rock-physics modeling. Then, we compare the observed and synthetic impedance, supported by production history data, evaluating their discrepancies and therefore, identify the properties and specific regions of the field where updates to the simulation model might be appropriate. In the case studied, the initial simulation model presents considerable mismatches with the observed seismic data. The inconsistencies can be caused either by the simulation model inaccuracy or uncertainties on the petro-elastic model. The pressure measurements at the wells (bottom-hole pressure) also present significant mismatches which are indicating an inaccurate simulation model. Furthermore, we update the initial simulation model using quantitative integration of 3D and 4D observed seismic impedance and well history data. Alternatively, the reliability of updated simulation model is improved which is validated by resolving the BHP discrepancies of well history-data. However some discrepancies were still observed for the 4D seismic data. Thus, in the last part of the proposed methodology, we calibrate the pressure dependency of petro-elastic model, referring to 4D observed and matched production history data, to ensure realistic values for changes in in-situ elastic parameters. This part highlights another important contribution of time-lapse seismic impedance data to

generate more reliable reservoir model, due to the difficulties of calibrating pressure sensitivity of the PEM using lab measurements.

The principal contribution of this article to the thesis is to evaluate the implementation of all previous articles (articles 1, 2 and 3) in a quantitative integration to maintain reliable reservoir model for a complex structural geology field which honor all available static and dynamic data.

2. ARTICLE-1: *Reservoir characterization using model based post-stack inversion: a case study in Norne field to show the impact of the number of wells in inversion*

Masoud Maleki, Alessandra Davolio, Denis José Schiozer

Article IBP1957-16 presented at the Rio Oil and Gas Conference & Exhibition, 24–27 October 2016, Rio de Janeiro.

Seismic inversion is the interpretation bridge between seismic data and geological information and is generally considered as a direct interpretation approach to evaluate different elastic characteristics in subsurface layers. The amplitudes of reflected seismic waves change at the interface between formations due to the different acoustic properties. It is therefore possible to mathematically invert seismic reflection data to obtain the acoustic impedance of formations on both sides of an interface. Although the inversion technique has evolved over the last 20 years, this technique is still influenced by many factors including seismic acquisition, processing, well-logs data, as well as others. Such influences sometimes lead to mismatches between the geological interpretation results from the impedance inversion and the spatial distribution of the actual reservoir. In this article, we analyze the problem of well constraint (the number and location of wells) in model-based post stack inversion. In practice, we applied an integrated workflow for a quantitative use of 3D post-stack seismic data using a commercial software in order to investigate the main influential factors and problems of 3D seismic inversion in the Norne Field such as the challenges of deviated well-logs information in the well to seismic calibration and the effect of increasing the number of wells in the inversion results. Our study indicates that the number and location of constrained wells will severely affect the accuracy of post-stack inversion results.

2.1. Introduction

Seismic impedance inversion stems from the synthesis of seismograms from well log data presented by Peterson et al., (1955) and Sengbush et al., (1961) under the assumption of plane-wave propagation, time-invariant seismic signal, and multiple and ghost free reflection. Following them, Lindseth (1979) and Becquey et al., (1979) developed Seislog inversion theory to recognize and interpret some geologic phenomena from impedance data. Then, many scholars further studied the mathematics, and formulated diverse approaches to the inversion, such as sparse impulse inversion (Levy and Fullagar, 1981), recursion inversion on the basis of discrete model and continuous model (Berteussen, 1983), auto-regression inversion (Walker and Ulrych, 1983), generalized linear inversion (Cooke and Schneider, 1983), model-based inversion (Russell and Hampson, 1991), and so on. In the model-based post stack inversion, an initial model is

needed as a background of observed seismic data due to the lack of low frequencies in the seismic data. This model represents a low frequency P-impedance volume, generated from well-logs data in order to guide the seismic inversion. Thus, the final result of model-based inversion is a P-wave impedance cube of the studied reservoir with advantages of maximizing the vertical resolution and minimizing tuning effects.

Contrary to the developing of various seismic inversion methods, it is recognized that many factors contribute to different results for the application of different approaches. For instance, Francis (1997) discussed the pitfalls of seismic inversion from the synthetic seismograms computation using well-logs data and well to seismic calibration to the impedance interpretation. Huang et al., (1995) studied the effects of the wavelet, including its frequency, phase, and time length, on inversion. They implied that bandwidth of used wavelet strongly influenced inversion, while its phase and duration had less influence. Shamsa and Lines (2010) implied that model-based inversion provides more control on the selection of the interested interval by choosing the weights of the seismic-initial model. However, the quality of the model-based inversion is partially related to the initial model, which is built by the well-log data and it is considered to be representative of the actual geological layers (Ellison, 1993). Consequently, the model based inversion is challenging in structurally geologically complex areas with few wells for control.

This study focuses on the discussion and analysis of the impact of well constraints in a model-based post-stack inversion applied to the Norne Field. We mainly focus on the effect of the number of wells in seismic forward modeling in a structurally complex geological area such as Norwegian Sea. Furthermore, we investigated the reservoir characterization using the reliable achieved inversion results to identify the main reservoir zones of the Norne Field.

2.2. Methodology

Considering to the non-unique nature of the seismic inverse problem, it is appealing to impose as many constraints as possible to confine the final impedance model. Thus, model-based inversion algorithm uses a convolutional model to incorporate more information from well-log data as a low frequency impedance model in connection with the seismic data. This method solves for the reflectivity iteratively, looking for differences

between the real seismic trace and the synthetic built from the model, and modifying the model to reduce these differences. In fact, the ultimate goal of model-based inversion approach is to minimize the below objective function (Equation 2.1).

$$\mathrm{J} = \mathrm{weight}_1 \times (T - W * r) + \mathrm{weight}_2 \times (M - H * r) \tag{2.1}$$

where T, W, r, M and H are the seismic trace, the wavelet, the final reflectivity, the initial guess of impedance model and the integration operator, respectively. Minimizing the first part of equation (T – W*r), forces a solution that honors the seismic trace and minimizing the second part (M - H*r), forces a solution that models the initial guess impedance. The weights (weight_1 and weight_2) indicate how the seismic trace and initial impedance model must be integrated to provide final inversion results. In stochastic model-based inversion, the constraint is considered to be soft as the model can deviate from the initial guess by setting different values for weights. It has to be noted that the values should be between 0 to 1 (e. g. if the weight1 is 0.6, the weight2 is 0.4). However, in constrained model-based inversion, weight2 is 0, and the final impedance values are set within upper and lower values as a percentage of the average impedance for the log (maximum impedance change), which the model cannot go beyond these values.

Thereby, the model-based inversion algorithm is an iterative procedure in which the impedance is allowed to change gradually to continuously improve the fit between the calculated synthetic trace and the real seismic trace. This algorithm produces a series of pseudo-velocity logs by upscaling the log data into layers or blocks. As a result, the models of pseudo-velocity logs have a coarser resolution than sonic or density logs calculated from well information. In fact, using the blocked model and the wavelet, a synthetic trace is calculated, which is then matched to the actual seismic trace. Note that the large blocking interval tends to produce a coarse blocky velocity structure. As the blocking interval becomes smaller (and therefore get a larger number of blocks), the model will have greater resolution and the synthetic trace will fit the seismic trace better, but the detail may be dependent on the initial guess and not on the real rocks properties measured by the acquired seismic data. Moreover, the model-based inversion process is very similar to deconvolution model in that reflection coefficients are being derived from the seismic data, using the known wavelet. However, this process can be unstable if the wavelet is band-limited and

the solution is to use pre-whitening to stabilize the process (same as the deconvolution procedure). For more details about the inversion algorithm refer to Russell (1988).

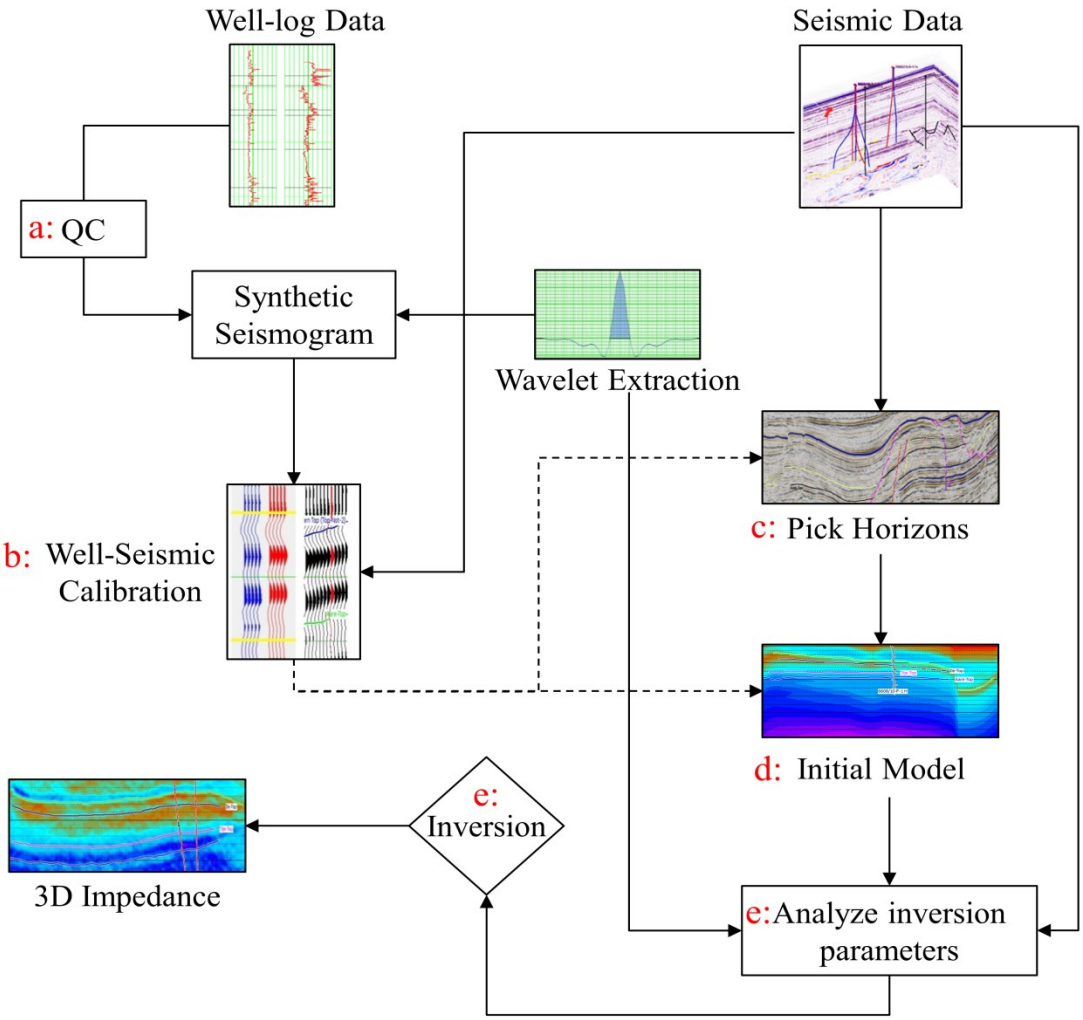

Figure 2.1. Workflow scheme of the 3D model-based seismic inversion (modified from Russell, 1998). Following a five-step approach: (a) perform the QC in the well-logs data; (b) calibrated the seismic and well-log data; (c) pick the main horizons in the seismic survey; (d) create the 3D P-impedance, time-domain starting model, using the well-log data, picked horizons and a low-pass filter; (e) analyze inversion parameters and run the 3D model-based inversion.

Accordingly, this work evaluates the impact of well constraint in a model based post-stack inversion applied to the Norne Field. Two post-stack inversions were run using different numbers of wells based on the workflow of model-based inversion (with same estimated wavelet). The summarized workflow for the 3D model-based inversion follows (Figure 2.1):

- (a) Perform the quality control in the P-wave sonic and density logs.

- (b) Calibrate the seismic and well-log data using the appropriate extracted wavelets for each well and computed synthetic seismogram at the well location.
- (c) Volumetric interpretation by picking the main reservoir horizons in the seismic survey, following the calibrated well-logs dada and well markers information.
- (d) Create the 3D P-impedance, time-domain starting model, using the main horizons picked in the seismic survey (which act as geological markers), well-log data and a low-pass frequency filter.
- (e) Analyze inversion parameters, and apply model-based inversion to the seismic survey to produce inverted impedance model.

2.3. Norne Field and dataset

The Norne benchmark case is based in a set of real oil field data organized by the Center of Integrated Operations in the Petroleum Industry (the IO Center), the Norwegian University of Science and Technology (NTNU) and Norne Field Operations (Statoil, ENI and Petoro). The Norne Field is located on a horst block in the southern part of the Nordland II area, with a complex structural geology and major faults. The horst block is approximately 9 × 3 km and consists of two separated oil compartments; Norne main structure (segments C, D and E) and the North-East segment (segment G). In the Norne Field, the hydrocarbons are found in sandstones from the Middle and Early Jurassic age and subdivided into the four different formations from top to base: the Garn, Ile, Tofte and Tilje formations. The top reservoir map and the segments of the Norne Field are shown in Figure 2.2, respectively.

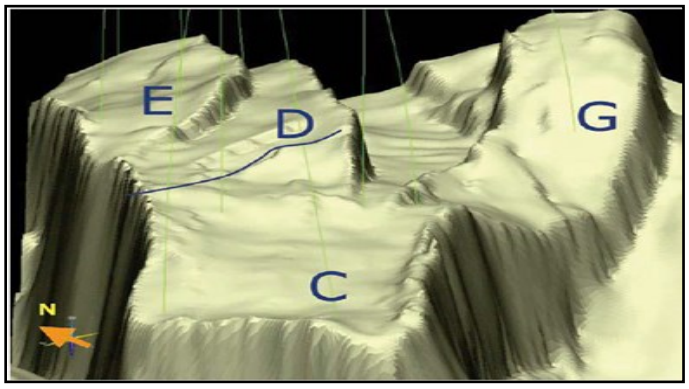

Figure 2.2. Top reservoir map showing Norne horst block with the four segments (modified from Osdal et al., 2006).

The dataset used in this article is a 3D post-stack seismic data which was carried out with a Q-marine vessel in 2001. In addition, we used the information of P-wave sonic and density logs of 9 wells (10-2, 10-4, B-4H, C-1H, C-3H, D-1H, D-4H, E-3H and F-1H) which were less deviated in the reservoir area to cover the entire seismic cube. Wells 10-2 and 10-4 are the vertical exploration wells, while wells B-4H, D-1H, D-4H and E-3H are the producer and C-1H, C-3H and F-1H are the injector wells. Figure 2.3 illustrates the location of 9 wells and post-stack seismic data of 2001 in the Norne benchmark dataset, respectively.

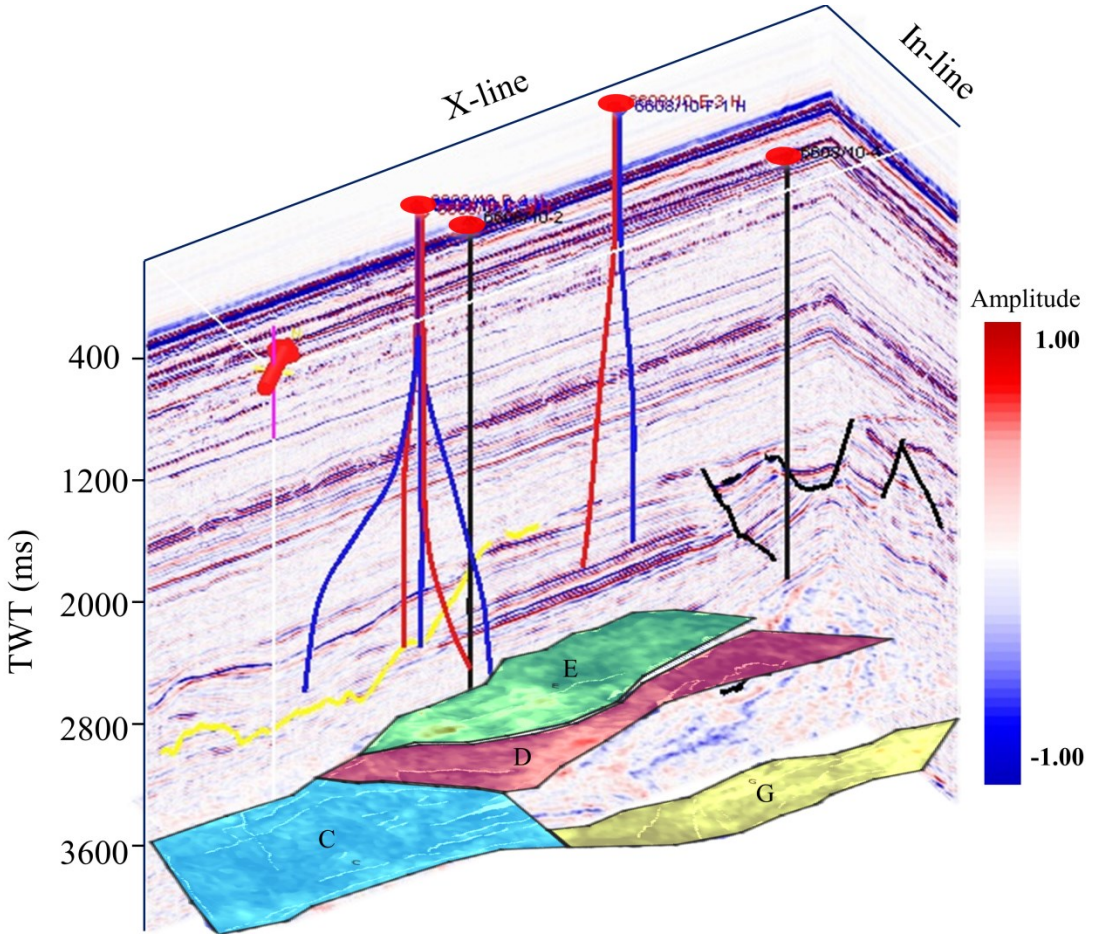

Figure 2.3. Database of the Norne benchmark including post-stack seismic data of 2001 and location of the nine well-logs. The black, red and blue colors denote the vertical exploration, producer and injector wells, respectively.

2.4. Application

In this study, analysis of the impact of well constraint is divided into two main steps: (1) model-based inversion using the two exploration wells of 10-2 and 10-4; (2)

model-based inversion using all the nine wells. Following the workflow of 3D model-based inversion (Figure 2.1), the first step of integrating well-logs data into the seismic inversion is well to seismic data calibration. However, this calibration is not straight forward in the Norne benchmark dataset due to the challenges of well to seismic tie in the deviated wells. Thereby, we extracted several statistical wavelets for each well and changed the size of correlation windows to obtain the best synthetic seismogram at the deviated well locations in order to tie the deviated logs within seismic data. For instance, as shown in Figure 2.4, after exhaustive tests and choosing a neighbored radius of eight samples along the deviation path of the well, fair correlations were achieved for the wells D-4H (90.7 %) and E-3H (86.2 %).

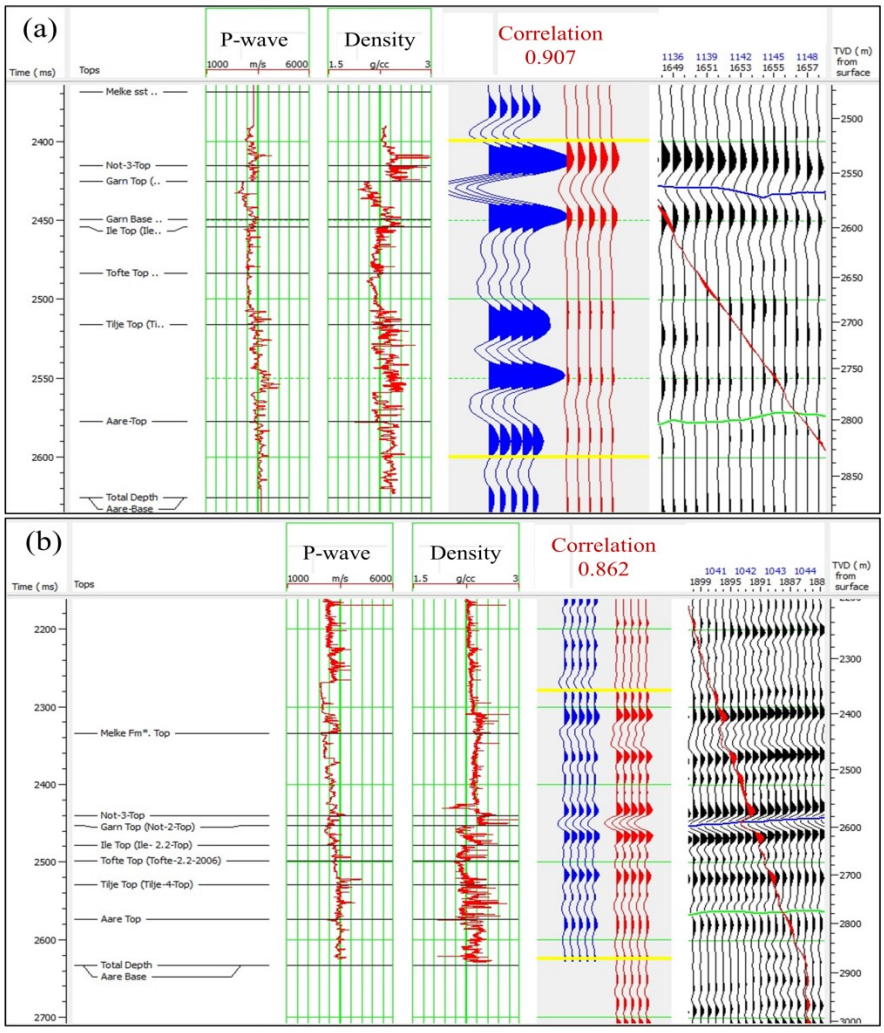

Figure 2.4. Well to seismic calibration of deviated wells (a) D-4H and (b) E-3H. The blue traces represent synthetic traces calculated from the sonic and density logs, while the red traces denote the composite traces extracted from the seismic data.

In the next step of inversion, the main reservoir formations of the Norne Field (top of Garn, Ile, Tilje and Aare formations) were interpreted in the seismic survey within the in-line and cross-line increments of 1 (Figure 2.5). Meanwhile, picked horizons of the top of Ile and Tilje formations were demonstrated that these two reflectors were able to be interpreted only in the western flank of Norne Field. It seems that the thinning of the reservoir interval between the top of Aare and Garn formations to the north supports the theory of episodic uplift and increased erosion to the north during the Middle and Early Jurassic time (as it is clearly shown in Figure 2.5).

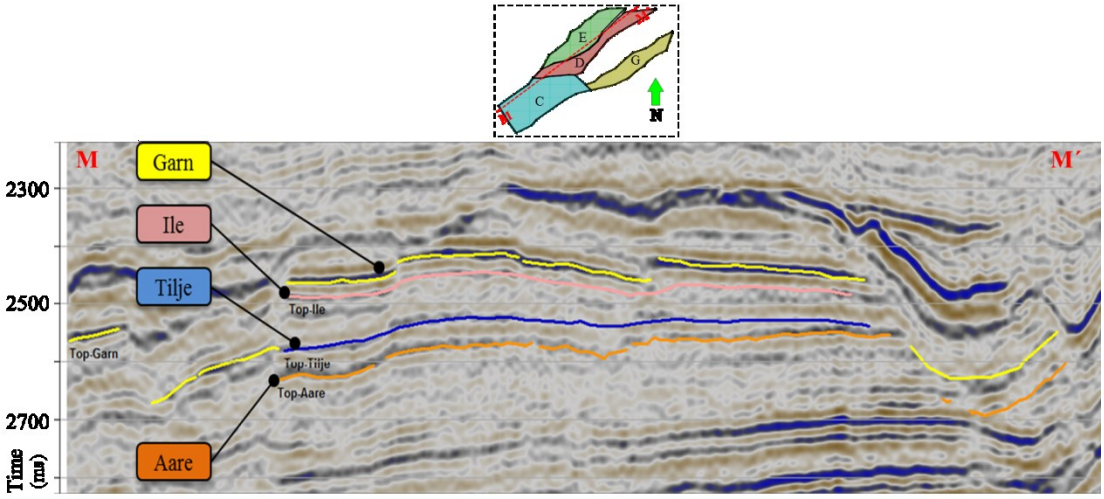

Figure 2.5. Interpretation of the main reservoir horizons. Location of the profile is given by the broken line in the thumbnail plot.

After a satisfactory well to seismic calibration and volumetric interpretation, construction of the initial impedance model was the next step of the inversion. Two initial models were built by interpolating the acoustic impedance logs from the nine wells (Figure 2.6a) and only two exploration wells (Figure 2.6b) over seismic survey (using the picked main horizons as interpolation guide). As shown in Figure 2.6, the initial impedance model derived by nine wells provided better continuity of the formations compared to the initial model extracted from two exploration wells.

The last step of the inversion procedure was to analyze the inversion parameters using cross plots of the initial impedance model and inverted impedance log. In this study, after testing different inversion parameters such as several block sizes (2 to 4 ms) and prewhitening percent (1% to 5%), we considered the same optimum procedure for both

inversions to compare the results (two- and nine-wells). The inversion parameters and profile plot of analysis using same parameters for the two and nine wells are shown in Table 2.1 and Figure 2.7, respectively. Analysis of the inversion constraint regarding two-wells highlighted the inverted synthetic correlation of 0.999 and inverted relative error of 0.023. Moreover, the analysis of the inversion constraint by nine-wells indicated the inverted synthetic correlation of 0.999 and inverted relative error of 0.031. Hence, the used inversion parameters (Table 2.1) provided high correlation and least error of inversions for both scenarios. It has to be noted that the both inversion analysis were performed at the well locations, which could not guarantee a high correlation for the entire survey.

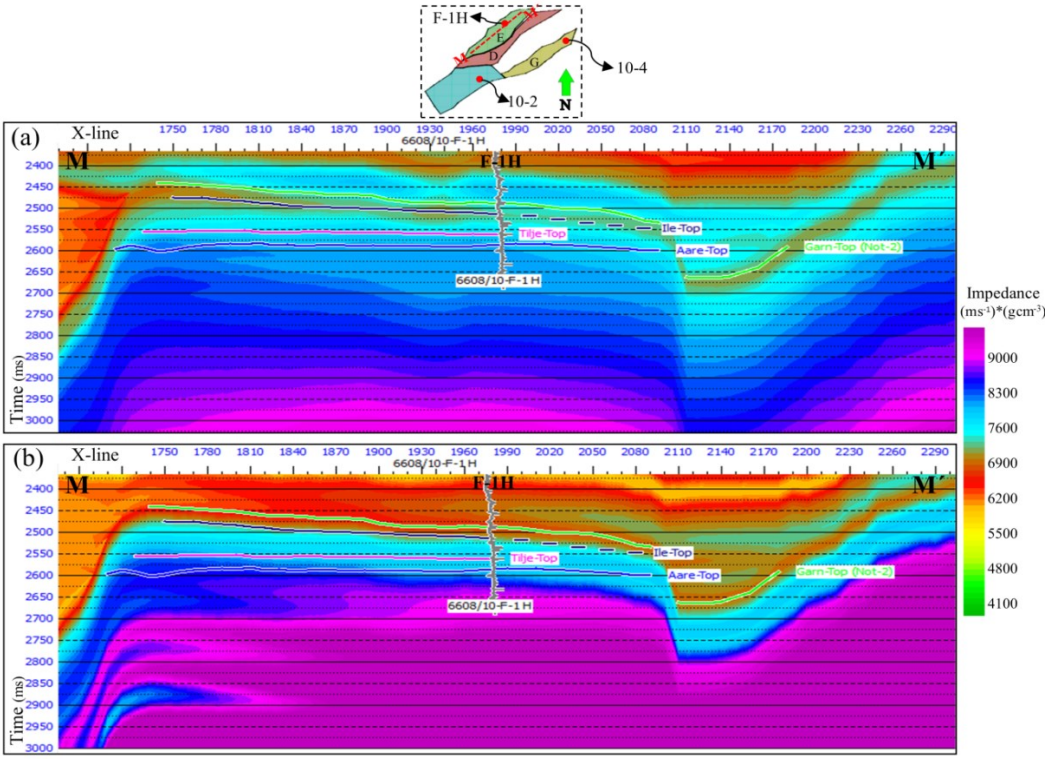

Figure 2.6. Profile of initial impedance models derived from (a) nine-wells, (b) two-wells. Location of the profile is given by the broken line in the thumbnail plot, and red dots denote well-head positions.

Table 2.1. Model-based inversion parameters.

Constraint	Maximum change of constraint	Average block size	Prewhitening	Number of iterations
Hard	80 %	2 ms	1 %	60

2.5. Results and discussion

Figures 2.8 and 2.9 illustrate the 3D impedance inversion results (using two exploration and nine wells) for the segments E and C, respectively. By comparison of

inversion results, it can be seen that the varied locations and number of well clearly affected the inversion results. We observed higher vertical resolution for the inverted impedance results derived from nine-wells compared to two-wells. The possible explanation is that since exploration wells are located in segment G and eastern flank of segment C, derived initial low-frequency impedance model could fail to reflect the actual geological model (due to the interpolation of well-logs along constrained layers). Thus, the inversion result of two exploration wells implied less continuity of layers compared to the inversion result using nine-wells, which may affect the reservoir characterization.

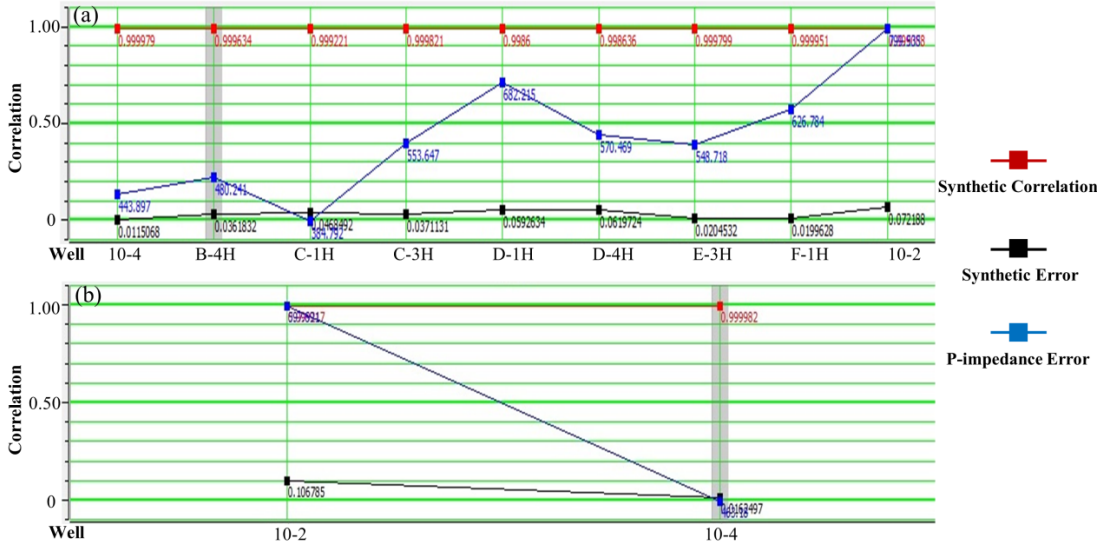

Figure 2.7. Profile plot of the inversion analysis for (a) nine-wells and (b) two-wells. The total, minimum and maximum deviations of impedance between the original log and inverted result (P-impedance error) for 9-well constrained inversion are 590.996 (m/s * g/cc), 384.792 (m/s * g/cc) and 799.535 (m/s * g/cc), respectively. The total, minimum and maximum deviations of impedance between the original log and inverted result (P-impedance error) for 2-well constrained inversion are 542.045 (m/s * g/cc), 463.18 (m/s * g/cc), and 591.691 (m/s * g/cc), respectively. Note that the maximum deviation between actual and inverted seismic trace (synthetic error) is 7.21% for 9-well constrained inversion, while this error is 10.6 % for 2-well constrained inversion.

We therefore interpreted the results of inverted impedance results using the nine-wells to highlight the main reservoir formations in the Norne Field. Figure 2.10 illustrates a profile throughout the 9-well constrained post-stack inversion results in the segments E and C. The impedance significantly decreased in the areas between Garn and Ile formations compared to the regions above top of Garn Formation, which it may be due to the presence of the gas-bearing sandstone. Meanwhile, the areas between top of Aare and Tilje formations implied higher impedance compared to the zones above the top of Tilje

Formation. It is in agreement with the geological knowledge, as it lies at the boundary between the reservoir sandstones of the upper formations and shaley sandstones of Aare Formation. Additionally, derived impedance results highlight that areas between Garn and Ile formations and below the top of Ile Formation are the possible main reservoirs due to their low impedance zones, which are consistent with the geological knowledge and previous interpretation on these zones (Statoil, 2004). However, main reservoir formations were separated by high impedance layers in the top of Ile and Tilje formations. Furthermore, it has to be noted that impedance decreases in the areas between the top of Garn and Ile formations are more significant compared to impedance decreases below the top of Ile Formation.

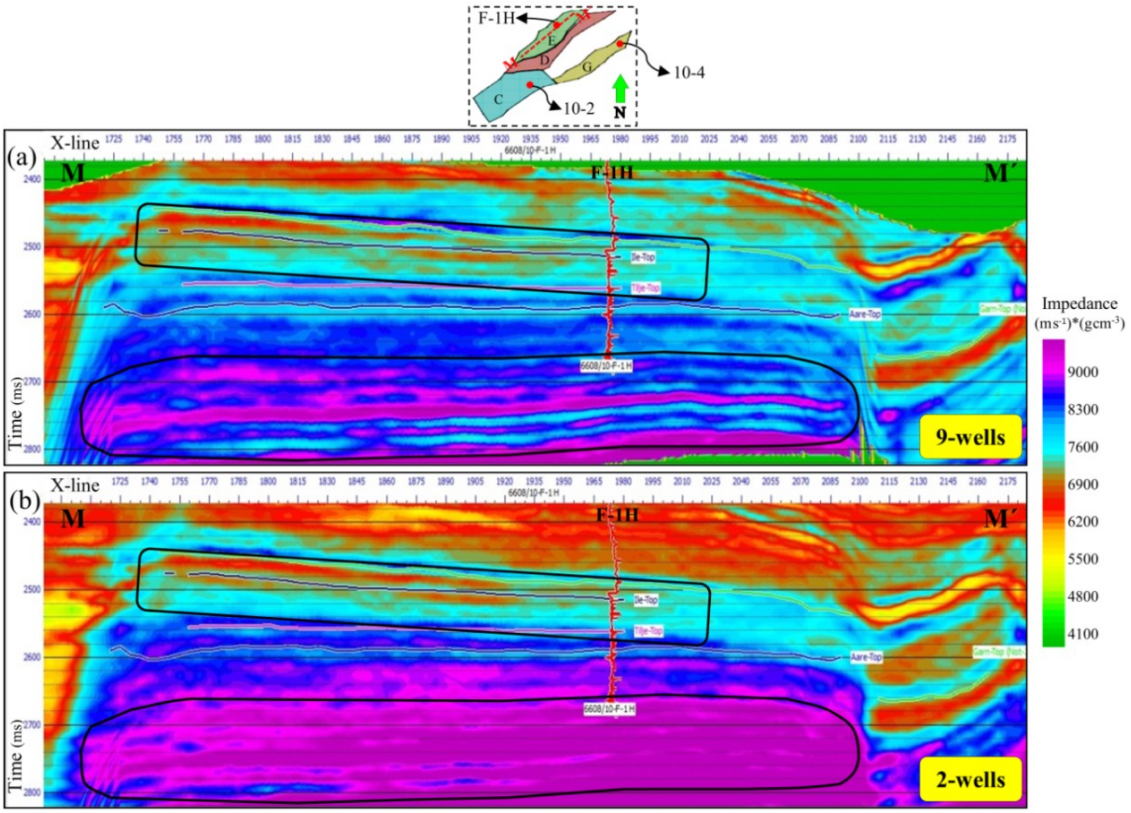

Figure 2.8. Profile of inverted impedance results for segment E derived from (a) nine-wells and (b) two-wells. The detached zones highlight improvement of vertical resolution throughout 9-well constrained post-stack inversion. Location of the profile is given by the broken line in the thumbnail plot, and red dots denote well-head positions.

Hence, we investigated the areas between top of Garn and Ile formations by computing the cross-plot of impedance against P- to S-wave velocity ratio (V_P/V_S) in order to interpret the fluid as well as lithology discrimination and describe the reservoir

conditions in terms of lithology and fluid content. Figure 2.11 illustrates the computed cross-plot for well C-3H. According to Goodway et al., (1997), the region having low values of impedance and V_P to V_S ratio is corresponded to gas-bearing sand, whereas the area having low values of impedance and high values of V_P to V_S ratio is considered to be a shaley formation. The zones of gas-bearing sandstone (A: low impedance and V_P/V_S) and Shaly formation (B: low impedance and high V_P/V_S) were interpreted according to the log data information of well C-3H (Figure 2.11a). Then, we compared the cross-section of zones A and B at well C-3H (Figure 2.11b) with the 9-well constrained post-stack inversion results (Figure 2.11c). Alternatively, zones A and B implied a strong match with low impedance areas throughout the Garn Formation and high impedance region above the tope of Garn Formation, respectively. We therefore considered zone B as a shaley cap-rock for the gas-bearing sand of Garn Formation (zone A).

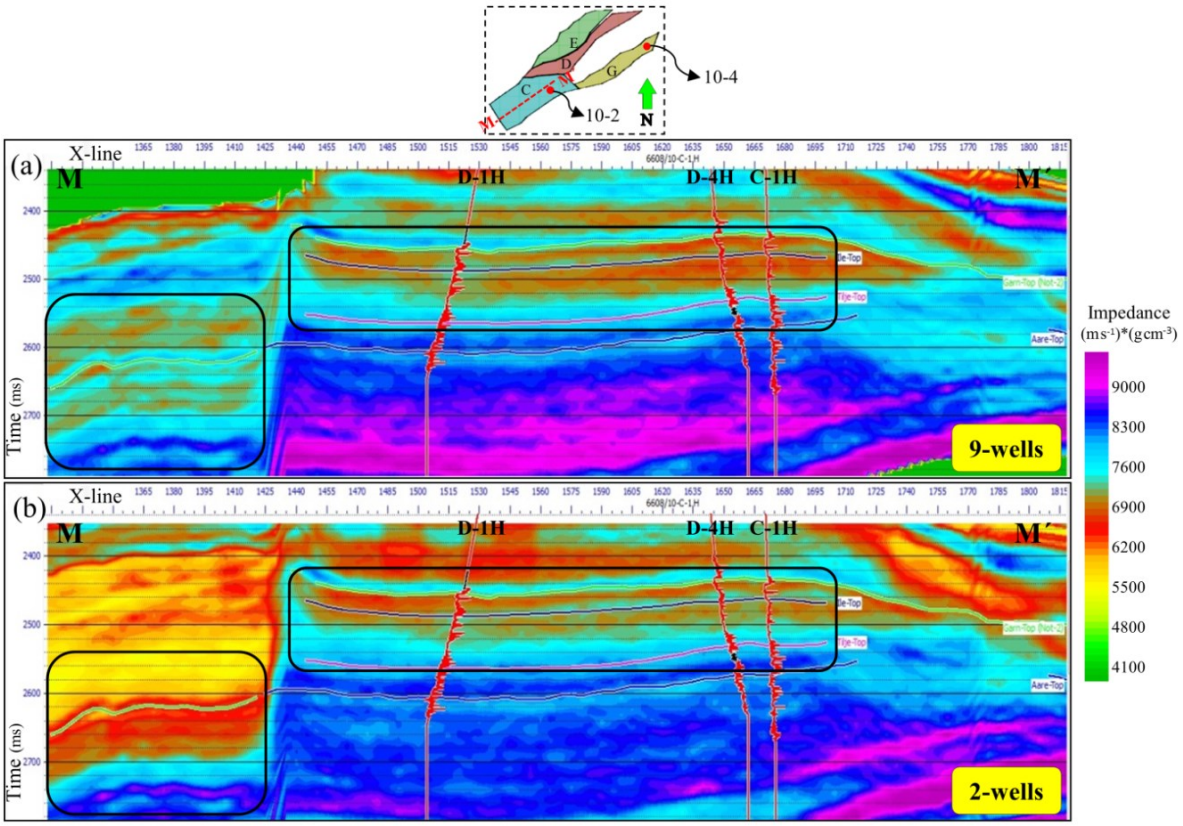

Figure 2.9. Profile of inverted impedance results for segment C derived from (a) nine-wells and (b) two-wells. The detached zones highlight improvement of vertical resolution throughout 9-well constrained post-stack inversion. Location of the profile is given by the broken line in the thumbnail plot, and red dots denote well-head positions of the exploration wells.

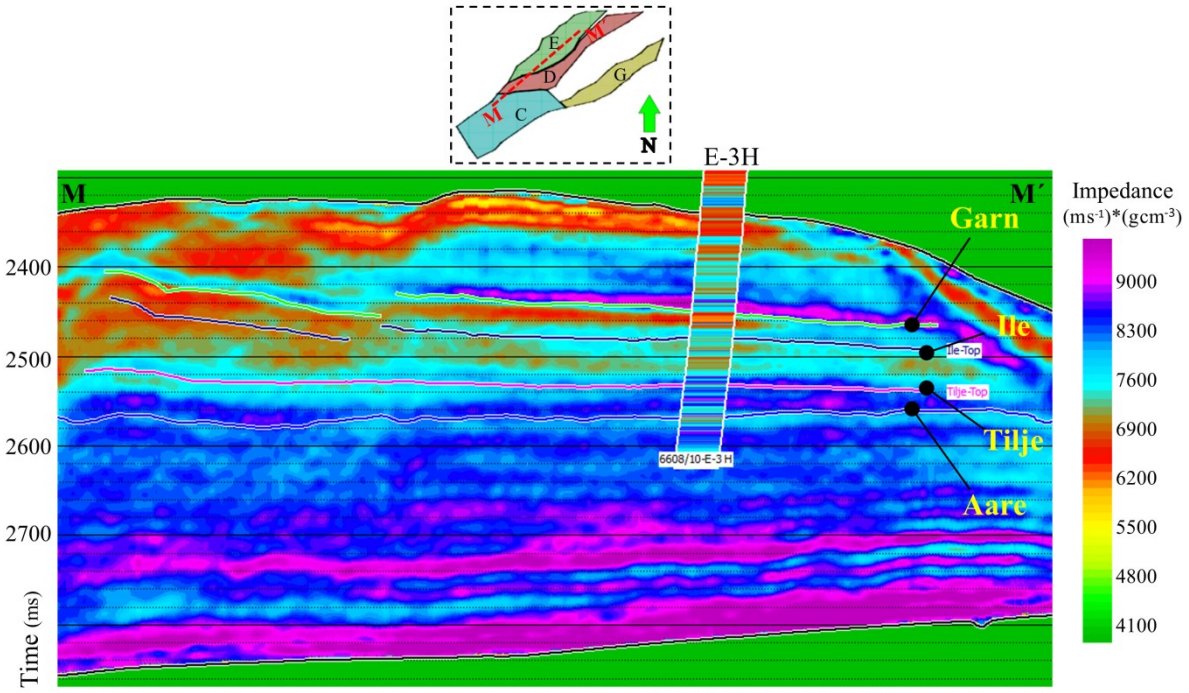

Figure 2.10. Profile of inverted impedance results from the 9-well constrained post-stack inversion. Location of the profile is given by the broken line in the thumbnail plot. Note the significant decreases in impedance for regions between the Garn and Ile formations and below the top of Ile Formation.

2.6. Conclusions

In this study we calibrated the deviated wells to seismic data using several statistical wavelets for each well. Then, we computed two different seismic initial models based on the nine and two exploration wells. Additionally, we performed varied 3D post-stack model-based inversion (within the same optimum procedure and wavelet) using different initial impedance models to evaluate the influence of well constraint (namely different number and location of wells) considered in the 3D model-based seismic inversion. In our case study, the 9-well constrained post-stack inversion implied reliable and more robust interpretation than 2-well constrained inversion for the structurally complex geological area of Norne Field. In fact, initial impedance model of nine-wells constraint would more likely meet requirements of an accurate model-based inversion for Norne seismic survey of 2001, in which are fundamental to the accuracy of the results as two-wells constraint inversion may lead to mismatches between the geological interpretation results from the impedance inversion and the spatial distribution of the actual reservoir. Eventually, despite the challenging seismic to well tie of the deviated wells, the seismic modeling outcome of the

9-well constrained inversion is more reliable to improve the reservoir characterization and to update the geological model in the Norne Field.

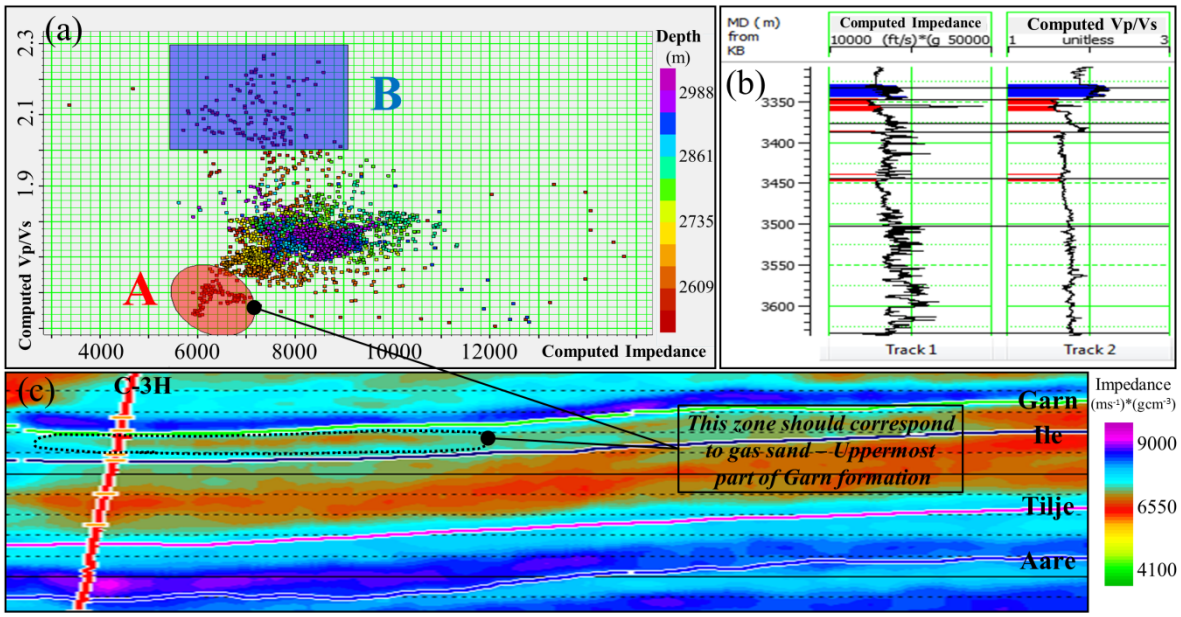

Figure 2.11. (a) Cross plot of P-impedance versus V_P/V_S for well C-3H. (b) Cross-section of interpreted zones (A and B) in the well C-3H. (c) Profile of inverted impedance results from the 9-well constrained post-stack inversion at location of well C-3H. Note the significant decreases in impedance for detached region (uppermost part of Garn formation) compared to upper formation.

3. ARTICLE-2: *Qualitative time-lapse seismic interpretation of the Norne Field to assess the challenges of 4D seismic attributes*

Masoud Maleki, Alessandra Davolio, Denis José Schiozer

Submitted to The Leading Edge journal

Presented at the IEEE/OES Acoustics in Underwater Geosciences, 25–27 July 2017, Rio de Janeiro.

Interpretation of time-lapse (or 4D) seismic data in terms of reservoir changes due to production posed many challenges in the Norne Field as the field experienced intense production activity from 1997 to 2006. For some segments within the field, both fluid movement and pressure changes have approximately the same degree of impact and possible opposite effects on the seismic data. Moreover, hardening anomalies could be caused due to the increase in water saturation or gas going back to solution, while softening anomalies could be related to the increase in pore pressure or decrease in fluid bulk modulus following the injection of gas. Thereby, for time-lapse seismic analysis to be most effective and less erroneous, different seismic attributes must be addressed to infer reservoir changes caused by production activity, such as seismic amplitude and impedance derived by seismic inversion. In the present work, we analyze the challenges of 4D seismic interpretation in the Norne benchmark case for the southern flank of segment C. Our study indicates that acoustic impedance differences derived by a 4D model-based inversion provide an increase in vertical resolution compared to standard seismic amplitude differences in the segment C. Furthermore, we present a comparison between results of a 4D model-based and coloured inversions to evaluate the confidence of inversion anomalies. Meanwhile, as this is a benchmark case, this study can be considered to enrich the discussions over qualitative and quantitative time-lapse seismic interpretation and to improve the reservoir characterization.

3.1. Introduction

Time-lapse seismic data (4DS) have proven to be an important tool in reservoir characterization and monitoring. When properly interpreted, 4DS can provide valuable information of production activities and their associated saturations and pressure changes. Thus, different seismic derived attributes (such as amplitude and impedance changes) are needed in achieving accurate interpretation and reducing the uncertainties attached to the 4D seismic analysis. The first level approach of interpreting the time lapse seismic anomalies is to compare the changes of amplitude from the actual 4D seismic datasets. However, opposed to seismic amplitude variations, which are sensitive to layer interface properties, inversion replaces the seismic signal by a blocky impedance response (Veeken

and Da Silva, 2004) to increase the vertical resolution, and also interdisciplinary communication (Tian et al., 2014).

Alternatively, reliable time-lapse seismic interpretation mainly depends on the quality of seismic surveys (e.g. repeatability and signal to noise ratio). Moreover, combinations of pressure and fluid saturation variations dominate the seismic response and affect their straight interpretations (Landrø, 2001). For instance, an increase in impedance is expected during water flooding, when water replaces oil or when gas goes back into solution (Johnston, 2013). Thereby, identifying the causes of 4D seismic anomalies in reservoir changes is often a challenge for most hydrocarbon reservoirs and there are complexities to obtain a successful and global 4D monitoring approach based on amplitude or impedance changes. Landrø et al., (1999) identified potentially undrained reservoir zones directly from time-lapse AVO (amplitude versus offset) and post-stack data in the Gullfaks Field. Tura et al., (2009) estimated the remaining oil thickness from conventional amplitude differences (4D stack data) in the Alba field (North Sea). However, interpretation of 4D seismic anomalies using standard seismic amplitude differences can be erroneous. Vedanti and Sen (2009) and Six et al., (2013) suggested that the 4D acoustic impedance inverted from seismic amplitude improved the distinguishing of reservoir changes (pressure and fluid effects) in the Balol Field of India and Moho Bilondo Field of Congo, respectively.

Thus, this study focuses on comparing the amplitude and impedance changes to evaluate the impact of different seismic attributes into the time-lapse seismic interpretation and shed light on the 4D seismic anomalies in the Norne Field (southern flank of segment C). Nevertheless, the Norne benchmark dataset is an ideal candidate for investigating the accuracy of amplitude and impedance attributes as it is known that the reservoir experienced intense production from 1997 to 2006. Accordingly, we generated differences volume of amplitude through the subtraction of the baseline (2001) and monitor (2006) seismic surveys for near, far and full stacks data. Meanwhile, we performed two approaches of 4D seismic inversion (model-based and coloured inversion) to evaluate the comparison between different time-lapse seismic attributes and certainty of inversion anomalies. Furthermore, we extensively investigated the reliable 4D anomalies and mapped the production activities to address their associated pressure and fluid saturation variations. It is worth mentioning that pre-stack inversion might be more appropriate to separate pressure

and fluid effects. However, we performed post-stack inversion as some regions of the angle stack volumes data for segment C (e. g. eastern flank of segment) presented low signal to noise ratio. Thus, we run full stack inversion to increase, as much as possible, the vertical resolution and produced clear images.

3.2. Nonre Field and benchmark dataset

In this study, The Norne benchmark case is a real dataset provided by Statoil and their license partners for research purposes, managed by the Norwegian University of Science and Technology (NTNU) and Norne Field Operations (Statoil, ENI and Petoro). The field is located on a horst block in the southern side of the Nordland II area within the Mid-Norwegian Margin (Figure 3.1a). The hydrocarbons are mainly found in sandstones of Lower and Early-Middle Jurassic age within Garn, Ile, Tofe and Tilje formations (Figure 3.1b). More details about Norne stratigraphy can be found in Dalland et al. (1988) and Swiecicki et al. (1998).

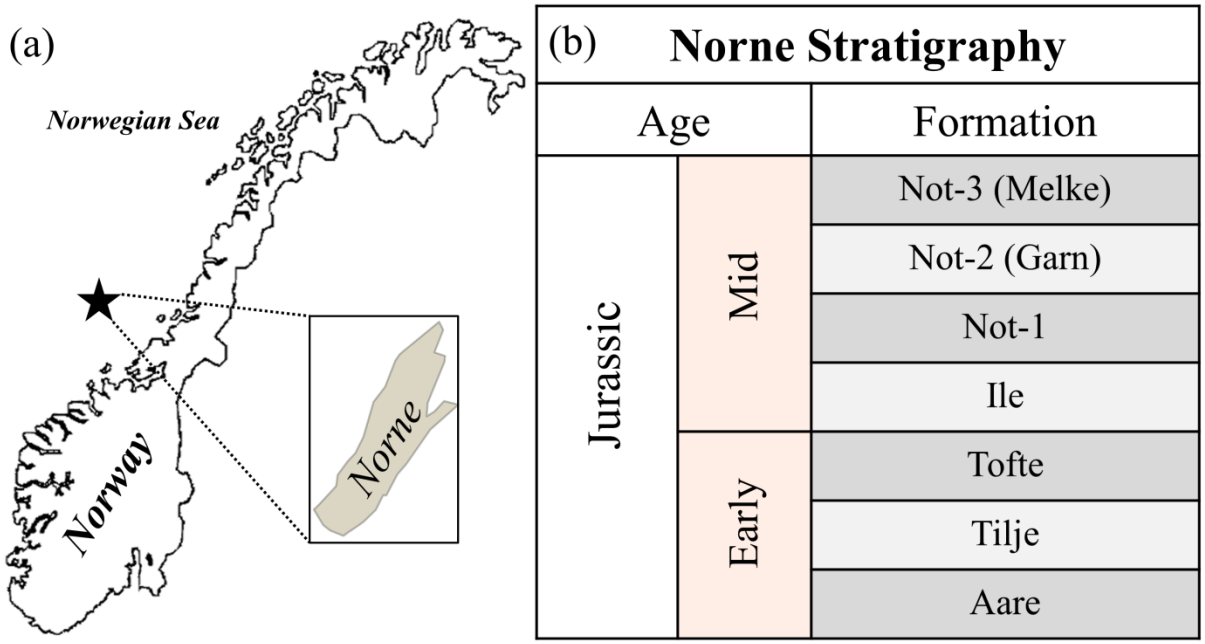

Figure 3.1. (a) Location of Norne Field in the Norwegian Sea. (b) Stratigraphy of the Norne Field. Hydrocarbons are mainly found in the Garn, Ile, Tofte and Tilje formations.

The seismic data used in this paper include nine 3D seismic cubes: near, far and full stacks acquired in 2001 (base survey), 2003 and 2006 (monitor surveys). Meanwhile, the frequencies contents of near, far and full stack are 10 to 65 Hz, 10 to 40 Hz and 10 to 60

Hz, respectively. Moreover, we constructed the base survey initial impedance model from P-wave sonic and density logs of nine-wells (10-2, 10-4, B-4H, C-1H, C-3H, D-1H, D-4H, E-3H and F-1H). Figures 3.2 and 3.3 highlight details of impedance logs in the reservoir zones of Norne Field, and the segments of field in the top reservoir and the locations of mentioned nine wells, respectively. Dots denote well-head positions (exploration wells marked by red dots) and black lines represent locations of the deviated sections.

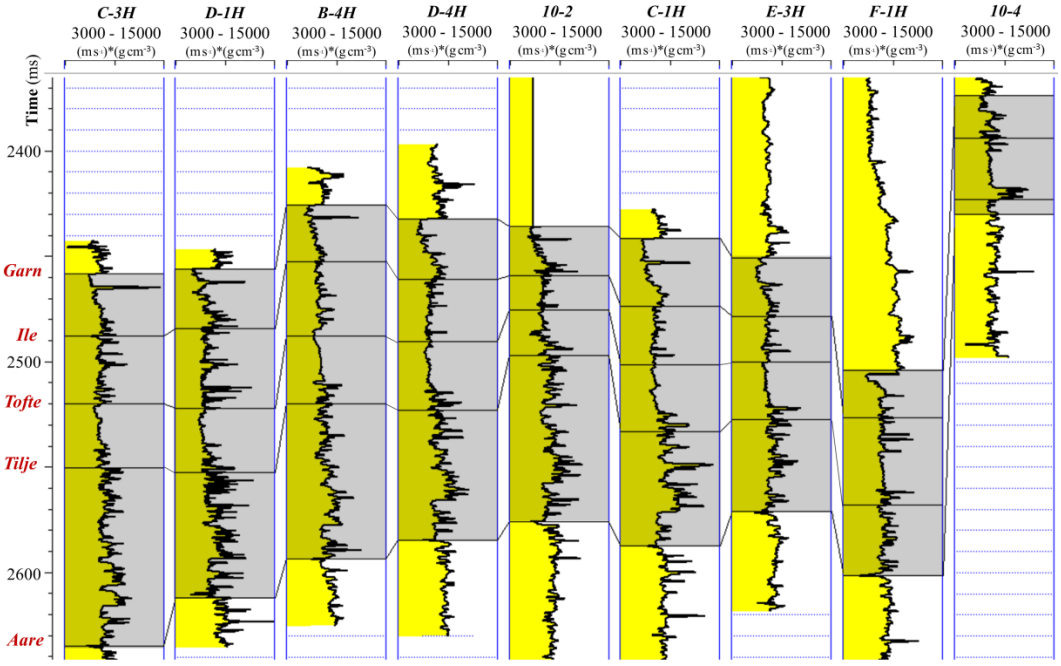

Figure 3.2. Impedance logs of wells 10-2, 10-4, B-4H, C-1H, C-3H, D-1H, D-4H, E-3H and F-1H) in the reservoir zones of Norne Field.

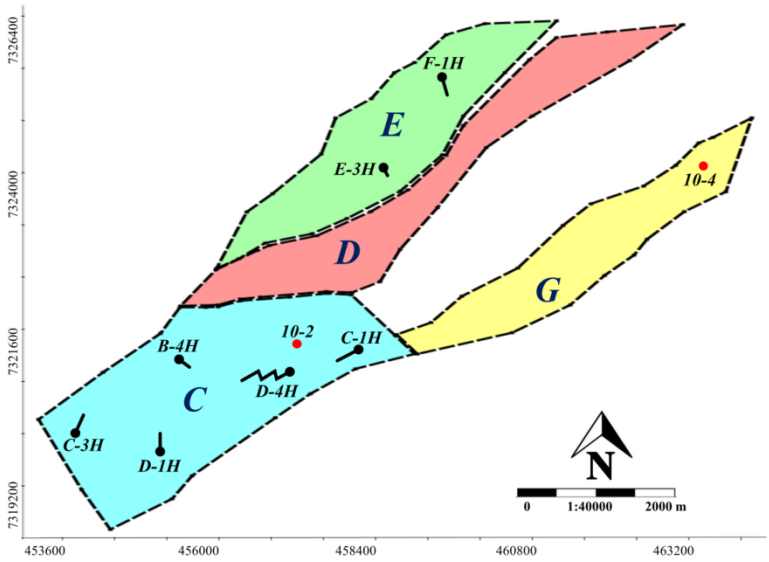

Figure 3.3. Segments of the Norne Field and locations of the 9 wells.

Segment C is located in the southern region of Norne Field and contains two injector wells of C-1H (water and gas) and C-2H (water). These injector wells were perforated before 1999, aimed at giving pressure support to the neighbouring producers and enhance the oil sweep. Figure 3.4 illustrates the injected water and gas rates of wells C-1H and C-2H up to 2007, respectively.

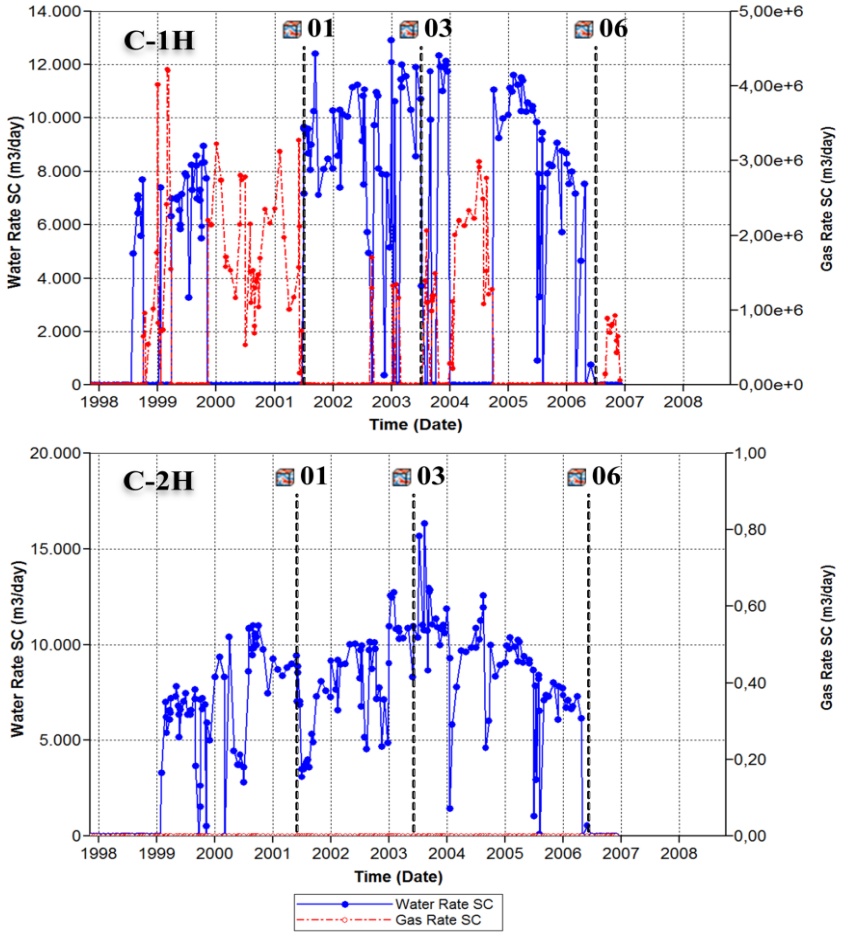

Figure 3.4. Injected water and gas rates of well C-1H (top) and C-2H (bottom).

3.3. Comparison of 4D seismic attributes

In this study, we divided the comparison of 4D seismic attributes and time-lapse interpretation into the two main steps. First, we evaluated the derived anomalies from conventional seismic amplitude changes to investigate the amplitude signals. Thus, difference volumes of near, far and full stacks data were generated through the

straightforward subtraction of the base (2001) and monitor seismic surveys (2006). Then, we compared amplitude signals within derived softening and hardening anomalies considering different procedures of 4D inversion (model-based and coloured inversion), to verify their similarities. The reason of using different 4D inversion methods is to improve the confidence of the observed impedance anomalies and evaluate possible artifacts generated by seismic inversion. However, a combination of pressure and fluid saturation variations may affect the 4D impedance interpretation. To describe this complex interpretation, consider the impedance variations in case of water replacing oil and gas going back into solution (Figure 3.5). Impedance increases considering both scenarios of water replacing oil and gas going back into solution. The explanation is that as water replaces oil, the rock bulk modulus stiffens as well as the rock density increases, therefore P-impedance increases. The same effect occurred when gas goes back into solution. Meanwhile, increases in pore pressure cause decreases in impedance. Thus, to overcome the mentioned challenge, we selected scenarios against the well history data to investigate the 4D seismic anomalies and to identify the related production-induced in the reservoir for the last part of the proposed workflow.

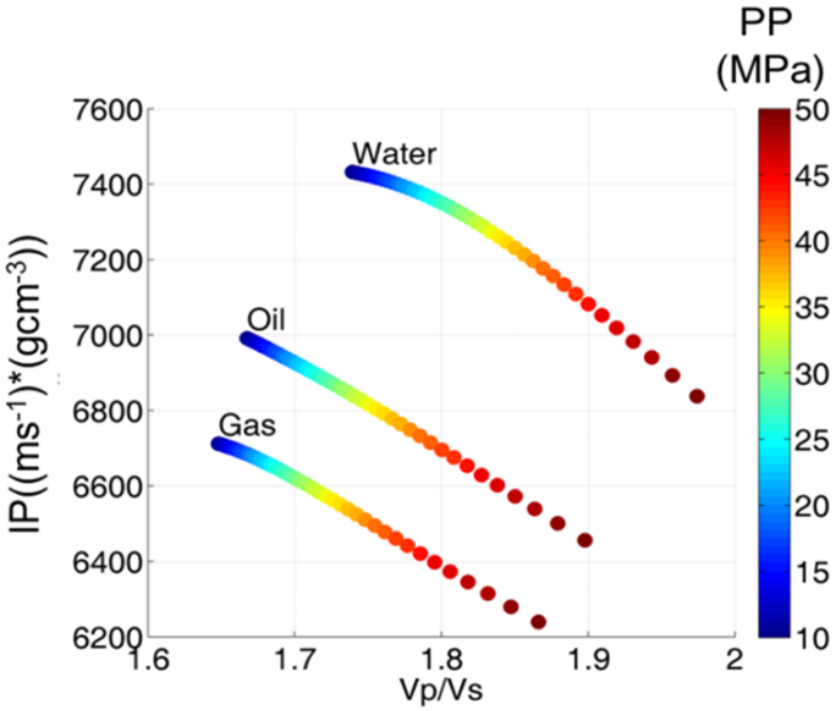

Figure 3.5. Impact of fluid saturation and pore pressure changes on impedance and V_P to V_S ratio. Color key represents the various values of pore pressure. Note the impedance increases considering water replacing oil and gas going back into solution. Meanwhile, increases in pore pressure cause decreases in impedance.

The summarized workflow for the 4D seismic interpretation (Figure 3.6) follows:

- (a) Generate the amplitude changes by subtraction of monitor and base vintages (near, far and full).
- (b) Estimate the impedance changes using both 4D model-based and coloured inversions.
- (c) Compare the observed 4D anomalies of amplitude and both estimated acoustic impedance changes (softening and hardening signals).

(d) Interpret the reliable 4D anomalies considering the well-history data to highlight the associated production-induced effects in the reservoir.

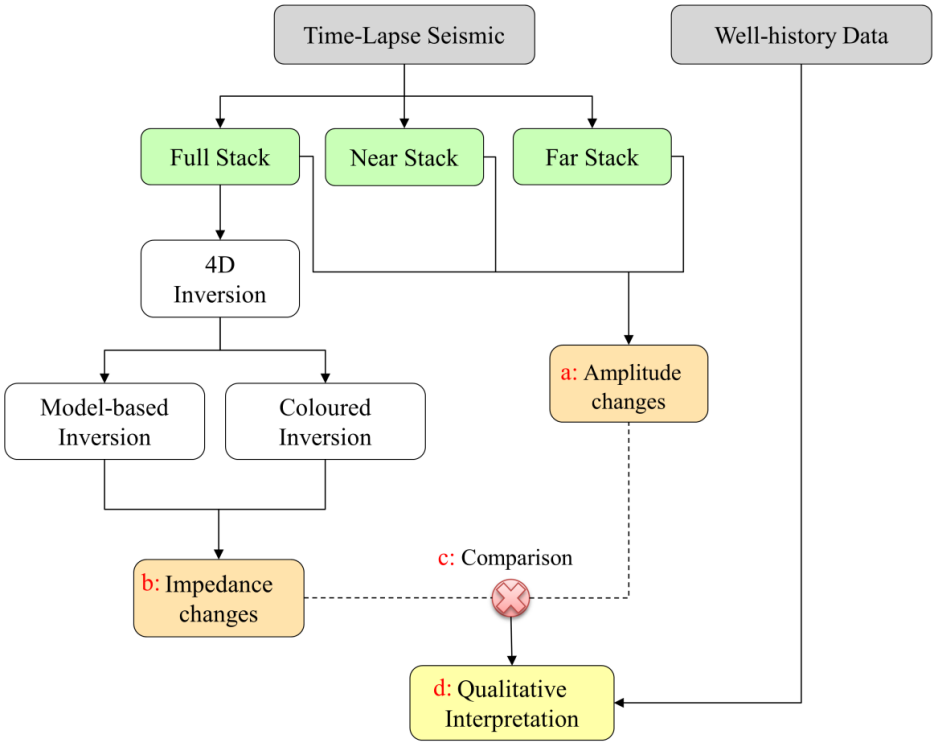

Figure 3.6. Workflow scheme of the 4D seismic interpretation. Following a four-step approach: (a) generate the amplitude changes; (b) estimate the impedance changes; (c) compare the observed 4D anomalies; (d) interpret the reliable 4D anomalies regarding the well-history data.

The 4D model-based inversion approach uses classical post-stack model based inversion algorithm (Russell and Hampson, 1991) but with different initial models for the base and monitor surveys. The method assumes two separate 3D model based inversions and computes the impedance variation by straightforward subtraction of the inverted acoustic impedance. This approach uses a low-frequency impedance starting model by well-logs data as prior for the base survey and P-wave velocity changes between base and

monitor surveys as priors for the monitor survey. Moreover, time-picking of the main reservoir horizons plays a key role in the 4D inversion since the picked horizons act as geological guides to generate the base survey starting model and build the updated low-frequency model for the monitor survey. In fact, interpreted horizons estimate the velocity changes by using the differences between horizon picks on the base and monitor surveys to evaluate the elastic properties that are in accordance with expected production effects (assuming that density is constant) to generate the monitor survey starting model. Herein, we generated the 3D P-impedance, initial model, using the main horizons picked in the base seismic survey (which act as geological markers), nine well-log data (as described in Maleki et al. (2016)) and a low-pass frequency filter that cuts frequencies above 10 Hz. Then, the low-frequency P-impedance model of the base survey was updated using time-shifted horizon information (assuming that density is constant) to generate the initial monitor model. For instance, Figure 3.7 illustrates the difference in the initial models for monitor and baseline surveys through segment C. Green represents negative impedance changes (decreasing impedance from 2001 to 2006) and the ellipses highlight that the most important changes were predominantly around the injectors C-1H and C-2H.

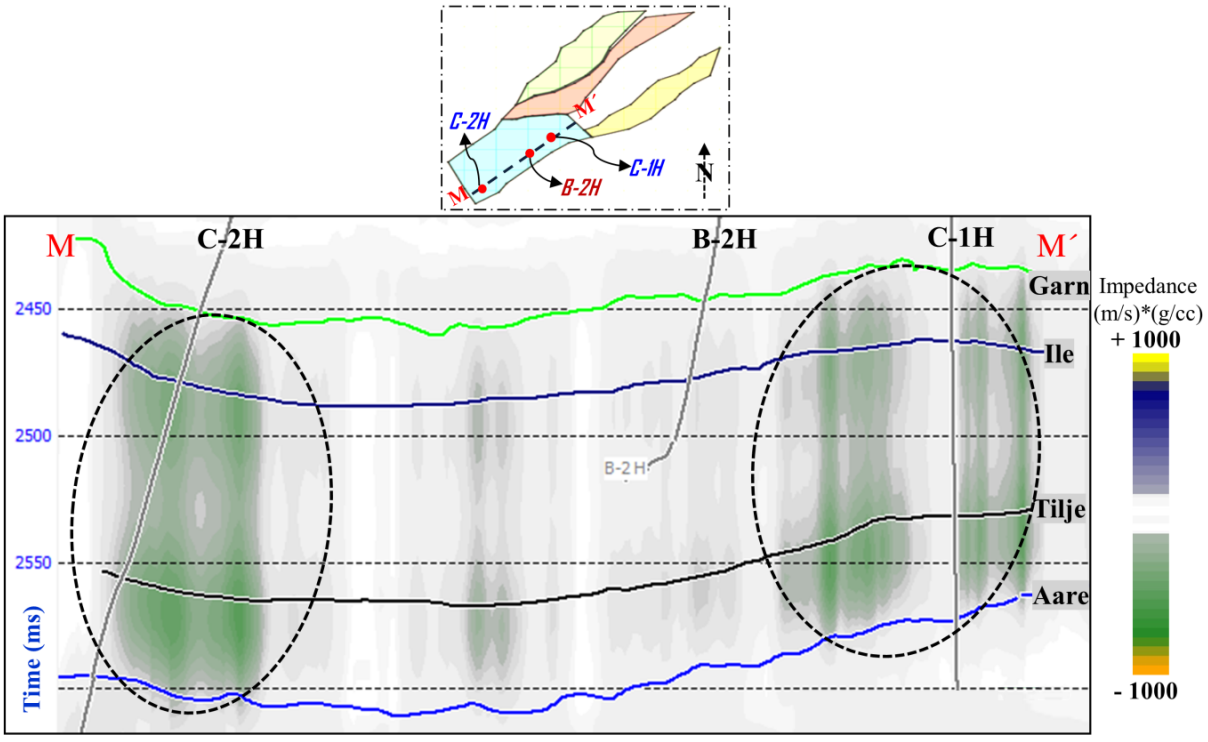

Figure 3.7. A cross-section of differences between the initial models for the base and monitor surveys through segment C showing, in green, negative impedance changes (decreasing impedance from 2001 to 2006) around the injectors C-1H and C-2H in the inserted ellipses.

Coloured inversion creates a smooth inversion operator, which transfers seismic data into a bandlimited acoustic impedance volume and matches the amplitude spectrum of the seismic to that of the acoustic impedance of the wells (Lancaster and Whitcombe, 2000). This approach generates an inversion operator based on the cross plotting of the well-logs data (impedance) versus amplitudes to derive a best-fit line to the data. Thus, coloured inversion is not dependent on the initial guess model compare to the model-based inversion method. However, coloured inversion only gives relative acoustic impedance which does not contain any low frequency components. For the studied case, we generated an inversion operator based on the cross plotting of the nine well-logs (same well logs mentioned for the model-based inversion) versus amplitudes to derive a best-fit line to the data. Alpha factor (slope of the line) was estimated by least-squares curve-fitting for each log over the zone of interest (Figure 3.8a). A general consistency between the wells can be observed, and a representative alpha factor of -0.848 (best-fit line) was chosen for the entire field. Then, coloured inversion operator (a single optimal filter) was constructed using this value of alpha factor in order to convolve this filter with the input seismic data and convert amplitudes into the acoustic impedance volume. Figure 3.8b illustrates the frequency spectrum of coloured inversion operator filter in this case. Furthermore, base and time-aligned monitor surveys were inverted separately as two separate 3D inversions and computed the impedance variation by straightforward subtraction of the derived acoustic impedance results.

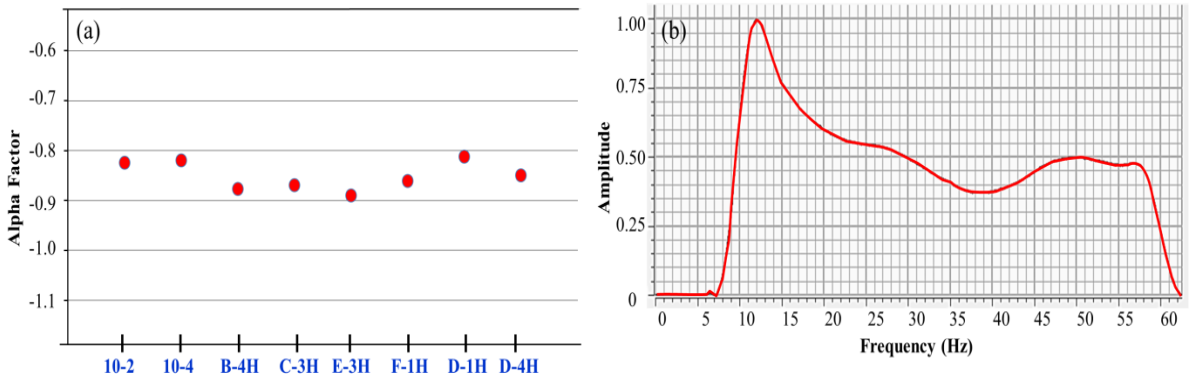

Figure 3.8. (a) Results of fitting curves to each 9 wells (alpha factor). A value of -0.848 was chosen to represent the alpha factor of entire field in this case. (b) Frequency spectrum of coloured inversion operator filter in this case.

3.4. Results and discussion

In the results of amplitude and impedance changes, we observed a wide range of hardening (increase in impedance over time) and softening signals (decrease in impedance over time) in the southern flank of segment C. Figure 3.9 illustrates vertical profiles through the difference volumes of near stack (Figure 3.9b), far stack (Figure 3.9c) full stack (Figure 3.9d), impedance changes of coloured inversion (Figure 3.9e) and impedance changes of model-based inversion (Figure 3.9f), between 2001 and 2006. Location of the profile is given by the broken line in the thumbnail plot and red dots denote well-head positions (Figure 3.9a).

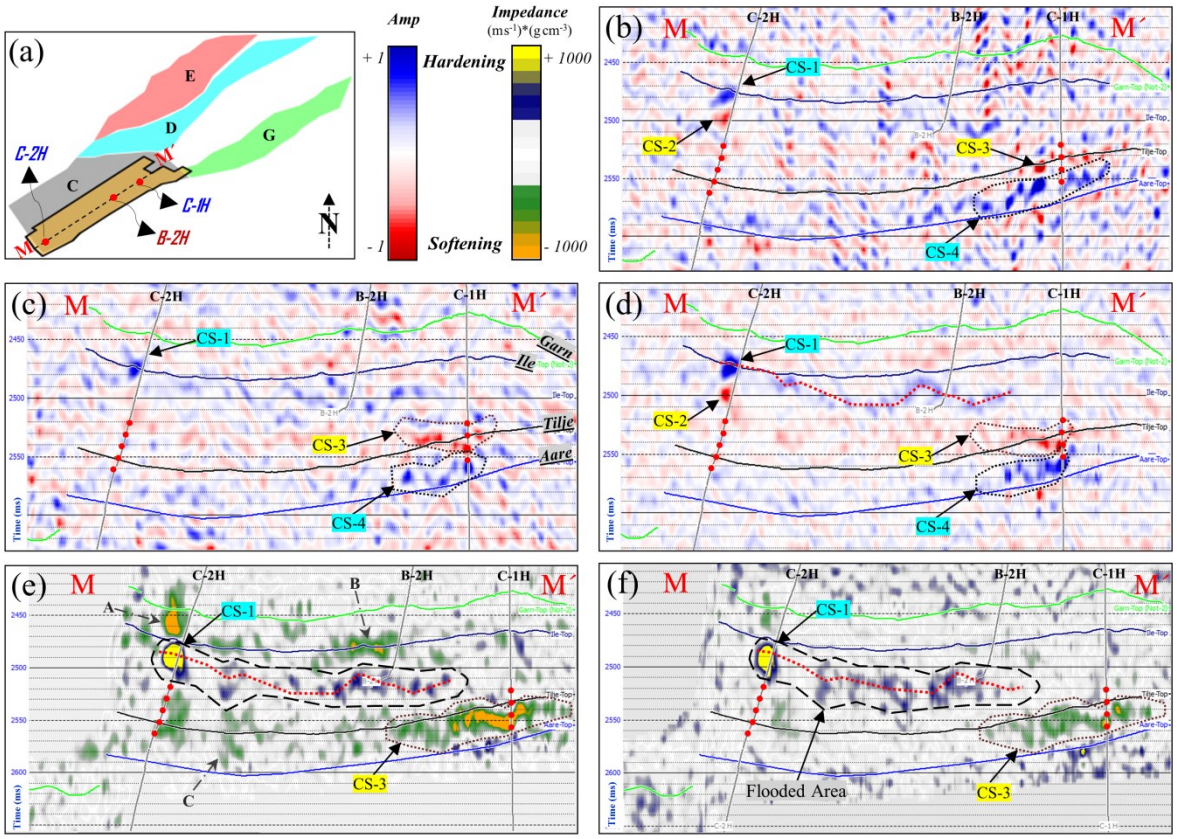

Figure 3.9. (a) Segments of the Norne Field and locations of the southern flank of segment C (marked by orange color). A profile of: (b) difference volume of near stack, (c) difference volume of far stack, (d) difference volume of full stack, (e) 4D coloured seismic inversion results, (f) 4D model-based seismic inversion results. Location of the profile is given by the broken line in the thumbnail plot and red dots denote well-head positions.

We noticed temporal variations in the impedance and amplitude changes throughout the profile (Figure 3.9). Moreover, it seems that the majority of softening and hardening anomalies occurred around the injectors C-2H and C-1H and areas surrounding the

producer B-2H. The response at top of Ile Formation (anomaly CS-1 in Figures 3.9b, 3.9c and 3.9d) highlights a hardening signal around the injector C-2H, which matches the results of 4D inversion (Figures 3.9d and 3.9e). Note that the both inversions presented a very similar hardening anomaly. Additionally, anomaly CS-1 spreads clearly along the injector C-2H to producer B-2H in the difference volume of full stack and results of 4D inversion (marked by the red dotted line in Figures 3.9d, 3.9e and 3.9f). We concluded that anomaly CS-1 might be solely driven by water saturation increases, as well history data showed that well C-2H continuously injected water from 1999 and water reached to well B-2H at the beginning of 2004 (Figure 3.10). The areas between Ile and Tofte formations (detached areas in the 4D inversion results) highlighted the probable flooded zone and water level rose from 2001 to 2006, which is much clearer than the oil water contact barely seen in the full stack data (Figure 3.9d). Alternatively, anomaly CS-1 was more concentrated around the injector C-2H, close to the top of Ile Formation, whereas injector C-2H completions were located in the deeper layers close to the top of Tilje Formation (marked by red color dots).

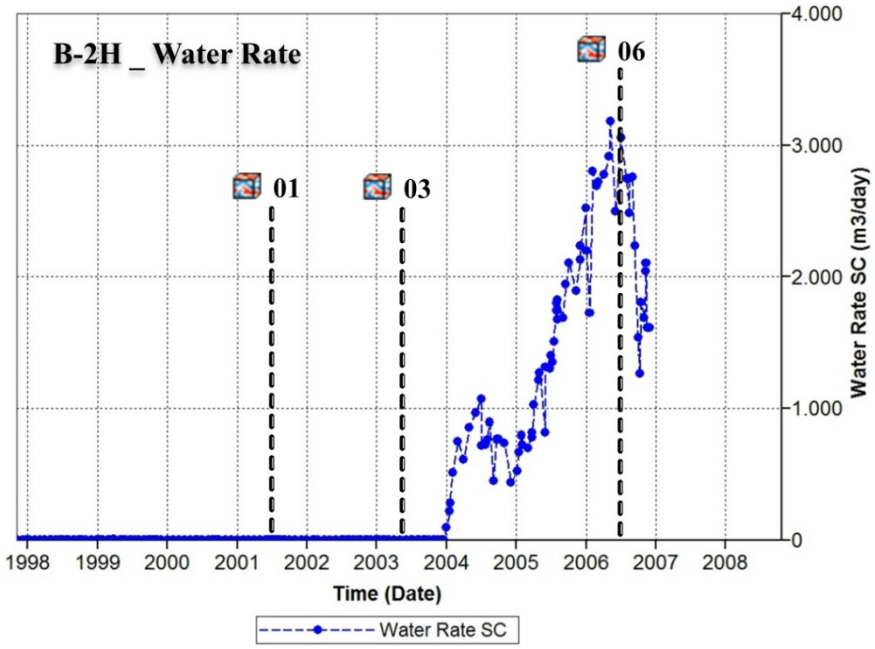

Figure 3.10. Well history data of producer B-2H (produced water rate).

Furthermore, we investigated the monitor seismic survey of 2003 to have more confidence in the interpretation of the anomaly CS-1. We performed two 4D model-based inversions for 2001 to 2003 and 2003 to 2006 in order to precisely monitor the movements

of anomaly CS-1. Figure 3.11 illustrates vertical profiles through the anomaly CS-1 for the impedance changes from 2001 to 2003 (2003 minus 2001) and 2003 to 2006 (2006 minus 2001); ellipse A highlights hardening anomaly in the impedance changes from 2001 to 2003, while ellipse B represents this hardening effect in the impedance changes from 2003 to 2006. It is clear that anomaly CS-1 moved-up around the well C-2H in the western flanks of segment C. Thus, injected water moved along the eastern side of major fault-1 (labelled 1) from the top of Tilje Formation toward the upper layers of Ile Formation. This explains the reason of location of anomaly CS-1 above the perforation of well C-2H for the inversion results of 2001 to 2006 (Figures 3.9e and 3.9f). However, the anomaly is concentrated around injector C-2H, which can be related to the microcracks caused by injection. Notably, it has to be mentioned that water did not reach to the producer B-2H till 2004 (Figure 3.10) which was in agreement with the inversion results (Figure 3.11a).

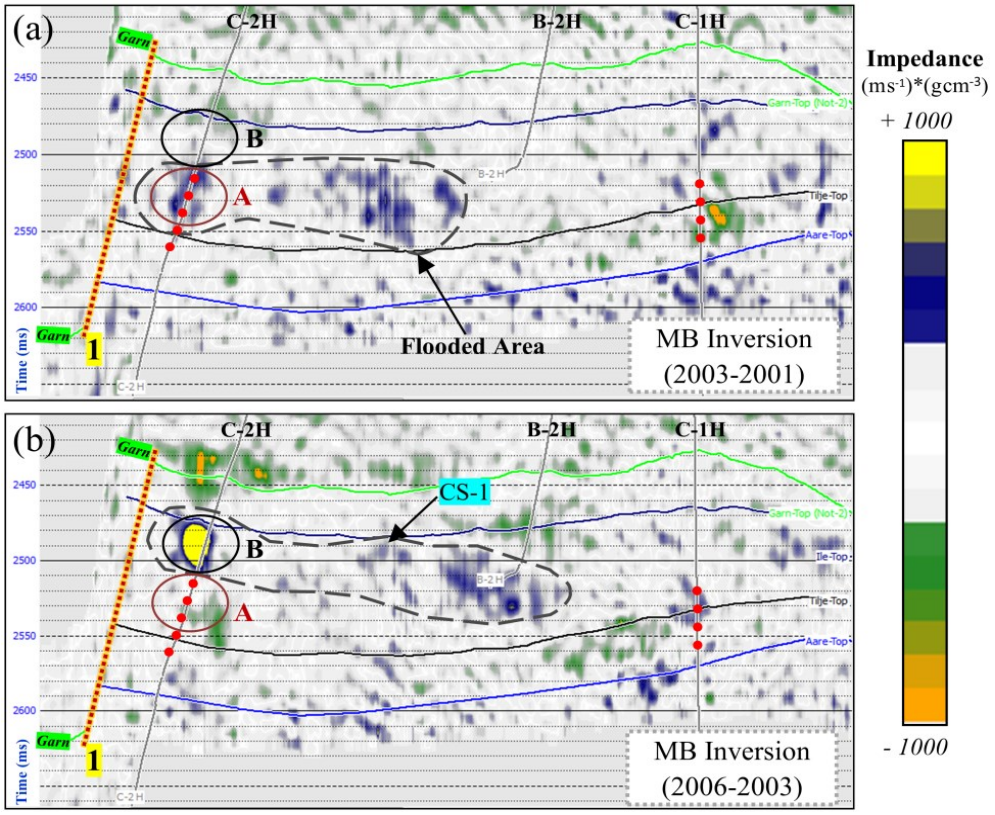

Figure 3.11. A profile of: (a) 4D impedance changes (model-based inversion) between the 2001 and 2003, (b) 4D impedance changes (model-based inversion) between the 2003 and 2006. Red dots denote perforation of wells C-2H and C-1H. Red dots denote perforations of injectors C-2H and C-1H. Ellipse A highlights hardening anomaly in the impedance changes from 2001 to 2003, while ellipse B represents this hardening effect in the impedance changes from 2003 to 2006.

Additionally, difference volumes of near and full stack between 2001 and 2006 showed a softening effect (anomaly CS-2) below the anomaly CS-1 (Figures 3.9b and 3.9d). However, this softening effect was absent in the difference volume of far stack and both 4D inversion results. The possible interpretation is that anomaly CS-2 is a side lobe of strong anomaly of CS-1 that was mitigated by inversion.

Similar to the areas around injector C-2H, the softening and hardening signals (anomaly CS-3 and CS-4) were observed around the injector C-1H at the difference volumes of seismic amplitude (Figures 3.9b, 3.9c and 3.9d). However, anomaly CS-3 was less clear in the near stack compared to the far and full stack. By contrast, anomaly CS-3 was revealed by both 4D inversion results and it looks to be much clear compared to anomaly CS-4 (Figures 3.9e and 3.9f). It highlights that the dubious seen 4D anomaly on the amplitudes may be explained as a softening signal as revealed by 4D inversion results. Furthermore, well C-1H was perforated in Tilje Formation (marked by red color dots) and consequently, we interpreted anomaly CS-3 due to the contribution effect of increased pore pressure and reduced fluid bulk modulus following the injection of gas in C-1H. Moreover, anomaly CS-4 was interpreted as a side-lobe effect of anomaly CS-3 since it is known that this anomaly was located in the aquifer zone (below the Tilje Formation) and 4D inversion mitigated it.

In general point of view, the estimated impedance changes provided more reliable hardening and softening effects compared to the amplitude differences as non-reliable anomalies were mitigated following the 4D inversion. It has to be noted that model-based inversion results presented clearer images of the reliable 4D anomalies compared to the coloured inversion results. For instance, the strong softening signals above anomaly CS-1 and around the Tilje Formation in the 4D colored inversion results (labelled by A, B and C) were considered as spurious signals (Figure 3.9e).

The continuity of the anomalies CS-1 and CS-3 can be seen in the maps (Figure 3.12) that highlights the changes in acoustic impedance between 2001 and 2006 from the 4D model-based inversion. Maps were generated in a window of 10 ms below the top of Ile and Tilje formations (locations of the maps are given by the broken lines in the plots of Figure 3.12). Figure 3.12a illustrates that the water movement is more concentrated in the eastern to center regions of the segment C. Moreover, the hardening signal is stronger

around the C-2H, which is likely to be caused by water movement up to 2006. Figure 3.12b shows the contribution path of pressure increases and fluid bulk modulus reduces that occurred in the deeper layers (below the top of Tilje Formation) around injector C-1H, in which is bounded to the northern part of region.

Eventually, Table 3.1 highlights the type of 4D signals and its agreement with inversion results in order to summarize the time-lapse seismic attributes comparison. It also shows the side-lobes, which has been eliminated by 4D inversion.

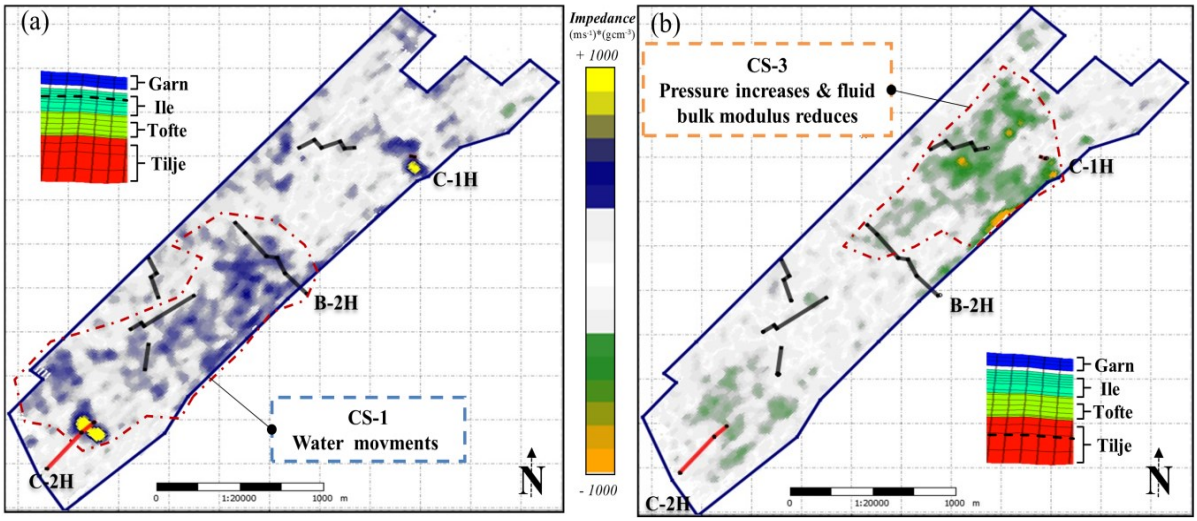

Figure 3.12. 4D impedance maps (model-based inversion) between the 2001 and 2006 through (a) anomaly CS-1, (b) anomaly CS-3. Locations of the maps are given by the broken lines in the plots.

Table 3.1. Description of each set of anomalies.

Anomaly	4D signal	Interpretation	Comparison
CS-1	Hardening	Increase of water saturation	Agreement with 4D inversion results
CS-2	Softening	Side-lobe	Eliminated by 4D inversion
CS-3	Softening	Increase of pressure & reduce of fluid bulk modulus	Agreement with 4D inversion results
CS-4	Hardening	Side-lobe	Eliminated by 4D inversion

3.5. Conclusions

Norne is an unique offshore field with strict 4D seismic interpretation for a case study. To overcome this difficulty, we presented different 4D seismic attributes and compared them to increase the interpretability of anomalies caused by intense production activities in the southern flank of segment C. Primary, difference volumes of amplitude were generated through the subtraction of the base and monitor seismic surveys. Then, we performed two different approach of 4D inversion in order to obtain the impedance variations up to 2006. Most of 4D anomalies were located in the borders of the eastern and western flanks of segment C around the injectors C-1H and C-2H. Moreover, inconsistencies were apparent between the anomalies derived from the 4D inversion and amplitude differences.

We have shown that inversion results improve the vertical resolution rather than the standard amplitude differences, where a better delineation of the water movements and pressure variations are achieved. In fact, 4D inversion mitigated the anomalies that are not caused by production activities and improved the confidence of time-lapse seismic interpretation for southern regions of segment C. However, the challenges are significant and time-lapse pre-stack inversion may improve the interpretation of seismic data by separating fluid effects and pore pressure effects. Additionally, since this is a benchmark case, these results could be integrated with deterministic and probabilistic history matching studies to improve reservoir monitoring and characterization in the Norne Field.

4. ARTICLE-3: *Using simulation and production data to resolve ambiguity in interpreting 4D seismic inverted impedance in the Norne Field*

Masoud Maleki, Alessandra Davolio, Denis José Schiozer

Journal of Petroleum Geoscience, October 2017

https://doi.org/10.1144/petgeo2017-032

The Norne Field started production in 1997 and up to 2006 the field experienced intense production activity, making the Norne benchmark case an ideal candidate to explore the challenges in interpreting complex time-lapse seismic data. Seismic amplitude changes and time-shifts are used as the first level approach to interpret the time-lapse differences and to update reservoir models. A common alternative is to invert the seismic data and obtain acoustic impedance variations caused by production activity, and to evaluate their possible interpretations. For this case study, we use a 4D inversion approach to invert the base (2001) and monitor (2006) seismic surveys in order to provide field-wide insights for the Norne benchmark case. We extensively interpret the observed 4D inversion anomalies and decouple, as much as possible, the effects of fluid and pressure variations, supported by production and reservoir engineering data. Moreover, we compare the inversion results with the simulation model from the Norne benchmark case to suggest areas of future modification to the simulation model. This research is intended as a resource to improve the quality of history matching or other 4D inversion methods applied to the Norne benchmark case, and to demonstrate a detailed time-lapse seismic interpretation within the reservoir segments of the Norne Field.

4.1. Introduction

Time-lapse seismic data have become increasingly important to monitor and manage reservoirs over the last few decades. According to Landrø (2010), there are various applications for 4D seismic surveys but 4D data are mostly used to monitor changes in producing hydrocarbon reservoirs. The objective of time-lapse seismic reservoir analysis is to provide information on the dynamics of fluids and production-induced changes within the reservoir. These dynamic changes can be mapped using seismic attributes such as amplitude differences in envelope and root mean square (RMS). However, estimating these 4D attributes is limited by vertical resolution and requires high-fidelity seismic data. Meanwhile, 3D and 4D seismic inversions have demonstrated their effectiveness and reliability to extract additional information from seismic data. In particular, inversion replaces the seismic signal by a blocky impedance response (Veeken and Da Silva, 2004) that is related to properties of the rock interval rather than to the interface, to which the seismic reflection amplitude responds, thereby facilitating interdisciplinary communication

(Tian et al., 2014). To quantitatively identify those production activities responsible for 4D seismic variations (hardening and softening effects), He and MacBeth (2009) recommended inverting 4D seismic data to the impedance domain. The benefits of 4D inversion on time-lapse seismic monitoring are the increases in vertical resolution (even when dealing with poor datasets) by converting the seismic reflectivity into volumetric impedance data (Tian et al., 2014) and the quantification of 4D effects in terms of P-impedance variations. Moreover, the derived acoustic impedance provides better-resolved information, compared to envelope or RMS amplitudes (Six et al., 2013), which can improve interpretability and, hence, reservoir characterization and management.

Over the past few years, various methodologies to invert time-lapse seismic data have been proposed. The inversion techniques are either deterministic or probabilistic, and can be classified based on their workflows (Tian, 2014). Abubakar et al. (2001), Sarkar et al., (2003) and Calvert (2005) presented 4D inversion as two separate 3D inversions. They inverted the base and monitor surveys separately, and computed the impedance variation by straightforward subtraction of the inverted acoustic impedances. Gluck et al., (2000), Lorenzen (2000) and Lafet et al., (2005) jointly inverted base and monitor surveys using a time-aligned base seismic survey with the subsequent monitor survey. This approach uses a single initial model to invert the base and monitor seismic data to quantitatively estimate representative changes of impedance. Williamson et al., (2007) integrated elements of image warping with impedance inversion to model both time-shifts and amplitude changes when formulating the 4D inversion. In this inversion, the authors assume that production-induced changes in the reservoir primarily affect the P-wave velocity, and cause observable time-shifts and amplitude changes between the monitor and base seismic data. Buland and El Ouair (2006) used the direct inversion of the amplitude differences between the time-aligned base and monitor seismic surveys when obtaining the impedance variations. Tian (2014) coupled the baseline and monitor seismic data in a Bayesian scheme in which the modelling errors are propagated from baseline to monitor to ensure their consistency.

However, while acoustic impedance derived from 4D inversion provides explicit information on changes in pressure and saturation within the reservoir, the impedance changes are saturation–pressure interdependent (Stovas and Landrø, 2005). Hence, identifying the causes of 4D acoustic impedances changes is often a challenge.

Misidentifying the causes may lead to interpretations that fail to reflect actual changes in the reservoir. For instance, a hardening effect (increased acoustic impedance) is expected when reservoir depletion causes pore compaction under increased effective stress. A similar hardening effect is expected during water flooding, when water replaces oil or when gas goes back into solution. Additionally, one of these effects may override all the others and dominate the seismic response (Landrø, 2001). This is a good example of why integrating different data types is important to decouple these competing time-lapse effects and reduce the uncertainties inherent in 4D reservoir seismic interpretation.

This study focuses on analysing and discussing the impedance anomalies derived from 4D inversion and predicted changes in time-lapse impedance for the Norne benchmark dataset. Several studies have analyzed 4D seismic data from the Norne Field: Osdal (2004), El Ouair et al., (2005), Lygren et al., (2005), Osdal et al., (2006), Aarre (2006) and Santos et al., (2016). Osdal et al., (2006) and Huang et al., (2013) also analysed Norne 4D data, giving examples of 4D inversion results in segments E and C. However, this paper discusses the interpretation of 4D acoustic impedances within the entire Norne Field, including all reservoir segments, which has the potential to improve reservoir monitoring and management. Furthermore, as the Norne Field is a publicly available benchmark case study, this detailed 4D acoustic impedance interpretation can provide complementary information to improve future history-matching, and offer a comparison for other 4D seismic inversion methods using the Norne benchmark data.

This paper focuses on interpreting actual reservoir changes from 4D acoustic impedance anomalies in the Norne benchmark dataset. We invert the base (2001) and monitor (2006) seismic surveys to access the time-lapse anomalies (softening and hardening signals). To thoroughly investigate inversion anomalies, we compare selected 4D inversion scenarios against well-history and engineering data to identify anomalies caused by production-related changes and the injected fluids. Furthermore, we analyse these scenarios and compare anomalies with the available flow-simulation model to suggest specific regions of the field where updates to the simulation model might be appropriate. Our study indicates that the combined interpretation of the time-lapse seismic inversion and production activities indicated by engineering data is key to understanding the 4D data within the reservoir segments of the Norne Field.

4.2. Norne Field

The Norne Field is located on a horst block in the Norwegian Sea, between the Vøring and Møre basins (Figure 4.1a). The horst block covers an approximate area of 9 × 3 km, and contains both oil and gas. In the Norne Field, the hydrocarbons are found in sandstone from the Middle and Early Jurassic age, and are subdivided into four different formations from top to base: the Garn and Ile formations of the Fangst Group; and the Tofte and Tilje formations of the Båt Group (Figure 4.1b). Specifically, oil is mainly found in the Ile and Tofte formations, and gas in the Garn (Not-2) Formation (Rwechungura et al., 2010). The porosity ranges between 25 and 30%, and permeability varies from 20 to 2500 mD (Steffensen and Karstadt, 1996; Osdal et al., 2006). Note that the Ile and Garn formations are separated by the shaley non-reservoir Not-1 Formation. The Not-1 Formation is a thin layer but acts as a very effective seal, breaking the communication between the reservoirs above and below it. The top of the heterolithic Aare Formation is the base of the reservoir and the shaley Not-3 Formation acts as a cap rock. More details about Norne stratigraphy can be found in Dalland et al., (1988), Swiecicki et al., (1998) and Correia and Schiozer (2016). The Norne Field is divided into four main fault blocks (Figure 4.2); the Norne main structure (Norne segments C, D and E) and the NE segment (Norne segment G) are contained by major tectonic faults and diagenetic carbonates, which also tend to prevent pressure communication between reservoir segments and impede fluid flow.

4.3. Norne benchmark dataset

The Norne benchmark case is based on a set of real oil-field data organized by the Centre of Integrated Operations in the Petroleum Industry (IO Centre), the Norwegian University of Science and Technology (NTNU) and Norne Field Operations (Statoil, ENI and Petoro). The time-lapse seismic dataset used in this paper includes a 4D-processed, post-stack base seismic survey (2001) and a monitor seismic survey from 2006. The seismic data were acquired using steered-streamer acquisition. The receiver array comprised six streamers with lengths of 3200 m at a depth of 8 m. The source was a single airgun array that operated at 140 bar (2000 psi) with depth of 6 m and shotpoint interval of 25 m. Besides seismic data, the dataset also comprises well logs, production and injection history data up to 2006, and a simulation model. The reservoir-simulation model contains

44 927 active cells (60 × 60 × 8.4 m), and is not seismic history-matched to the production and injection data. By 2001, the field had 26 wells: 17 producers, seven injectors and two exploration wells. Maleki et al., (2016) analysed the impact of well-log constraints, including the number and locations of wells, in 3D post-stack, model-based inversion of the Norne Field base survey from 2001. Their results showed that the number and locations of well logs considered in the 3D inversion are fundamental to the accuracy of the results. A nine-well constrained inversion (with seven deviated wells) gave better results and more robust acoustic impedance interpretation than an inversion constrained by only the two exploration wells. Therefore, in the current study, we constructed the base survey initial impedance model from P-wave sonic and density logs of nine wells (10-2, 10-4, B-4H, C-1H, C-3H, D-1H, D-4H, E-3H and F-1H). Figure 4.2 illustrates the segments of the Norne Field in the top reservoir and the locations of the nine wells.

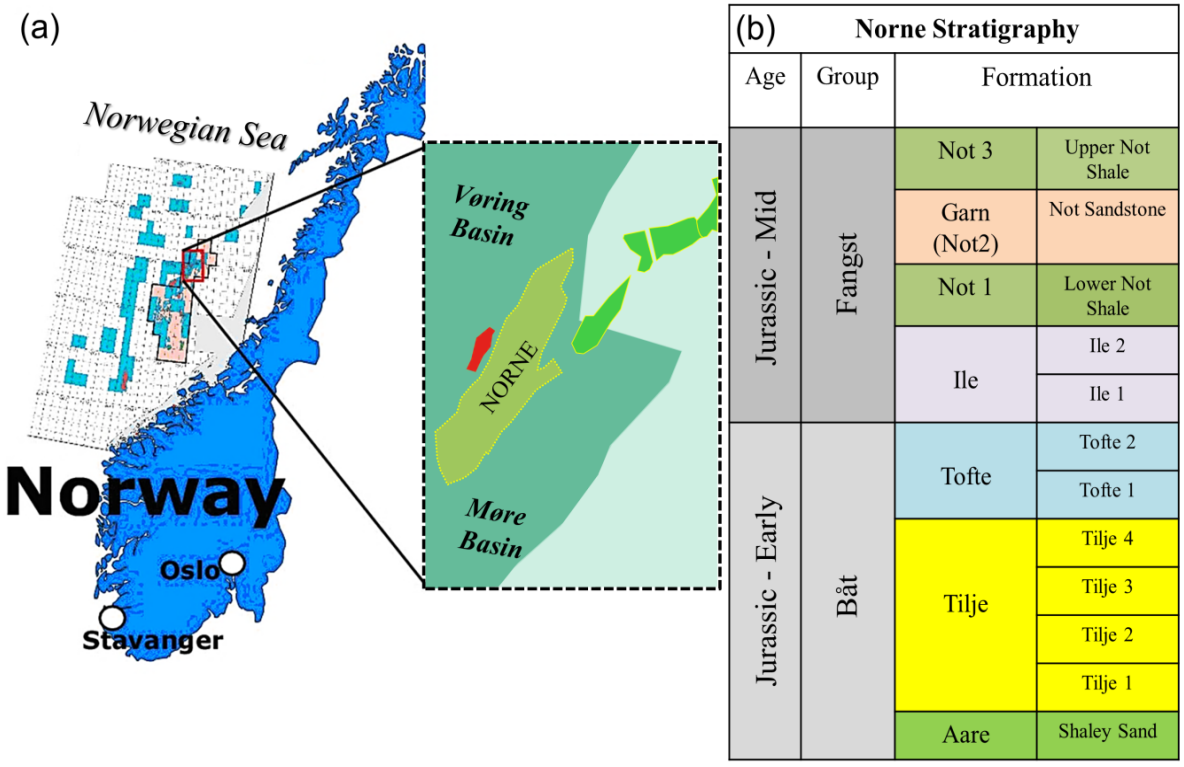

Figure 4.1. (a) Location of the Norne Field in the Norwegian Sea (modified from Huang et al., 2013). (b) Stratigraphy of the Norne Field. Hydrocarbons are mainly found in the Garn, Ile, Tofte and Tilje formations.

Figure 4.2. Segments of the Norne Field in the top reservoir map and locations of the nine wells. Dots denote well-head positions (exploration wells marked by red dots) and black lines represent the locations of the deviated sections. The field is confined by major tectonic faults and compartmentalized by a series of minor faults.

4.4. Time-lapse inversion and interpretation

In this study, the interpretation is divided into two main steps. First, we inverted the Norne base and monitor surveys using a 4D post-stack, model-based inversion from Hampson-Russell software. We then referenced the production activity and engineering data to comprehensively interpret the observed 4D impedance anomalies (softening or hardening signals) to suggest causal factors: pressure changes, fluid variations or changes unrelated to production activity.

The 4D inversion uses a post-stack, model-based inversion algorithm but with different initial models for each vintage. The method applies two separate 3D model-based inversions and computes the impedance change by straightforward subtraction of the inverted acoustic impedance volumes. Model-based inversion is based on the 1D time-

domain convolutional model which progressively updates the model until the resulting derived synthetic matches the stacked seismic trace (Russell and Hampson, 1991). This method iteratively solves for the reflectivity by estimating the differences between the real seismic trace and a synthetic formed from the model, and modifies the model to minimize the difference. However, seismic data are band-limited and inversion is dependent on the starting model to provide added low-frequency data that are below the bandwidth of the seismic data. This approach uses a low-frequency impedance starting model from well-log data as a prior for the base survey, and P-wave velocity changes between base and monitor surveys as priors for the monitor survey. The velocity changes derive from the sought variations in rock properties that cause time-shift observations estimated by differencing horizon picks on the base and monitor surveys. These time-shifts are used to update the initial P-impedance model by creating a series of scalars that are, in effect, low-frequency signals caused by production-induced changes in the reservoir. Outside the reservoir, the initial model of the monitor seismic survey remains the same as for the base seismic survey; while inside the reservoir, the monitor survey model is updated according to the time-shifts. Thus, the input data of the 4D inversion are base and monitor seismic traces, time-aligned monitor seismic traces, effective source wavelets, well-log data before the base vintage (including P-wave sonic and density logs), and horizon time-shifts. The output results are 3D impedance models for each vintage. The summarized workflow for the 4D model-based inversion (Figure 4.3) follows:

- (a) Volumetric interpretation by picking the main reservoir horizons in the base survey.
- (b) Create the 3D P-impedance, time-domain starting model, using the main horizons picked in the base seismic survey (which act as geological markers), well-log data (from the previously mentioned nine wells) and a low-pass frequency filter that cuts frequencies above 10 Hz.
- (c) Re-pick the main horizons in the monitor survey (without time-shift corrections) to capture the sought production-induced velocity changes in the reservoir.

- (d) Update the low-frequency P-impedance model of the base survey (using velocity changes from step (c) and assuming that density is constant) to generate the monitor survey starting model.
- (e) Analyse inversion parameters, and apply model-based inversion to the base and time-aligned monitor surveys to produce inverted base and time-aligned monitor impedance volumes.

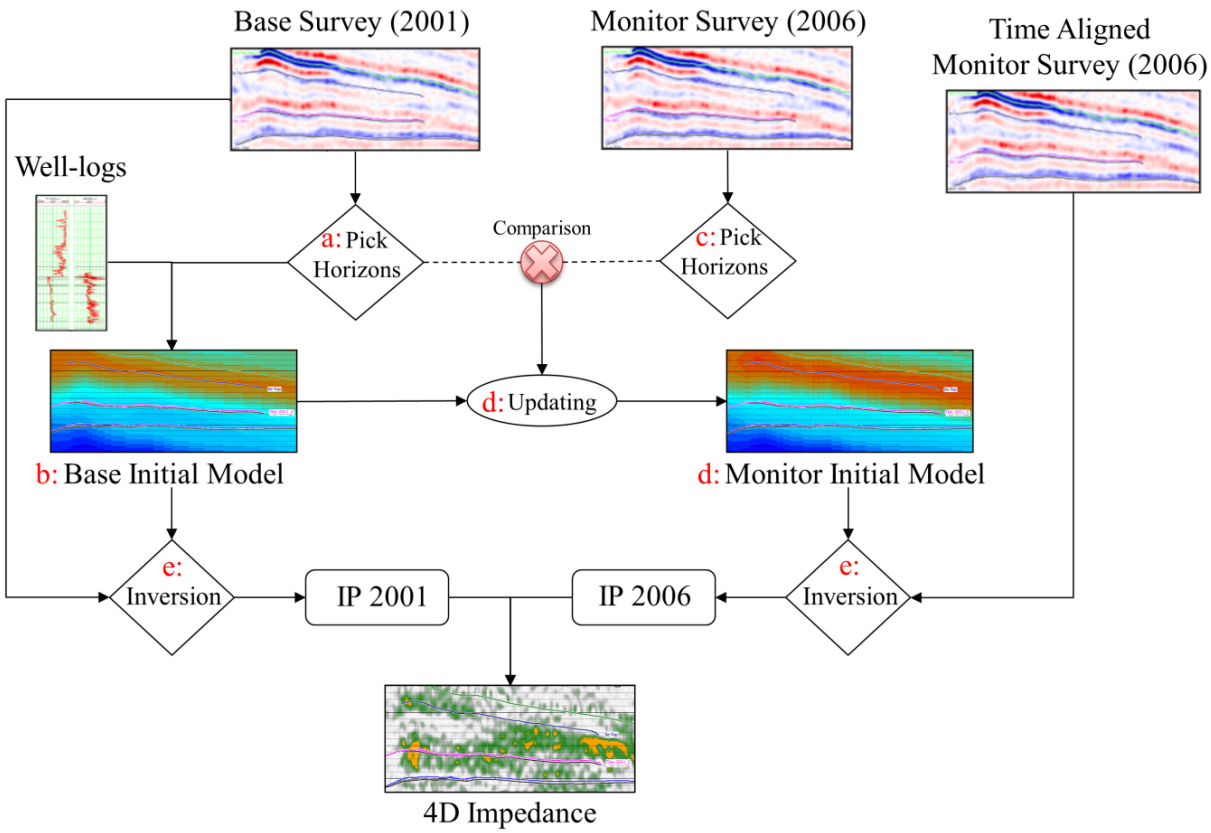

Figure 4.3. Workflow scheme of the 4D seismic inversion. Following a five-step approach: (a) pick the main horizons in the base survey; (b) create the 3D P-impedance, time-domain starting model, using the well-log data, base horizons and a low-pass filter; (c) re-pick horizons in the monitor survey (without time-shift corrections); (d) update the low-frequency P-impedance model of the base survey to generate the monitor starting model; and (e) analyse inversion parameters and run the 4D inversion.

Time-picking of the main reservoir horizons plays a key role in the 4D inversion since the picked horizons act as geological guides to generate the base survey starting model and build the updated low-frequency model for the monitor survey. The main horizons of the Norne Field (the top of the Garn, Ile, Tilje and Aare formations) were picked in the baseline survey. Additionally, two of these horizons (top of the Tilje and Aare formations) were re-picked in the uncorrected monitor survey to estimate the time-shift

signal that is assumed to result from production effects. The Garn Formation defines the top of the Norne reservoir and the Aare Formation the base of the Norne reservoir. Also note that in this 4D inversion approach, the time-shifts need to be allocated to different horizons within the reservoir interval (for thick reservoir zones), because the production activity does not change velocity uniformly from the top to the bottom of the reservoir. This is particularly applicable in the Norne reservoir as some zones present a hydrocarbon column of 140 m (e.g. segment C, and the southern regions of the segments E and D). For example, as shown in Figure 4.4, following exhaustive re-picking of the Tilje and Aare formations (in-line and cross-line increments of one trace), we estimated 2 and 4 ms time-shifts, respectively, by straightforward subtraction of the monitor and base picked horizons on the western side of section. In fact, re-picking the tops of the Tilje and Aare formations localized the zone where the known production was expected to produce a time-shift signal, while a single interpreted horizon (top of the Aare Formation) could have led to an unreliable 4D inversion, which might not accurately represent the reservoir changes by smearing the response.

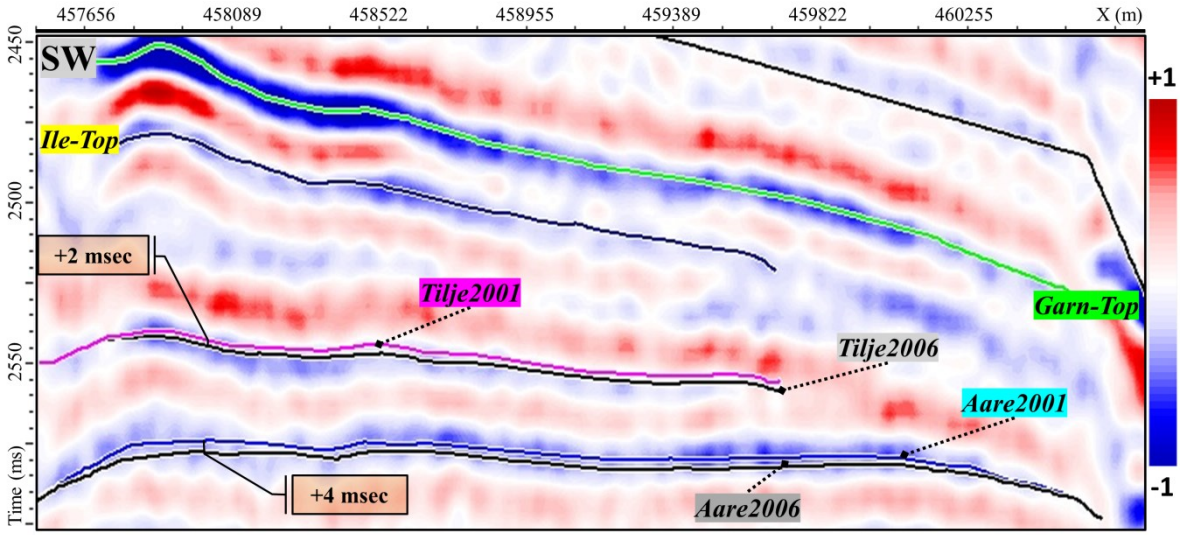

Figure 4.4. SW–NE section through the monitor seismic survey (2006). The Garn Formation represents the top of Norne reservoir and Aare Formation is the base. The time shift between the Tilje Formation in 2006 and 2001 is +2 ms in the west section, and +4 ms for the Aare Formation 2006 and 2001.

After a satisfactory volumetric interpretation and re-picking the monitor survey horizons, we generated the starting models as the next step of the 4D inversion. First, the 3D initial base model was built by interpolating the acoustic impedance from time-

converted logs in the nine wells over the 2001 base seismic survey and applying a 10 Hz low-pass frequency filter, as described in Maleki et al., (2016). Then the initial monitor model was constructed based on the time-shifted horizon information and the initial base model properties. The differences between horizon picks on the base and monitor surveys generate a series of scalars, or multipliers, to approximate the impedance changes, and are applied to the interval impedance values from the baseline starting model to provide the low-frequency monitor starting model. Figure 4.5 illustrates the difference in the initial monitor and base acoustic impedance models through segment E. Green represents negative impedance changes (decreasing impedance from 2001 to 2006) and the ellipses highlight that the most important changes were predominantly below the top of Ile Formation.

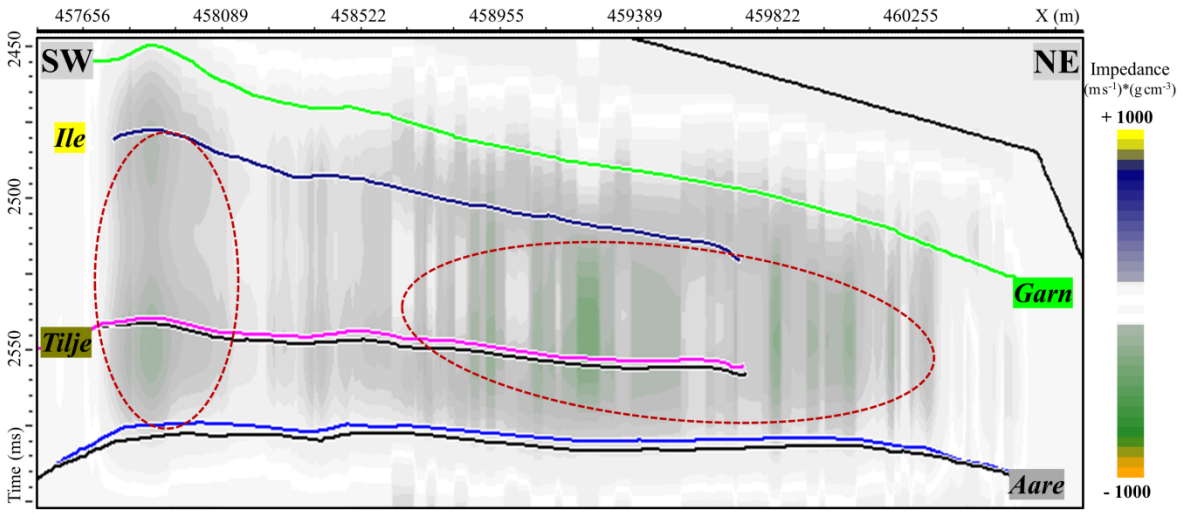

Figure 4.5. A cross-section of differences between the initial models for the base and monitor surveys through segment E showing, in green, negative impedance changes (decreasing impedance from 2001 to 2006) below the top of the Ile Formation in the inserted ellipses.

In the fifth and final step of the inversion, we tested and selected the inversion parameters. In this study, after testing different inversion parameters – such as the type of constraint (to set the maximum allowable deviations in impedance from the initial model), several block sizes (2–4 ms), the pre-whitening percentage (1–5%) and the number of iterations (10–90) – we selected the parameters of hard constraint (with 80% allowable deviations in impedance), an average block size of 2 ms, pre-whitening of 1%, a maximum number of iterations of 60 and a zero-phase wavelet of 200 ms length (derived statistically from the data around the reservoir) to apply the 4D inversion to the entire seismic surveys and generate the impedance volumes for each vintage.

Using the 4D inversion results, we analysed the entire inverted volume (including impedance difference maps and cross-sections) to identify the 4D seismic impedance anomalies from 2001 to 2006 (hardening and softening effects). Next, we checked all the observed 4D impedance anomalies for consistency with the production activities, including well-history data. Finally, we compared the interpreted anomalies with the available simulation model, evaluating the similarities.

4.5. Results and discussion

In the 4D seismic inversion results, we observed a wide range of anomalies that we interpret as being caused by the intensive production-injection activity from 2001 to 2006 in the reservoir segments. Figure 4.6 maps the normalized root mean square (NRMS) of the 4D inversion results, illustrating the P-impedance variations; the higher the NRMS, the greater the difference in impedance between the base and monitor surveys. The NRMS was computed in a window covering the entire reservoir (the regions bounded by the top of the Garn and Aare formations) between 2001 and 2006. The observed NRMS indicated that the acoustic impedance variations were distinct to each segment. We therefore decided to assess the reservoir segments separately and interpret the 4D inversion anomalies for all the reservoir segments. Starting from the top left, we follow the segments (E, D, C and G) to the bottom right.

4.5.1. Segment E

Segment E is located in the NW region of the Norne Field, with minor and major faults displacing most formations. The water injectors F-1H and F-3H were drilled in 1999, aimed at giving pressure support to the neighbouring producers within the Ile, Tofte and Tilje formations. We noticed temporal variations of impedance throughout the entire segment, and after generating maps at different depths (Figure 4.7) we observed that anomalies were concentrated around the injectors. Changes in acoustic impedance from the 4D inversion results are shown in Figure 4.7a for below the top of the Ile Formation and Figure 4.7b for around the top of the deeper Tilje Formation. Close examination reveals that most P-impedance reductions occurred around the injectors F-1H and F-3H (anomalies SE-1 and SE-2), while impedance increased slightly in areas surrounding the southern flank of segment E above the top of the Tilje Formation (anomaly SE-4). Figure 4.7a suggests

three sub-zones (zones A, B and C) in segment E below the Ile Formation, in which the effects on 4D inversion caused by injector wells in sub-areas A and C were more pronounced than sub-area B.

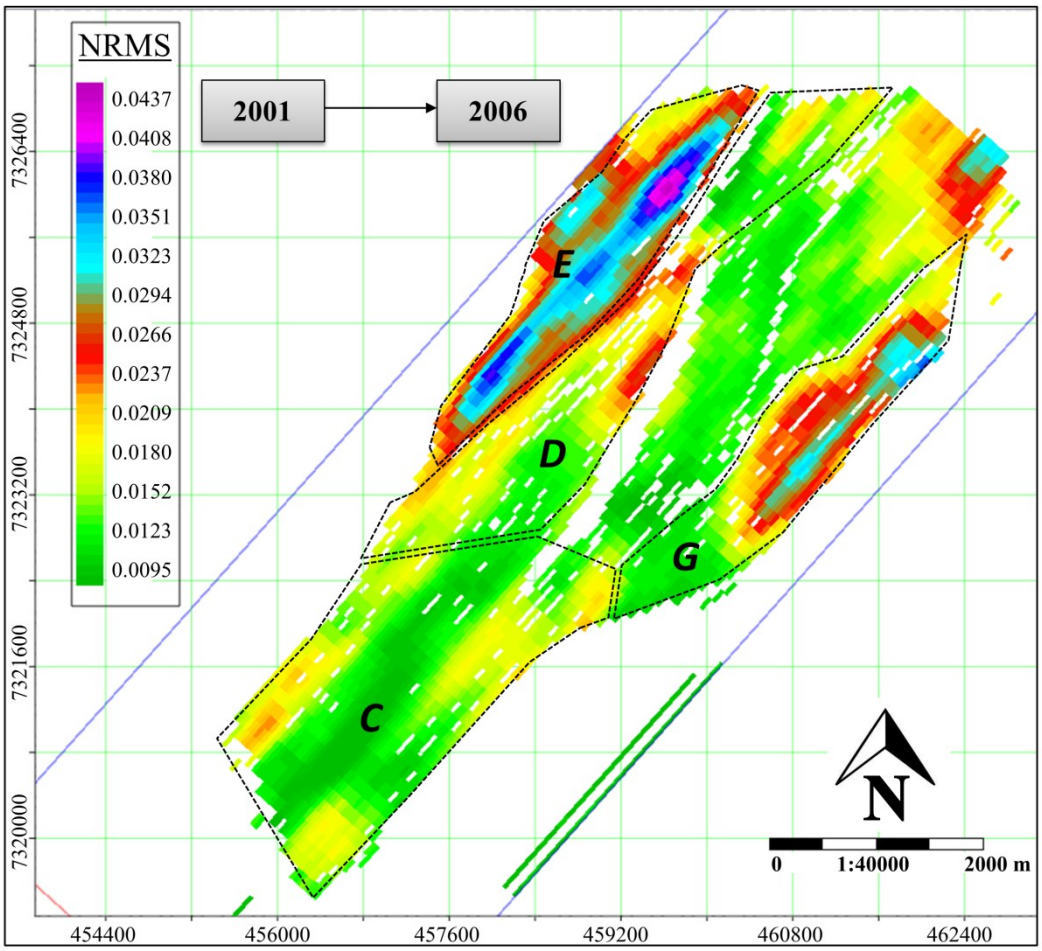

Figure 4.6. Normalized RMS map of 4D inverted impedance differences over the Norne reservoir interval between the 2001 base and 2006 monitor surveys (scale is 0.09–4.37%).

Figure 4.8a illustrates a 2006 – 2001 impedance difference section through injectors F-1H and F-3H. Herein, the decrease in acoustic impedance over time (in orange) indicates a strong softening signal below the top of the Ile Formation (anomaly SE-1) and through the top of the Tilje Formation (anomaly SE-2). The anomalies, SE-1 and SE-2, appear concentrated around the injectors, and are likely to result from increased pore pressure. Increased pore pressure weakens the pressurized rock framework and reduces the P-wave velocity, consequently decreasing acoustic impedance (Johnston, 2013). The decreased acoustic impedance suggests that pressure effects overrode the saturation effects on the

acoustic impedance variations around the water injectors F-1H and F-3H. This is because a pore-pressure increase can reduce the matrix bulk modulus and velocity more than an increase in water saturation increases fluid velocity (Johnston, 2013). The increases in pore pressure appear detectable and well pronounced. Meanwhile, simulated pore-pressure changes (Figure 4.8b) correlate nicely with anomaly SE-2 as the pore pressure also increased in the southern region of segment E around injector F-3H.

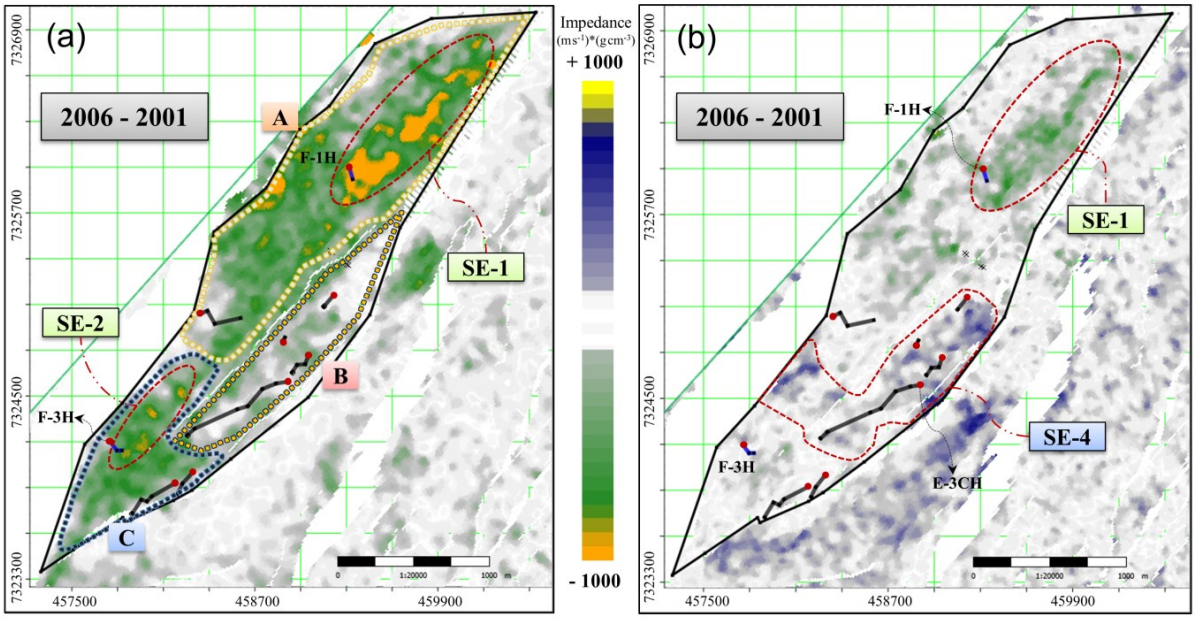

Figure 4.7. 4D acoustic impedance maps between the 2001 and 2006 surveys for (a) below the top of the Ile Formation and (b) above the top of the Tilje Formation. Black lines represent the locations of the deviated producer wells, while dark blue lines represent the locations of the deviated injector wells; red dots denote well-head positions. Regions in orange and green delineate areas with decreased impedance from 2001 to 2006. (a) Highlights the three subzones in segment E (A, B and C), and the pronounced impact on 4D seismic data caused by injectors F-1H and F-3H.

In contrast, we observed an inconsistency between the P-impedance variation and simulated pore-pressure changes in the northern region of segment E (anomaly SE-1). The results of the 4D inversion implied a strong decrease in impedance, as in the southern flank, while the simulation model showed a minor increase in the pore pressure compared to the increased pore pressure around the F-3H injector. The actual pressure values from the simulation model for anomaly SE-1 increased from c. 260 bar (2001) to 275 bar (2006) and the velocity sensitivity to this pressure change is small, as shown in Osdal et al., (2006). This suggests that the simulation model should be reconsidered, particularly in the southern flank.

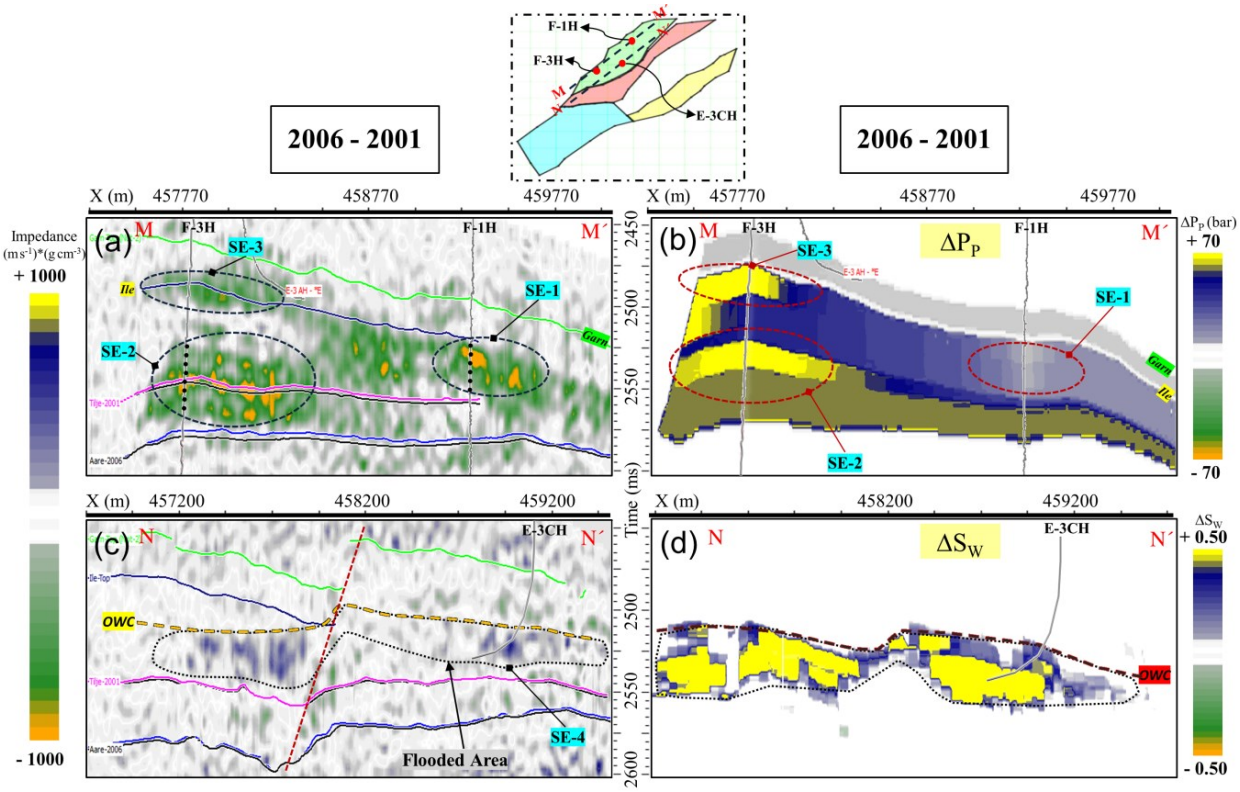

Figure 4.8. Profiles of the inverted impedance difference and simulation model for segment E. Locations of the profiles are given by the broken lines in the thumbnail plot, and red dots denote well-head positions. (a) Cross-section of the inverted impedance difference around injectors F-3H and F-1H (black dots denote completion of injectors). Anomalies SE-1, SE-2 and SE-3 highlight regions where softening (decrease in impedance) is most evident. (b) Crosssection of the simulation model showing pore-pressure changes around injectors F-3H and F-1H. (c) Cross-section of the inverted impedance difference in the southern flank of segment E. The black dotted region shows the location of the hardening signal (increase in impedance) and probable water flooding. (d) A cross-section of the simulation model showing water-saturation changes in the southern flank of segment E. Note the good correlation between the increase in water saturation and the detached region of (c).

Moreover, we observed a strong increase in pressure below the top of the Ile Formation (anomaly SE-3) on the simulation model (Figure 4.8b), which was less strongly seen on the 4D inversion compared to anomaly SE-2 (Fig. 8a). The possible explanation is that as the pressure estimated by the simulation model increased from c. 230 to 300 bar for anomaly SE-3 and from 280 to 350 bar for anomaly SE-2 (from 2001 to 2006), anomaly SE-3 experienced a weaker reduction in velocity compared to anomaly SE-1 according to the relationship between pressure and velocity in the Norne Field that is described in Osdal et al., (2006). Also, the 4D impedance anomaly extends above the top of the Ile Formation, while the simulation shows the anomaly to be confined below the top of the Ile Formation. Thus, the sealing layer seems to be a less complete pressure barrier for this region.

Concerning the SE-4 anomaly, in Figure 4.8c, we observe a hardening effect (an increase in acoustic impedance over time) between the Ile and Tofte formations (the areal extent of this anomaly can be seen in Fig. 4.7b). Well-history data for producer E-3CH indicates that this well had produced a substantial amount of water since 2005 and it is likely that anomaly SE-4 is caused by increased water saturation. These observations indicate that the areas between the Ile and Tofte formations were partially water flooded, and we interpreted the oil–water contact (OWC) (represented by the yellow dashed horizon in Figure 4.8c) uniformly below the top of the Ile Formation. The impedance anomaly SE-4 broadly matches the simulated water-saturation change (Figure 4.8d), although there are some differences in detail.

4.5.2. Segment D

Segment D is located in the NW region of the Norne Field and is separated from segment E by a major fault, sealing this area. The water injector F-2H, drilled in 1999, was completed in the Ile and Tofte formations to provide pressure for the producers in the entire segment D. As with segment E, we observed variations in impedance throughout the entire segment. Figure 4.9a maps acoustic impedance changes, from the 4D inversion, below the top of the Ile Formation and Figure 4.9b shows these changes at the bottom of the Ile Formation. Similar to segment E, P-impedance decreased around the injector well by 2006. Anomaly SD-1 (Figure 4.9a) is localized at the centre of the segment, and major faults (labelled 1 and 3) apparently prevented this anomaly from spreading beyond the eastern and western flanks of segment D. In deeper layers, segment D displays increased acoustic impedance (Figure 4. 9b) in the SW and SE regions. In addition, the well-history data for producers E-1H and B-3H showed significant increases in water production from 2002 to 2006. Thus, anomaly SD-2 may be caused by water movement, which has raised the OWC up to 2006.

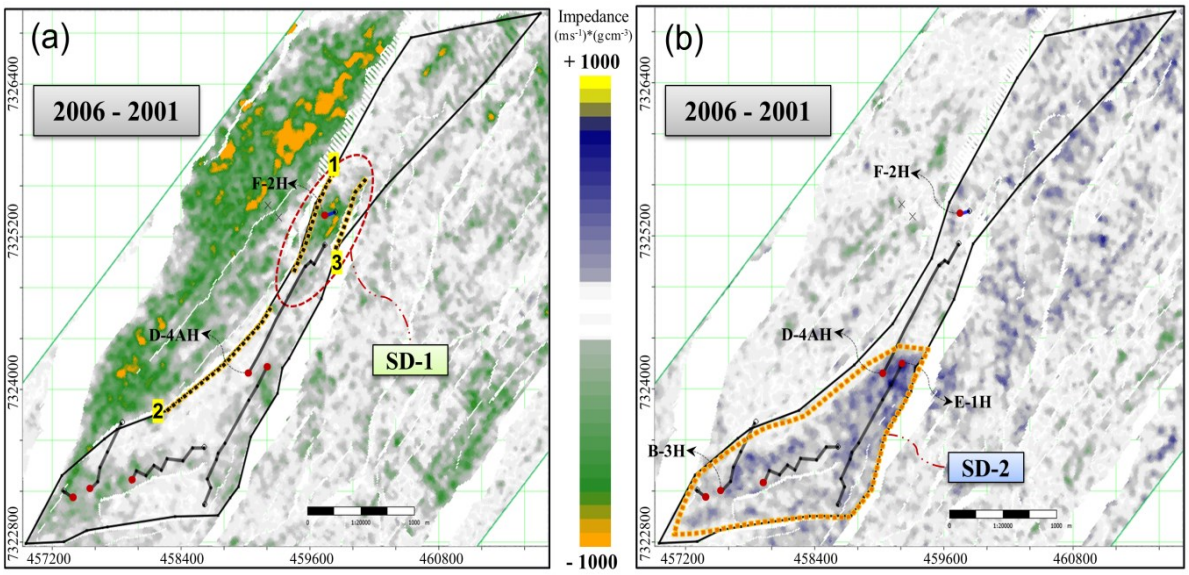

Figure 4.9. 4D acoustic impedance maps between the 2001 and 2006 surveys for (a) below the top of the Ile formation and (b) the bottom of the Ile Formation. Black lines represent the locations of the deviated producer wells, while dark blue lines represent the locations of the deviated injector wells; red dots denote well-head positions. Anomaly SD-1 delineates regions around the F-2H injector between the major faults (black dotted lines), while anomaly SD-2 shows the hardening signal (increase in impedance) in the SW and SE regions of segment D.

Figure 4.10a shows acoustic impedance changes around injector F-2H. At this location, anomaly SD-1 is a softening signal below the top of the Ile Formation. This suggests that the effect of the increased pore pressure dominates the effect of water replacing oil around injector F-2H. The simulated pore-pressure change (Figure 4.10b) is consistent with the observed 4D anomaly as the pore pressure increases more around the injector than in the rest of the section. Producing wells E-1H and B-3H, drilled between the Ile and Tilje formations, have high water cuts indicating that ellipses A and C (Figure 4.10a) represent zones of water replacing oil, with the main western fault (fault-2) offsetting the zones of water movement. In addition, fault 2 acted as a possible pressure barrier. Figure 4.10a supports this, as fault-2 is located in the transition region between the hardening and the softening anomalies (marked by ellipses A and B). However, there is no lateral change in simulated pore pressure around fault-2 (Figure 4.10b), highlighting an area where the simulation model may be reconsidered for this region. Similar to segment E, a strong hardening effect (anomaly SD-2 in Figure 4.10c) was observed in the deeper zone between the Ile and Tilje formations, and reflects the increase in water saturation and reduction in pore pressure near the producer (at well E-1H). It is likely that the regions

between the Ile and Tofte formations were partially flooded with water, and we identified the OWC below the top of the Ile Formation. Nevertheless, simulated water-saturation changes show an increase in water saturation in the deeper zone between the Ile and Tilje formations (Figure 4.10d), matching the inversion results.

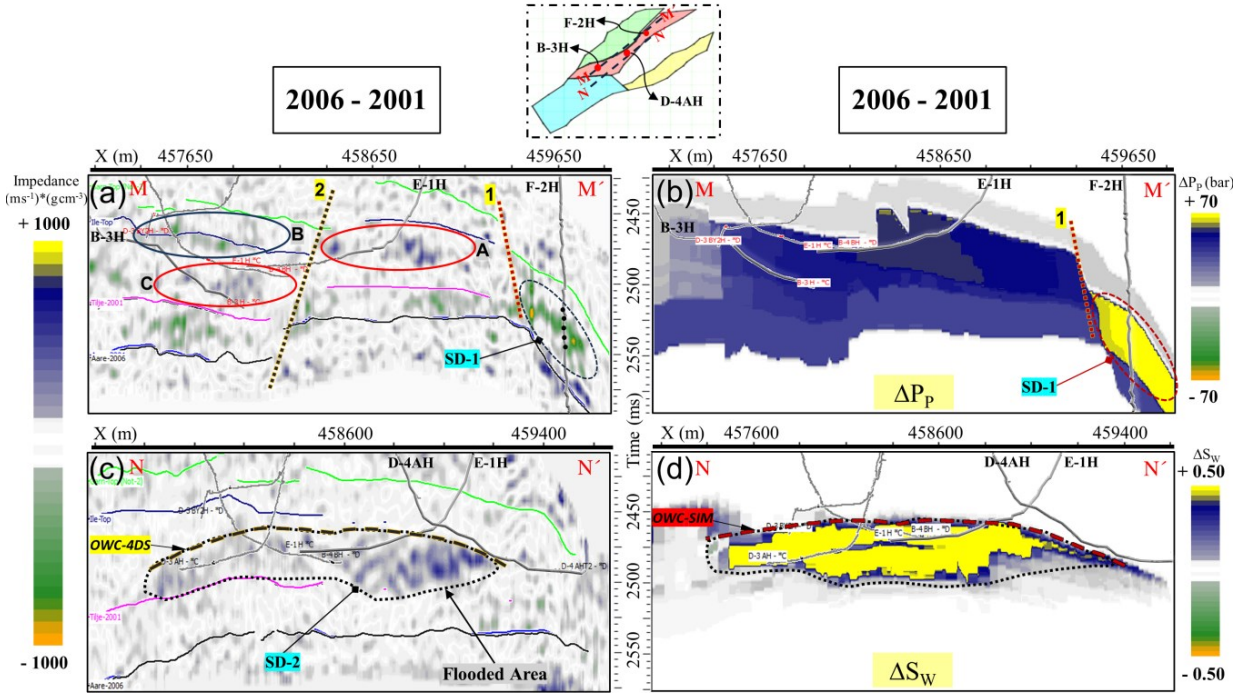

Figure 4.10. Profiles of the inverted impedance difference and simulation model for segment D. Locations of the profiles are given by the broken lines in the thumbnail plot, and red dots denote well-head positions. (a) A cross-section of the inverted impedance difference showing decreased impedance around injector F-2H (black dots denote the completion of F-2H). (b) A cross-section of the simulation model showing increased pore pressure around injector F-2H. (c) A cross-section of the inverted impedance difference in the southern flank of segment D. The black dotted region shows the location of the hardening signal and the potentially water-flooded area. (d) A cross-section of the simulation model showing the water-saturation changes in the southern flank of segment D.

Notably, the simulation model for well D-4AH produced far less water than the flow rates recorded by the well-history data between July 2003 and January 2006 (Figure 4.11). It strongly suggests that water reached the producer D-4AH. A possible explanation may be that, as the completions of well D-4AH are located in the Garn Formation, injected water from F-2H reached this zone. However, interpreting an increase in water saturation based on the inversion results for this region might need some care due to the thinning of the reservoir interval between top of the Garn and Ile formations to the north affecting seismic amplitudes.

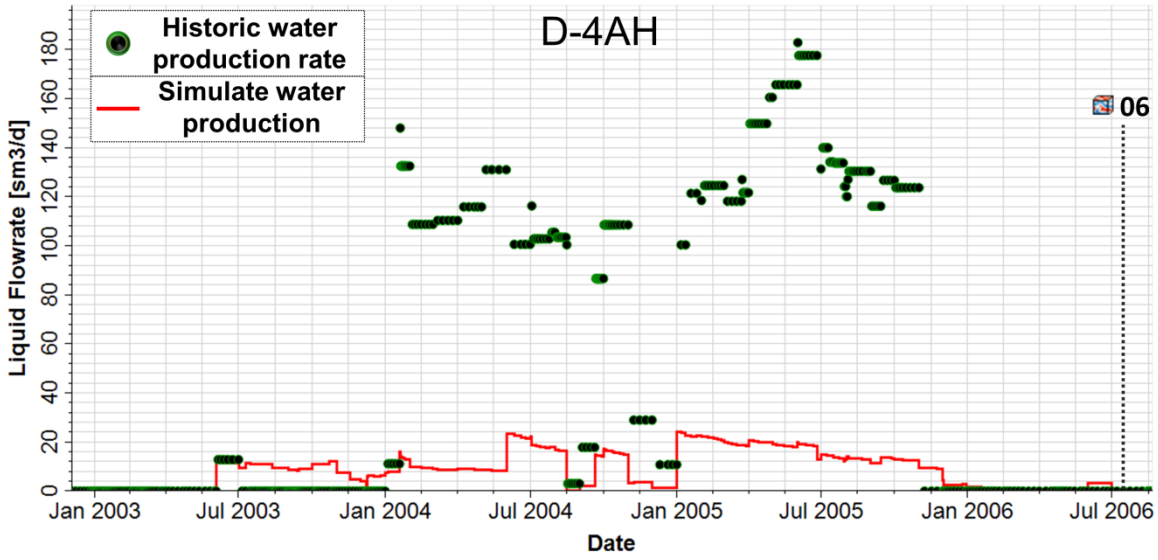

Figure 4.11. Water rate for well D-4AH. Green points are the history data and the red line shows the simulation results.

4.5.3. Segment C

Segment C is located in the southern region of Norne Field, and contains four injector wells: C-1H, C-3H and C-4AH (water and gas), and C-2H (water). These injector wells were perforated before 1999, except well C-4AH, which started injecting in January 2004 to increase pressure for neighbouring producers and to enhance the oil sweep across the Ile Formation. Here, we observe variation in impedance mainly in the eastern region of segment. Figure 4.12a maps acoustic impedance differences below the top of the Garn Formation and Figure 4.12b maps these below the top of the Ile Formation. The areas surrounding the producer wells showed slight changes in impedance, while greater differences in impedance were observed around the injector wells (anomalies SC-1, SC-2 and SC-3).

Anomalies SC-1, SC-2 and SC-3 are mainly located in the eastern region of segment C (marked by red dotted ellipses in Figure 4.12), and we therefore focused on interpreting anomalies around the injector wells C-2H, C-4AH and C-1H. Figure 4.13a illustrates the acoustic impedance changes around injector C-2H. Anomaly SC-1 is an increase in impedance, indicating strong hardening of the signal across the Ile Formation. Since the hardening signal is concentrated around the well location and C-2H injected water from 1999 until 2006, anomaly SC-1 might be solely driven by water-saturation increases and not a pressure-related anomaly. Injected water (higher density) replaces

produced oil (lower density) and increases the P-impedance (Johnston, 2013) but, as seen above, a pore-pressure driven reduction in rock-frame modulus can dominate the impedance change. Furthermore, well B-2H started producing significantly more water after January 2004, highlighting that the detached area was partially flooded and the OWC rose to the upper part of the Ile Formation (see Figure 4.13a). Comparing the SC-1 anomaly with the simulated model, we note that the simulated pore pressure below the top of the Ile Formation remained almost constant (Figure 4.13b). Meanwhile, the water saturation in this region increased significantly from 2001 to 2006 (Figure 4.13c). However, the simulated water saturation spreads along the Ile Formation, and is not concentrated around injector C-2H and producer B-2H, as in Figure 4.13a. We also note that injector C-2H completions were located in deeper layers, below the SC-1 seismic anomaly. We conclude that further investigation in this zone are necessary to better interpret the 4D seismic signal, especially at SC-1, and improve matching with the simulation model.

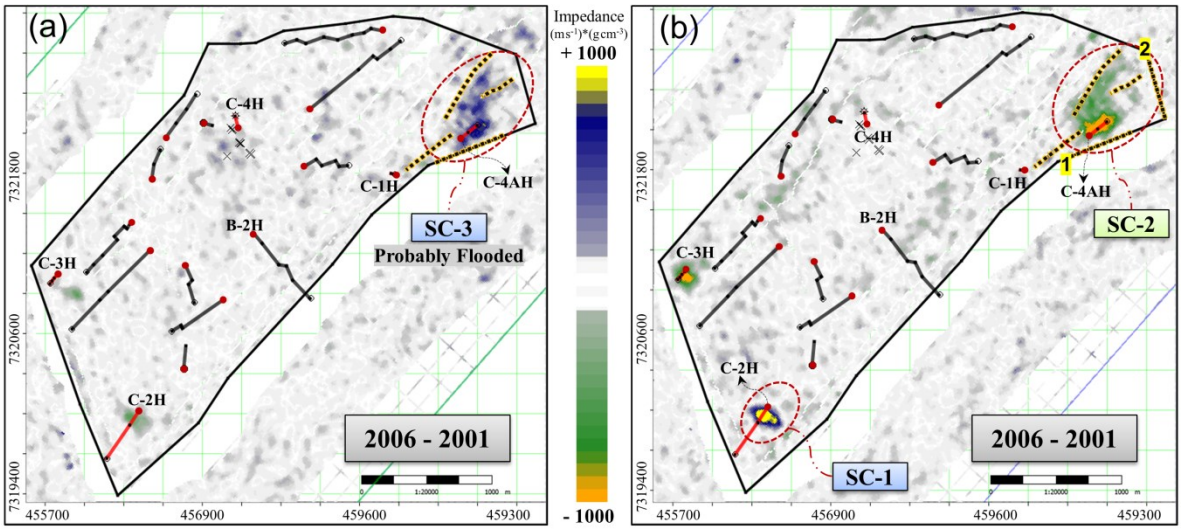

Figure 4.12. 4D acoustic impedance maps between the 2001 and 2006 surveys for (a) below the top of the Garn Formation and (b) below the top of the Ile Formation. Black lines represent the locations of the deviated producer wells, while dark blue lines represent the locations of the deviated injector wells; red dots denote well-head positions. In (a), the NE flank of segment C is probably water flooded around the top of the Ile Formation.

Figure 4.13d illustrates the softening (anomaly SC-2) and slight hardening of the signal (anomaly SC-3) around gas and water injector C-4AH. Based on well information, C-4AH injected water into the Ile Formation until January 2005, which is a water-saturated layer in this region, and gas injection started in 2005, lasting 6 months. We therefore

conclude that the likely cause of anomaly SC-2 is a combination of increased pore pressure and reduced fluid bulk modulus, due to the 6 month injection of gas. It is probable that anomaly SC-2 is concentrated around injector C-4AH because gas injection was relatively short. The gas could have remained local to the injector, while pore pressure would have travelled much faster through the reservoir. This would explain the almost-uniform increase in simulated pore pressure for the entire region (Figure 4.13e) which is not localized around injector C-4AH. However, a local hardening effect, visible at well C-4AH below anomaly SC-2 (Figure 4.13d), led us to question the interpretation: as the local hardening lies in the aquifer, below the top of the Tilje Formation, a cause is difficult to identify and might therefore be due to a poor time-pick or a processing artefact.

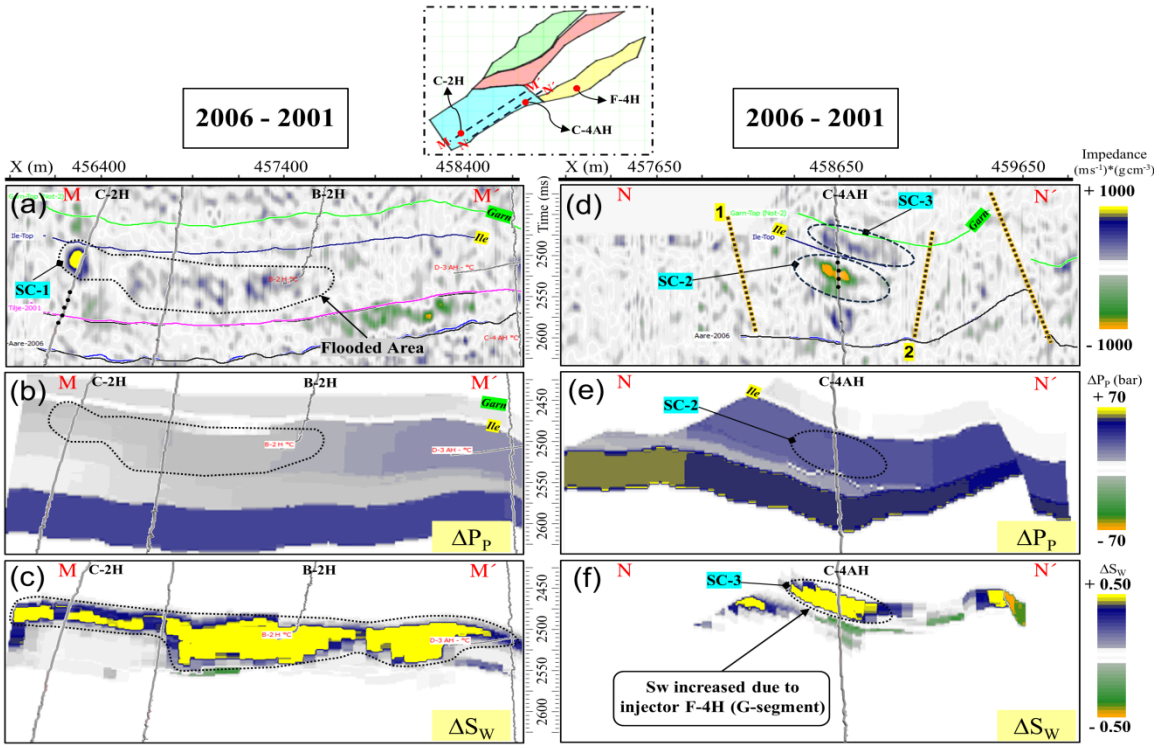

Figure 4.13. Profiles of the inverted impedance difference and simulation model for segment C. Locations of the profiles are given by the broken lines in the thumbnail plot, and red dots denote well-head positions. (a) A cross-section of the inverted impedance difference showing a strong hardening signal around the injector C-2H (black dots denote the completion of C-2H). (b) A cross-section of the simulation model showing no pore-pressure change around anomaly SC-1. (c) A cross-section of the simulation model showing a significant increase in water saturation around anomaly SC-1. (d) A cross-section of the inverted impedance difference showing anomalies SC-2 (softening signal) and SC-3 (hardening signal) around the injector C-4AH (black dots denote the completion of C-4AH). (e) A cross-section of the simulation model showing a gentle increase in pore pressure around anomaly SC-2. (f) A cross-section of the simulation model showing the significant increase in water saturation around anomaly SC-3.

We also cannot rule out that the hardening anomaly SC-3 could be a result of a significant increase in water saturation (Figure 4.13d) due to flooding from injector C-4AH reaching the Garn Formation. This interpretation agrees with that of Huang et al., (2013) but is slightly uncertain since the Not-1 Formation (the thin layer between the Garn and Aare formations) is known to act as a sealing layer due to its shale content. Possible explanations are that fractures in the Not-1 Formation may have developed due to overpressure during injection in well C-4AH, which carried injected water from the Ile Formation through the Not-1 Formation, or water encroachment from the aquifer in this region. Alternatively, the simulated water-saturation change (Figure 4.13f) suggests that water from injector F-4H in segment G has crossed the segment boundary, reaching the top of the Garn Formation around anomaly SC-3. The analysis shows that compartmentalization in the simulation model may still require reconsideration, even when there is a good match with observed anomalies.

4.5.4. Segment G

Segment G is located in the NE region of Norne Field and contains hydrocarbon only in the Garn Formation, the uppermost interval. Producer E-4AH was drilled in the upper part of the Garn Formation in 2000, and the water injector F-4H was perforated downflank (toward the aquifer zone) in September 2000 to provide more pressure for the northern region of the segment. As with segments E and D, we observe variations in impedance in the entire segment. Figure 4.14a maps inverted acoustic impedance differences below the top of the Garn Formation and Figure 4.14b maps these around the bottom of the Tilje Formation, above the top of the Aare Formation. The softening signal SG-1 spreads from the area around injector F-4H, up along the western side of fault-1 and was also observed in the northern region of segment G (anomaly SG-2). However, there is a strong softening signal in the areas surrounding the entire segment G around the bottom of reservoir (anomaly SG-3).

Figure 4.15a illustrates a greater decrease in acoustic impedance updip of the completion zone of injector F-4H (anomaly SG-1) compared to the areas around producer E-4AH (anomaly SG-2). The injector was active from September 2001 and the producer was shut-in in 2005, due to water production. Thus, it is likely that after the 2005 shut-in, without the producing well to limit the pressure build-up, the pressure increased sufficiently

in the NE flank of segment G to lower the impedance. It strongly indicates that the effects of increasing pore pressure, between 2001 and 2006, caused anomalies SG-1 and SG-2. However, the weaker anomaly SG-2 compared to anomaly SG-1 could be due either to competing effects (water flood and pressure increase) or to a lower pressure in SG-2 compared to that in SG-1.

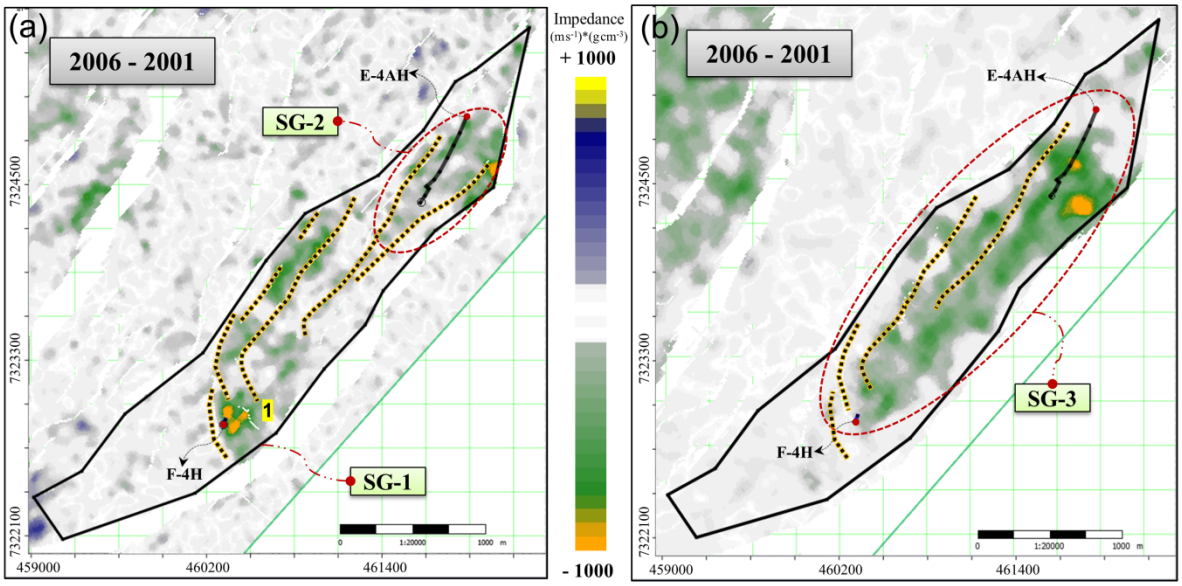

Figure 4.14. 4D acoustic impedance maps between the 2001 and 2006 surveys for (a) below the top of the Garn Formation and (b) around the bottom of the Tilje Formation. Black lines represent the locations of the deviated producer well, while dark blue lines represent the locations of the deviated injector well; red dots denote well-head positions. In (a), the areas surrounding injector F-4H and producer E-4AH show decreases in acoustic impedance, while a significant softening anomaly that spreads across the entire segment G (anomaly SG 3) can be seen in (b).

Following the above interpretation, the most probable path of water flooding is from the injector F-4H, along the western side of fault-1 through the NE region of segment G and to the heel-end of producer E-4AH. However, anomaly SG-3 showed a decrease in acoustic impedance around the base of the Tilje Formation that was spatially consistent along section but in disagreement with the small pressure change from the simulation model (Figure 4.15b). This anomaly could be attributed to the increased pore pressure as injector F-4H pressurized the entire segment G by injecting water from 2001. The simulation results showed higher increases in pore pressure in the upper region (c. 200 bar for anomaly SG-1 and 170 bar for anomaly SG-2) compared to smaller changes in the middle (about 35 bar for anomaly SG-3). Despite the fair agreement of the simulation model with the inversion results in the upper regions, further scrutiny of the assumed

compartmentalization in the simulation model is suggested, or a rock physics analysis of the sensitivity of impedance to pressure variations. Concerning the local hardening signal below well E-4AH, this could not be addressed to water replacing hydrocarbons through aquifer movement or injection, as this region is an aquifer zone with no well activity. The possible explanation could be porosity loss as a result of compaction. However, we considered this to be an uncertain interpretation that needs further investigation in this zone.

Finally, we catalogued the anomalies for all the segments in Table 4.1 in terms of the type of 4D signals and their match with the simulation model in order to summarize the time-lapse interpretation.

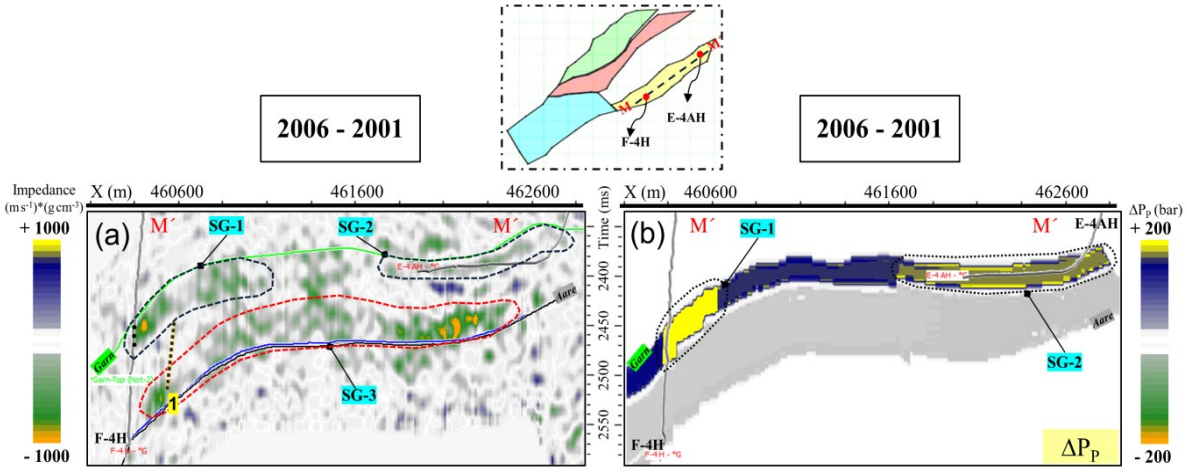

Figure 4.15. Profile of the inverted impedance difference and simulation model for segment G. Location of the profile is given by the broken line in the thumbnail plot, and red dots denote well-head positions. (a) A cross-section of the inverted impedance difference showing the softening anomalies of SG-1, SG-2 and SG-3 (black dots denote the completion of F-4H). (b) A cross-section of the simulation model showing higher increases in pore pressure around anomalies SG-1 and SG-2 compared to the smaller changes in the middle region.

4.6. Conclusions

The challenges facing time-lapse seismic interpretation of the Norne benchmark case are significant due to the intense production activity between 2001 and 2006. Moreover, time-lapse changes in the inverted seismic impedance using a post-stack, model-based inversion algorithm are unable to separate the effects of changes in saturation and pore pressure. However, by inverting the base (2001) and monitor (2006) seismic surveys to acoustic impedance and comparing its changes with well production history and flow

simulation, we have shown how it is possible both to identify likely causes of 4D anomalies and to highlight parts of the (non-history-matched) flow model for further inspection.

In this approach, we obtained the low-frequency impedance starting models using base survey well logs and 4D relative changes in P-wave velocity, from a comprehensive reinterpretation of the main horizons, which guided estimations of the time-lapse changes in acoustic impedance. However, the inverted 4D impedance anomalies resulted from competing production effects, such as pore-pressure and saturation changes, associated with the injection of water and gas and the production of oil. Accordingly, to avoid mismatches between the interpretation of softening/hardening signals and the actual dynamic reservoir anomalies, we considered the reliability of the observed anomalies, referring to production/injection history data. The 4D acoustic impedance anomalies in reservoir segments E, D, C and G were reviewed together with the flow-simulation and injection/production histories to seek consistency in interpreted changes in pore pressure and water saturation. As the difference sections and maps showed, most softening anomalies were located in areas surrounding injector wells, where increased pore pressure, softening the frame modulus, dominated increased water saturation, stiffening the fluid modulus. Despite these softening effects, the fluid-gradient change (zones with rising water levels replacing hydrocarbon) caused the increases in impedance that can be seen mainly in segments E, D and C, where the water contact rise in these segments is a consequence of the production activity up to 2006.

Inconsistencies were apparent between the anomalies derived from the 4D inversion and those provided by the simulation model for the northern region of segment E, the southern region of segment C and the bottom of segment G. These inconsistencies suggest re-examination of both simulation model assumptions on compartmentalization and seismic horizon picking or processing to achieve reconciliation. As a corollary, a fair match between observed inversion anomalies and simulation model predictions in other regions is not always an indication that no updates are needed in the simulation model or the inversion.

We have shown that joint interpretation of time-lapse seismic inversion with the flow-simulation model results builds confidence in identifying the production effects in the Norne benchmark case, and provides valuable input for reservoir characterization and

monitoring. Indeed, combined interpretation is key to understanding production/injection effects within the reservoir segments of the Norne benchmark case. However, further interpretation support might be achieved from time-lapse amplitude v. offset (AVO) analysis to provide both compressional and shear impedance anomalies that could improve the interpretation of seismic data by separating fluid effects from rock framework effects. Additionally, these results could be used to guide a seismic history-matching procedure to update the simulation model in the parameterization phase, for instance. Finally, as this is a benchmark case, other 4D inversion methods can be considered to enrich the discussions over 4D seismic interpretation.

Table 4.1. Description of each set of anomalies

Segment	Anomaly	4D Signal	Simulation Model
E	SE-1	Softening	Disagreement
	SE-2	Softening	Agreement
	SE-3	Softening	Agreement
	SE-4	Hardening	Agreement
D	SD-1	Softening	Agreement
	SD-2	Hardening	Agreement
C	SC-1	Hardening	Disagreement
	SC-2	Softening	Agreement
	SC-3	Hardening	Agreement
G	SG-1	Softening	Agreement
	SG-2	Softening	Agreement
	SG-3	Softening	Disagreement

5. ARTICLE-4: *Quantitative integration of 3D and 4D seismic inverted impedance into reservoir simulation model updating in the Norne Field*

Masoud Maleki, Alessandra Davolio, Denis José Schiozer

Submitted to Geophysical Prospecting journal

The ultimate goal of reservoir simulation in reservoir surveillance technology is to estimate long-term production forecasting and to plan development and management of petroleum fields. However, maintaining reliable reservoir models which honor available static and dynamic data, involve inherent risks due to the uncertainties in space and time of the distribution of hydrocarbons inside reservoirs. Recent applications have shown that these uncertainties can be reduced by quantitative integration of seismic data into the reservoir modelling workflows to identify which areas and reservoir attributes of the model should be updated. This work aims using seismic data to reduce ambiguity in calibrating reservoir flow simulation model with an uncertain petro-elastic model (PEM), proposing a circular work-flow of inverted seismic impedance (3D and 4D) and engineering studies, with emphasis on the interface between static and dynamic models. The main contribution is to develop an updating procedure for adjusting reservoir simulation response before using it in the production forecasting and enhance the interpretive capability of reservoir properties. Accordingly, the workflow evaluates consistency of reservoir simulation model and inverted seismic impedance, assisted by production history data, to close the loop between reservoir engineering and seismic domains. The methodology is evaluated in a complex, faulted, sandstone reservoir, the Norne benchmark field, where a significant reservoir behavior understanding (about the static and dynamic reservoir properties) is obtained towards the quantitative integration of seismic impedance data. This lead to diagnose the reservoir flow simulation reliability and generate an updated simulation model consistent with observed seismic and well production-history data, as well as, a calibrated petro-elastic model. Furthermore, as Norne Field is a benchmark case, this study can be considered to enrich the discussions over deterministic or probabilistic history matching studies.

5.1. Introduction

The geoscientists and reservoir engineers attempt to build reliable reservoir models, which provide a better understanding of field planning and management. This motivated the development of integration between wide ranges of well-known techniques including time-lapse seismic data, reservoir flow simulation and history matching. Reservoir management requires simulation models to improve understanding of complex flow

behavior in reservoirs, and to provide a long term perspective on the future performance of the reservoir (Hoffman and Caers, 2007; Lucia, 2007). Moreover, reservoir simulation models are intended to represent the variation in the dynamic properties over the production time to establish the reservoir management plans (Hoffman, 2005; Fanchi, 2001). However, the reliability of the predictions of simulation models as a stand-alone procedure depends on knowledge of rock and fluid properties such as the distribution of heterogeneities, relative permeability, faults location and transmissivity, and the production mechanism that control the reservoir performance.

Nowadays, among the different technologies that contribute to reservoir management, the role of time-lapse seismic data (or 4DS) is critical at different stages of life of the field cycle due to its unique character to capture the fluid flow behavior during production (Johnston, 2013). 4DS can be a rich source of information to reduce the uncertainty related to reservoir properties, in which allowing the improvement of the knowledge of geological framework and a more effective reservoir management. It provides new data describing the dynamic behavior of reservoir fluids in between the wells, often providing a surprise relative to preconceived views of reservoir flow, or even stratigraphy. Time-lapse seismic data have been tried in several fields to date, and proven to be a well-established and mature technology to optimize field and enhanced oil recovery operations (Landrø et al., 1999; Koster et al., 2000; Strønen and Digranes, 2000; Johnston, 2013) by imaging production induced changes within the reservoir and providing invaluable information about reservoir heterogeneity (Greaves and Fulp, 1987; Tura and Lumley, 1999; Koster et al., 2000; Landro, 2001; Tura et al., 2005).

Meanwhile, the possibilities for integration of 4D seismic attributes data into the reservoir simulation updating process should be considered as it can be integrated in form of seismic amplitude, acoustic impedance or any other seismic-derived attribute. Time-lapse seismic attribute must reflect a good understanding of character of the seismic prior to its integration in the simulation model in order to be most effective and less erroneous. It seems that, inverted impedances provide better results than the seismic amplitudes for 4D interpretation, allowing detection of subtle changes in repeatedly acquired seismic data (Ayzenberg et al., 2013). Furthermore, inverted impedance converts the seismic reflectivity into volumetric impedance data that are more suited to cross-domain comparison (Tian et

al., 2014). For instance, the advantage of 4D seismic impedance attribute to capture the effect of pressure and saturation variations (with reasonable degree of success) has been highlighted in the Draugen Field (Guderian et al., 2003), UKCS turbidite reservoir (Stephen et al., 2006), Girassol Field (Roggero et al., 2007) and Norne Field (Maleki et al., 2017). Moreover, techniques for inverting for 4D changes are now readily available.

Another aspect to highlight is how to incorporate the 4D seismic data within reservoir flow simulation. 4D seismic response can be integrated either qualitatively (such as interpreting likely causes of 4D anomalies due to changes in saturation and pore pressure) or quantitatively (by adding seismic derived attributes inside in the objective function of a history matching process). Most 4D seismic interpretation remains qualitative in the literature (Johnston, 2013) and it was recently discussed in Byerley et al., (2016) and Maleki et al., (2017). Byerley et al., (2016) used time lapse seismic data to implement an optimized well operating strategy for the Surmont heavy oil field and Maleki et al., (2017) identified the production effects in the Norne Field utilizing the joint interpretation of 4D seismic inversion with the flow-simulation model results.

However, the multidisciplinary nature of reservoir modeling demands more quantitative approach to integrate 4D seismic data. Amini (2014) used simulation model to generate synthetic time-lapse seismic data during different stages of production which in turn were compared to measured time-lapse data. More recently, 4D seismic has been used quantitatively in reservoir simulation model updating processes as a constraint into history matching, by defining a procedure to match not only the well production data but also 4D seismic attributes (Gosselin et al., 2003; Lygren et al., 2005; Skjervheim et al., 2007; Stephen et al., 2008; Peters et al., 2010). For instance, Roggero et al. (2012) proposed an assisted history matching technique to update reservoir models with 4D seismic data in a quantitative way, in which represented a significant improvement in the reservoir modeling process. Moreover, the updates derived by 4D seismic data integration may not make geological sense as characterizing the static reservoir framework demands reliable geological knowledge before proceeding with the history matching workflow. Alternatively, the geological framework and property distributions of the reservoir can be defined by the 3D seismic data as it is associated to the static reservoir framework (Tian et al., 2014). Thus, instead of having only history production data at well locations (few

points in the reservoir), spatial variations of static and dynamic properties derived by 3D and 4D seismic data also become accessible to update reservoir simulation parameters iteratively, in order to match both the observed seismic and production data and measures the quality of the matching. Under this type of analysis, seismic and reservoir engineering studies are linked in a circular work-flow to provide better production forecast, with the emphasis being placed on the interface between static and dynamic models, seismic and rock physics.

Nevertheless, quantitative evaluation of consistency between seismic data and reservoir flow simulation relies on petro-elastic modelling (PEM) which links the reservoir simulation to elastic parameters and provides the logical cross-domain comparison. The parameters in PEM should be calibrated according to the specific field of study to ensure realistic values for changes in in-situ elastic parameters due to production activity. The main inputs to PEM are mineral and fluid properties, dry rock model, and a pressure sensitivity model for velocities. Calibrated parameters of rock frame and fluid properties are computed by well-logs data, while related calibration to pressure sensitivity are evaluated by repeated well logging and core measurements. However, there are difficulties in calibrating the pressure sensitivity of the PEM with lab measurements (Osdal et al., 2006) and in case of absent of repeated well logging or not enough core measurements, 4D seismic data can be useful to evaluate the pressure sensitivity of PEM.

This paper presents a successful development of a circular workflow in an engineering-consistent manner to reduce ambiguity in calibrating reservoir flow simulation model with an uncertain PEM. The central ingredient in this scheme is to generate a quantitative integration of inverted seismic data (3D and 4D) that allows a robust reservoir simulation model updating process, in agreement with information from seismic data when performing a history matching. The methodology is evaluated in a complex, faulted, sandstone reservoir, the Norne Field to validate its efficiency and analyze the confidence level of quantitative integration. There are several research where highlighted the beneficial of 4D seismic data for better reservoir behavior understanding in the Norne Filed: Osdal and Alsos (2002), Lygren et al., (2005), El Ouair et al., (2005), Osdal et al., 2006, Boutte (2007), Cheng and Osdal (2008), Dadashpour et al., (2009); Huang et al., (2011), Aschjem (2013), Huang et al., (2013), Yan (2014), Santos et al., (2016) and Maleki et al., (2017).

However, this study addresses in more details the evaluation of consistency between the reservoir simulation model and seismic impedance data (3D and 4D) of Norne Field, assisted by production history data, to provide geologically consistent reservoir models that could match production data, static data, and available geological knowledge.

To thoroughly investigate, we convert the inversion results of base (2001) and monitor (2006) seismic surveys to the simulation scale to access the observed impedance models (3D and 4D). Alternatively, synthetic impedance models (3D and 4D) are calculated using a reservoir flow simulation model and rock-physics modeling. Then, we compare the observed and synthetic impedance models, supported by production history data, evaluating their discrepancies and therefore, identify the properties and specific regions of field where updates to the simulation model might be appropriate. In the case studied, the initial simulation model presents considerable mismatches with the observed seismic data. The inconsistencies can be caused either by the simulation model inaccuracy or uncertainties on the petro-elastic model. The pressure measurements at the wells (bottom-hole pressure) also present significant mismatches which are indicated an inaccurate simulation model. Furthermore, we update the initial simulation model using quantitative integration of 3D and 4D observed seismic impedance and well history data. Alternatively, the reliability of updated simulation model is improved which is validated by resolving the BHP discrepancies of well history-data. However some discrepancies were still observed for the 4D seismic data. Thus, in the last part of the proposed methodology, we calibrate the pressure dependency of petro-elastic model, referring to observed 4D model and matched well production data, to ensure realistic values for changes in in-situ elastic parameters. This part highlights another important contribution of time-lapse seismic impedance data to generate more reliable reservoir model, due to the difficulties of calibrating pressure sensitivity of the PEM using lab measurements. Our study indicates that the quantitative incorporation of inverted seismic data and reservoir flow simulation (in an iterative loop), that matches the production data and honors other static and dynamic data, is key to maintain a reliable reservoir model for the Norne Field. Additionally, as Norne Field is a benchmark case, these results can be considered to enrich the discussions over deterministic and probabilistic seismic history-matching studies.

5.2. Norne Field

The Norne Field was discovered in the mid-Norwegian Sea, offshore Norway, in December 1991 and development drilling started in August 1996. The field is located between Vøring and Møre basins on the Norwegian Continental Shelf and the reservoir is a flat horst structure (around 3×9 km in extent) at a depth of 2500 – 2700 meters (water depth of 380 m) with a trend of northeastern-southwestern (Figure 5.1). The reservoir rocks divided into two separated oil compartments; the Norne main structure (segment D, E and C), and the NE segment (segment G), that are situated in a fault complex in the Norwegian Sea (Figure 5.1). The compartments are bounded by the major horst structure and compartmentalized by minor associated faults (Huang et al., 2013), which also tend to prevent pressure communication between reservoir segments and impede fluid flow.

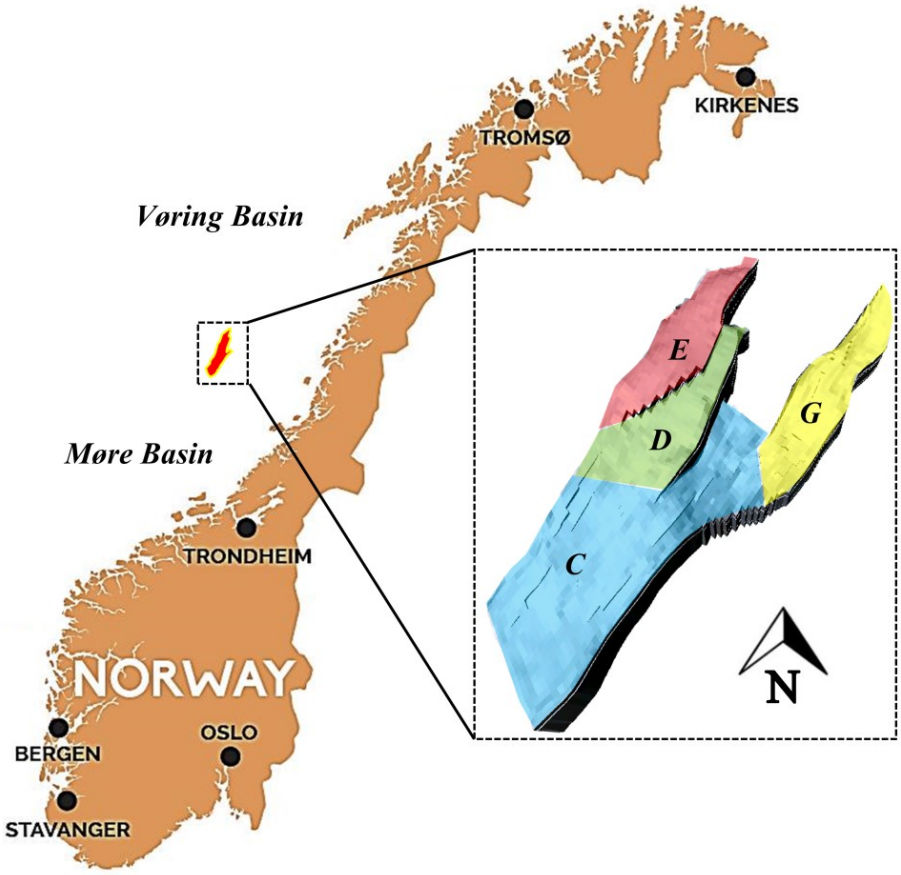

Figure 5.1. Location and segments of the Norne Field in the Norwegian Sea.

In the Norne Field, the hydrocarbons are found in sandstone from the Middle and Early Jurassic age, and are subdivided into the Garn and Ile formations of the Fangst

Group; and the Tofte and Tilje formations of the Båt Group (Dalland et al., 1988; Hammer et al., 2010) as shown in Table 5.1.The top of the heterolithic Aare Formation is the base of the reservoir and the shaly Not-3 Formation (Melke Formation) acts as a cap rock for the reservoir. The Not-1 Formation behaves as an effective seal, preventing communication between the Garn and Ile Formations (the reservoirs above and below it) during production. Notably, 80% of the initial oil is located at the Ile and Tofte formations, and the free gas is in the Garn Formation (Rwechungura et al., 2010). Most of the sandstones formations in the Norne have good reservoir properties, with porosity in the range of 25-30%, permeability between 20 and 2500 mD, net-to-gross values range from 0.7-1 and water saturation 12-43% for the hydrocarbon zones (Rwechungura et al., 2010; Steffensen and Karstadt 1996; Osdal et al., 2006). Additionally, the reservoir thickness varies over the entire field from 260 m in the southern region to 120 m in the northeast part, due to increasing erosion to the north in Ile and Tilje formations (Verlo and Hetland, 2008). More details about Norne stratigraphy can be found in Dalland et al., (1988), Swiecicki et al., (1998) and Correia (2017).

5.3. Dataset preparation

The Norne benchmark case is based on a set of real oil-field data organized by the Centre of Integrated Operations in the Petroleum Industry (IO Centre), the Norwegian University of Science and Technology (NTNU) and Norne Field Operations (Statoil, ENI and Petoro). It has a wide variety of data, including reservoir flow simulation model of full field in Eclipse format, well logs data, production and injection history data up to 2006 and time-lapse seismic data. More details on the data provided within the benchmark case can be found in Verlo and Hetland (2008).

The simulation model contains 44 927 active cells (60 × 60 × 8.4 m) with 22 layers (corresponding to the actual change of lithology as shown in Table 5.1), in which comprises the entire field. The initial simulation model used in this study is provided by a geostatistical parameterization technique based on the pilot wells method in the CMG-IMEX format to address the lack of a geological model (Correia 2017). Correia (2017) used the pilot point method (De Marsily et al., 1984) and geostatistical assumptions for the benchmark reservoir-simulation model to provide geologically consistent reservoir model

and modelled a high-resolution geogrid including their petrophysical properties (porosity, permeability and net-to-gross ratio) that were controlled by the facies models. In fact, the porosity, net-to-gross ratio and permeability distributions are directly related to the geostatistical facies models. Although the model is geologically consistent, it is not perfectly history matched, in which is improved in this work.

Tabe 5.1. Early-Middle Jurassic stratigraphy of the Norne Field and reservoir zonation from the simulation model. Hydrocarbons are mainly found in the Garn, Ile, Tofte and Tilje formations.

Norne Stratigraphy				**Reservoir Zonation** (from the simulation model)
Age	Group	Formation		Layer number
Jurassic - Mid	Fangst	Not-3	Upper Not Shale	_
		Garn (Not-2)	Not Sandstone	K-01 to K-03
		Not 1	Lower Not Shale	K-04
		Ile	Ile-2	K-05 to K-08
			Ile-1	K-09 to K-11
Jurassic - Early	Båt	Tofte	Tofte-2	K-12 to K-15
			Tofte-1	K-16 to K-18
		Tilje	Tilje-4	K-19
			Tilje-3	K-20
			Tilje-2	K-21
			Tilje-1	K-22
		Aare	Shaley Sand	_

Wells including logs data from 29 oil producers, 10 water injectors and two exploration wells, in which by 2001, the field had 24 wells: 17 producers and 7 injectors. Production history-data of fluid rates (Oil rate (Qo), water rate (Qw), gas rate (Qg) and gas-

oil-ratio) and historical injection fluid rates (Qwi, Qgi) are available for 22 producers and 9 injector wells, respectively. The bottom-hole pressures (BHP) are also recorded for some producer wells up to December 2006.

Besides engineering and well-logs data, the dataset also comprises post-stack seismic data of 2001 base and 2006 monitor surveys. Maleki et al., (2016) analyzed the impact of well log constraints, including the number and locations of wells, in 3D model-based inversion of the Norne Field base survey from 2001. Their results highlighted that the varied locations and number of well were clearly affect the inversion results. The nine-well constrained inversion (10-2, 10-4, B-4H, C-1H, C-3H, D-1H, D-4H, E-3H and F-1H) provided higher vertical resolution and more robust acoustic impedance interpretation than an inversion constrained by only the two exploration wells. Moreover, Maleki et al., 2017 used model-based 4D inversion approach to invert the base (2001) and monitor (2006) seismic surveys in order to compute the related impedance variations to production activity in the Norne Field. They used model-based inversion algorithm with different initial models for each vintage; a low frequency impedance starting model from well-log data as a prior for the base survey, and 4D relative changes in P-wave velocity between base and monitor surveys as priors for the monitor survey. Their study showed that joint interpretation of time-lapse seismic inversion with the flow-simulation model results builds confidence in identifying the production effects in the Norne benchmark case, and provides valuable input for reservoir characterization and monitoring. Thereby, in the current study, the observed seismic impedance data (3D and 4D) are provided by 3D and 4D seismic inversion results (using nine wells) of Maleki et al., 2016 and Maleki et al., 2017.

Furthermore, used parameters for deriving a suitable petro-elastic model for the Norne Field are presented in Table 5.2. The main inputs of PEM are mineral and fluid properties, dry rock model, and dependency of velocity changes to pressure. The fluid and rock properties are provided by Suman (2013), Briceno et al., (2016) and Norne benchmark data. Moreover, MacBeth (2004) proposed equations that relate effective stress and the bulk and shear modulus of dry rock frame. His equations are controlled by parameters that are measured from lab measurements and effective pressure which is the difference between the overburden pressure and the pore pressure. However, here we used a modified

equations of MacBeth (2004) as proposed by Briceno et al., (2016) to calculate the bulk modulus of dry rock frame (Equations 5.1 and 5.2):

$$k_{dry}^{(dyn)} = k_{dry}^{(st)} \frac{1 + E_k e^{-Peff\ initial/Pk}}{1 + E_k e^{-Peffmon/Pk}} \tag{5.1}$$

and

$$\mu_{dry}^{(dyn)} = \mu_{dry}^{(st)} \frac{1 + E_\mu e^{-Peff\ initial/P\mu}}{1 + E_\mu e^{-Peffmon/P\mu}} \tag{5.2}$$

where Ek, Pk, Eμ and Pμ are the rock stress sensitivity constants estimated in MacBeth (2004). P_{eff} initial is the reservoir pre-production effective pressure and $P_{eff\ mon}$ is the effective pressure at the monitor survey time. We used measurement values of West of Shetland region for Pk and Pμ as described in MacBeth (2004). Moreover, Ek and Eμ were set to 3 and 2, respectively following the work of Santos (2017). The values for overburden and underburden were assigned using the average of the available well logs, as described in Table 5.3. Eventually, we used well-known fluid substitution equation proposed by Gassmann (1951) to compute the bulk modulus (k and μ) in the PEM.

Table 5.2. Main PEM parameters used in this study.

Fluid properties	Temperature (°C)	98.3 °C
	Salinity	50.000 ppm
	API of oil	29.6
	Gas gravity	0.85
Sand properties	Bulk modulus (k)	29 GPa
	Density (ρ)	2728 kg m^{-3}
	Shear modulus (G)	25 GPa
Clay properties	Bulk modulus (k)	16 GPa
	Density (ρ)	2663 kg m^{-3}
	Shear modulus (G)	7 GPa
Stress sensitivity parameters	Frame bulk modulus (k_{inf})	10.23 GPa
	P_k	5.62 MPa
	E_k	3
	μ_{inf}	4.88 GPa
	P_μ	7.97 MPa
	E_μ	2

Table 5.3. Parameters for over and underburden in the PEM.

Overburden	V_p	2900 m/s
	Density (ρ)	2400 kg m^{-3}
	V_s	1500 m/s
Underburden	V_p	3000 m/s
	Density (ρ)	2400 kg m^{-3}
	V_s	1550 m/s

5.4. Reservoir model updating workflow

This work proposes a reservoir model updating procedure which quantitatively integrates seismic and engineering data to close the loop between both domains. Mismatches between the two datasets (in presence of trustful PEM) would ideally mean that the simulation model has inaccuracies and should be calibrated to the observed seismic impedance data. One of the key aspects in a petro-elastic modeling is the pressure dependence of bulk and shear modulus. This relation comes from core measurements which very often do not match observed 4D signals, making it very uncertain. Thus, we propose to first ensure that the simulation model provides reasonable pressures estimates, which in our case are supported by BHP measurements and then revisit the petro-elastic modeling, evaluating the calibration of the pressure sensitivity. Hence, the methodology is divided into three stages to resolve ambiguity in calibrating reservoir flow simulation model with an uncertain PEM. First, comparisons of the observed (inverted from seismic data) and synthetic (computed from simulation model) 3D impedance models provide a detailed updating of the static reservoir framework (e. g. porosity and net-to-gross) to add realistic heterogeneities into the model. Then, comparisons of observed and synthetic 4D impedance models (considering the updated model from previous step), estimate the updating for dynamic reservoir properties. These two steps improve the reliability of reservoir model using quantitative integration of observed seismic impedance (3D and 4D) and relying on production-history data. Meanwhile, the pressure sensitivity of petro-elastic model is calibrated for the field, referring to observed 4D model and matched well production data.

It has to be noted that the comparison of synthetic and observed seismic impedance must be with the same scale (or grid). The chosen scale (seismic or engineering) should contain the capability of computational efficiency and straightforward ability to run multiple times. Thus, before moving on updating workflow, all the observed impedance

models generated at the seismic domain are converted to depth (using appropriate velocity model), and then, scaled to the simulation grid. The scaling procedures are mainly based in averaging methods and therefore normally followed by a smooth effect to maintain as much as possible the fine scale heterogeneities seen in the seismic domain. However, depending on the reservoir characteristics and on each reservoir parameter, different scaling methods are proposed in the literature and available in the commercial software. After capturing the desired observed seismic impedance in engineering scale, the static and dynamic properties of the referenced simulation model are captured during different stages of production at the selected time-steps (same time as seismic datasets are acquired). Furthermore, the synthetic impedance models are generated through a petro-elastic model to convert the extracted dynamic and static properties to elastic properties (P-wave velocity, S-wave velocity and density).

Moreover, the preliminary comparison is evaluated in the 3D domain to capture uncertainties in the parameters that are of direct impact to the reservoir volumetrics. One advantage of preliminary comparison in 3D domain is to provide pore volume information of reservoir that aims to validate the geological modeling. For instance, higher impedance in the observed data could indicate the demands of lower porosity (decreases in pore volume) for the model as 3D acoustic impedance has a high correlation with porosity. Thus, these modifications are considered to be used as input for the new reservoir simulation model to run it again in order to improve the match between the observed and synthetic 3D impedance models. Furthermore, with the new reservoir volumetric model regarding the first stage of comparison, the impedance change predictions from the simulation model are now compared directly to the inverted 4D seismic impedance changes. The particular feature of 4D comparison is to reduce the uncertainty ranges of the dynamic reservoir properties according to their particularities and maintain consistency with the physics of flow. For example, one of the possibilities of a hardening effect (increased acoustic impedance) is water flooding, when water replaces oil. Thus, a hardening signal in the observed data can indicate the demands of permeability modifications. Thereby, these two comparison steps are mainly concentrated in the parameterization step to identify the properties and specific regions of the field where updates might be appropriate.

Meanwhile, the comparison steps are supported by well production data, where each modification in the simulation models is quantified and diagnosed during the assisted history matching. In fact, comparison between observed and synthetic anomalies from 3D and 4D domains, combined with the production-history data, can provide significant insights to the overall confidence levels of the reservoir simulation model updating process. Moreover, the deviations of production-history data throughout initial and updated simulation models can be evaluated either visually or calculated using the normalized quadratic deviations with sign (NQDS) as described in Avansi et al., 2016.

For remained poorly matched areas (after the updating steps), if the well history matching is in acceptable range, subsequently the inconsistency can be related to the rock-physic modeling. This fact leads us to revisit the PEM, especially the stress sensitivity of the model. For instance, higher values for softening effect are observed in the 4D seismic inversion results when compared with the 4D synthetic impedance derived by simulation model. Moreover, time-lapse interpretation indicates that the softening anomaly is caused due to the pore pressure increases. Additionally, the updated simulation model presents a good bottom-hole pressure (BHP) match for the wells in the same region which is a good indicative of fair pressure estimates from the simulation model. Thereby, the pressure sensitivity of PEM should be calibrated in order to capture the approximate same values for both observed and synthetic 4D impedance models. This is a good example of why the last step of methodology avoids the generation of unrealistic property values by calibrating the pressure sensitivity of PEM and overcomes potential instability problems that frequently affect the reliability of reservoir simulation model updating.

The summarized workflow for the quantitative integrations of 3D and 4D seismic impedance data to update the reservoir flow simulation model and calibrate the pressure sensitivity of PEM (Figure 5.2) follows:

- (a) Convert the seismic impedance models (3D and 4D) to engineering scale by converting the seismic data to depth domain and scaling it to the simulation model scale.
- (b) Compute the synthetic impedance models (3D and 4D) using the initial reservoir simulation model (to extract static and dynamic properties for the selected time-steps) and rock physics modelling.

- (c) Preliminary comparison of observed and synthetic impedance models in 3D domain (from steps (a) and (b)) to update the parameters that are related to static reservoir properties.
- (d) Secondary comparison of observed and synthetic impedance models in 4D domain (from steps (a) and (b)) to update the parameters that are related to dynamic reservoir properties.
- (e) Analyze the matching of production-history data and updated reservoir flow simulation models (from steps (c) and (d)).
- (f) Evaluate if it is necessary to update the PEM, referring to the observed 4D impedance (from step (d)) and matched production-history data (from step (e)).

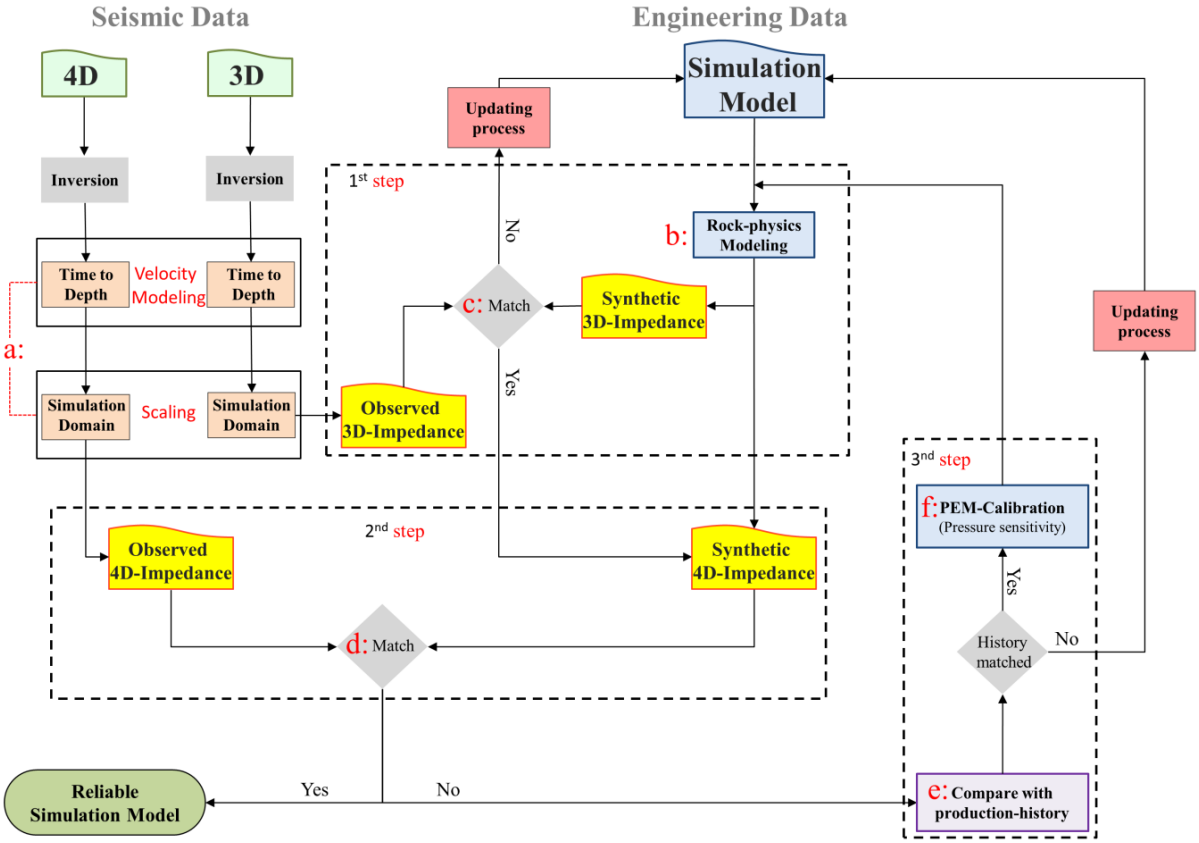

Figure 5.2. Workflow scheme of updating the reservoir flow simulation model. The seismic side of the flowchart provides observed static (3D) and dynamic (4D) seismic impedance models, while the engineering side contains the initial reservoir flow simulation model. Following a five-step approach: (a) convert the seismic impedance models to engineering scale; (b) compute the initial synthetic impedance models (3D and 4D) using the initial reservoir simulation model; (c) preliminary comparison of observed and synthetic impedance models in 3D domain; (d) secondary comparison of observed and synthetic impedance models in 4D domain; (e) analyze the matching of production-history data and updated reservoir flow simulation models; and (f) calibrate the pressure sensitivity in PEM setting.

Eventually, it is important to note that the specific contributions of updating steps are highlighted by the dashed black boxes in Figure 5.2. Moreover, these steps must run in a loop until all the mismatches caused by simulation model errors and uncertain PEM can be validated, to obtain a fair confidence levels of realistic reservoir model.

5.5. Results and discussion

This section presents the application and results that outcome from the proposed reservoir updating workflow in the segments E and D of Norne Field. We compared the synthetic and observed seismic data for each zone of these segments to analyze the confidence level on reservoir simulation updating, considering the uncertainties from synthetics seismic impedance models, and production-history data agreement. We attempted to implement the updating workflow in the segments E and D of Norne Field for two main reasons; first, these segments present challenges regarding the understanding of the production behavior. Segments E and D experienced intense production activity up to 2006, where several wells are producing close to each other at the same time. Second, Maleki et al., (2017) interpreted the 4D seismic impedance anomalies for the entire Norne reservoir segments from 2001 to 2006 and their results highlighted that 4D features such as softening (due to pore pressure increases) and hardening signals (due to water saturation increases) were detectable and well pronounced in the segments E and D. Herein, these segments are particularly applicable to validate the efficiency of methodology.

Segment E is located in the NW region of the Norne Field (Figure 5.3). The water injectors F-1H and F-3H were drilled in 1999, aimed at giving pressure support to the neighboring producers within the Ile, Tofte and Tilje formations. Producer wells in this area which produced after 2001 are E-2H, produced between November 1999 and July 2005 in the Ile Formation; E-2AH, opened in May 2005 aiming to produce oil in the Ile Formation and E3-AH, which produced horizontally along Not-2 Formation (Garn Formation) between December 2000 and January 2005. Segment D is located in the NW region of the Norne Field and is separated from segment E by a major fault, sealing this area (Figure 5.3). The water injector F-2H, drilled in 1999, was completed in the Ile and Tofte formations to provide pressure for the neighboring producers and to enhance the oil sweep across the segment D. Well E-1H opened from July 1999 aiming to produce oil in the Ile-2

until December 2006. Well B-4BH produced horizontally in Ile-1 Formation that produced between 2001 until reaching a high water production in 2003. Well B3-H produced in the Ile-1 and Tofte-2 Formations from July 1999 up to December 2006. Well D3-AH was perforated in the Tofte-2 Formation and produced from mid-2000 to June 2005. Well D3-BH is the side-tracks from D3-AH which started production February 2006 in the Ile-2 Formation. Additionally, the petrophysical reports of producer E-1H and injector F-3H have been demonstrated that upper layers of Garn Formation (Garn-3 and Garn-2) comprise free gas around these wells.

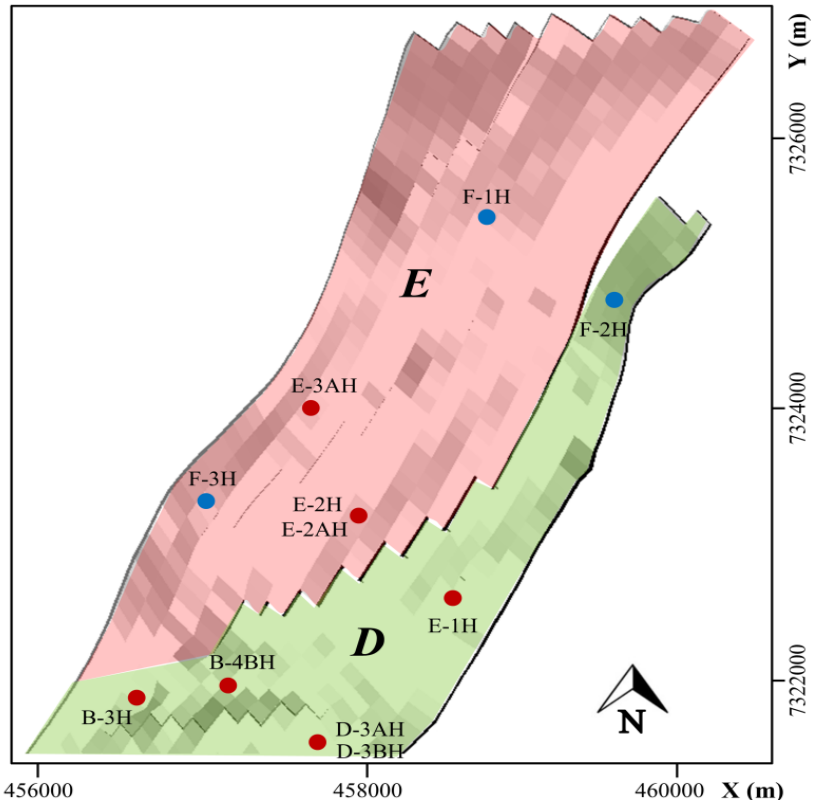

Figure 5.3. Location of the producers and injectors in the top reservoir map of segments E and D. Blue dots denote well-head position of injectors, while red dots represent well-head positions of producers.

The first step of methodology is to convert the observed seismic impedance (3D and 4D) to simulation scale, in order to increase the certainty of comparisons between observed and synthetic impedance models. We built a 3D velocity model by using the available velocity data of Norne benchmark dataset (average velocity) and converted the observed impedance data to depth domain. Then, we scaled the results to simulation grid utilizing seismic resampling method (arithmetic averaging) to maintain as much as possible the fine scale heterogeneities seen in seismic domain. Figure 5.4 illustrates the observed 3D and 4D

seismic impedance models in the simulation scale after the scaling and re-gridding, respectively. Then, we run the initial simulation model in IMEX-CMG software to extract the static (porosity and net-to-gross) and the dynamic properties (pore-pressure and fluid saturation of oil, gas, and water) in 2001 and 2006. Since the baseline seismic survey (2001) is generated after production starts in 1999, we extracted the initial pore-pressure, porosity and net to gross in July 1999 (initial time). Eventually, the captured static and dynamic properties were converted into the elastic properties (V_P, V_S and density) using the PEM (presented in the dataset preparation section) to generate the synthetic 3D impedance of baseline survey 2001 and synthetic impedance variations from 2001 to monitor survey of 2006.

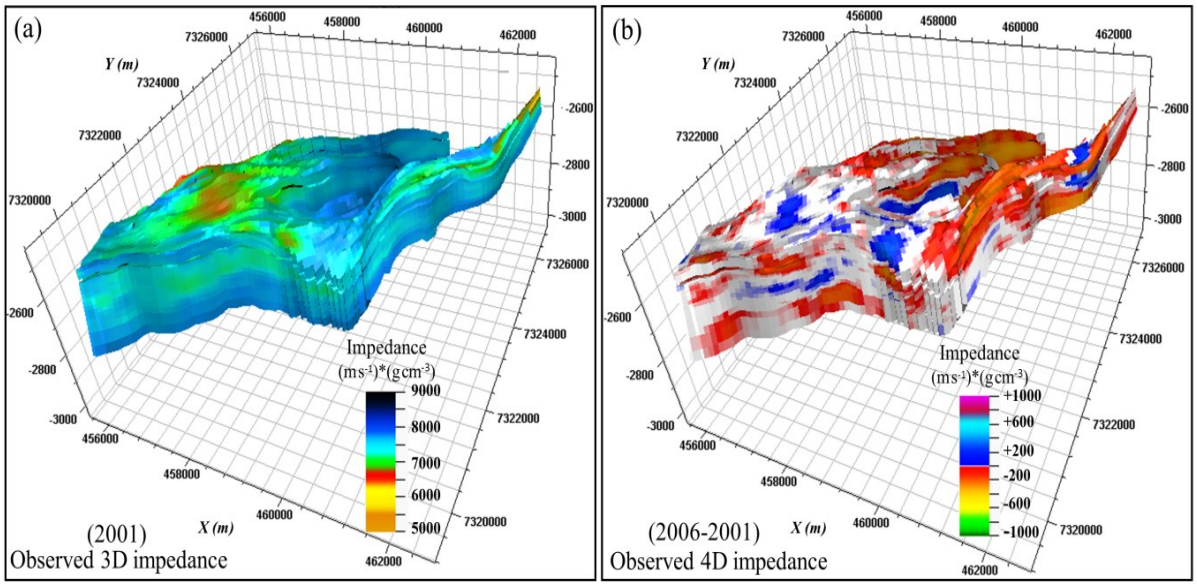

Figure 5.4. Observed seismic impedance in the simulation scale over the Norne reservoir for (a) baseline survey of 2001 (3D) and (b) impedance variations from 2001 to 2006 monitor survey (4D).

Following scaling and seismic modeling, we compared the observed and synthetic 3D impedance of baseline 2001 to evaluate the petrophysical parameters that are of direct impact to the reservoir volumetric. Figure 5.5 illustrates profiles of observed and synthetic 3D impedance models across the segments E and D. Here, we noticed several discrepancies throughout the Ile, Tofte and Tilje formations, where greater inconsistencies were apparent in deeper layers. The areas surrounding the eastern (below the top of Ile Formation) and western regions (below the top of Tofte Formation) of section implied higher impedance in the observed 3D impedance model (Figure 5.5b), rather than the 3D impedance response of initial simulation model (Figure 5.5a). This suggests that the pore volume of initial

simulation model in these regions should be diminished to enhance the matching of observed and synthetic 3D impedance models. Thereby, the porosity of Ile, Tofte and Tilje formations was decreased for the initial simulation model, while the porosity for some regions of Garn Formation (above the sealing Not-1 Formation) was increased (as porosity has a high correlation with 3D seismic impedance). For example, ellipse A highlighted higher impedance in the response of initial simulation model compared to observed impedance model for some zones of Garn Formation in the southern region of segment D (Figure 5.5).

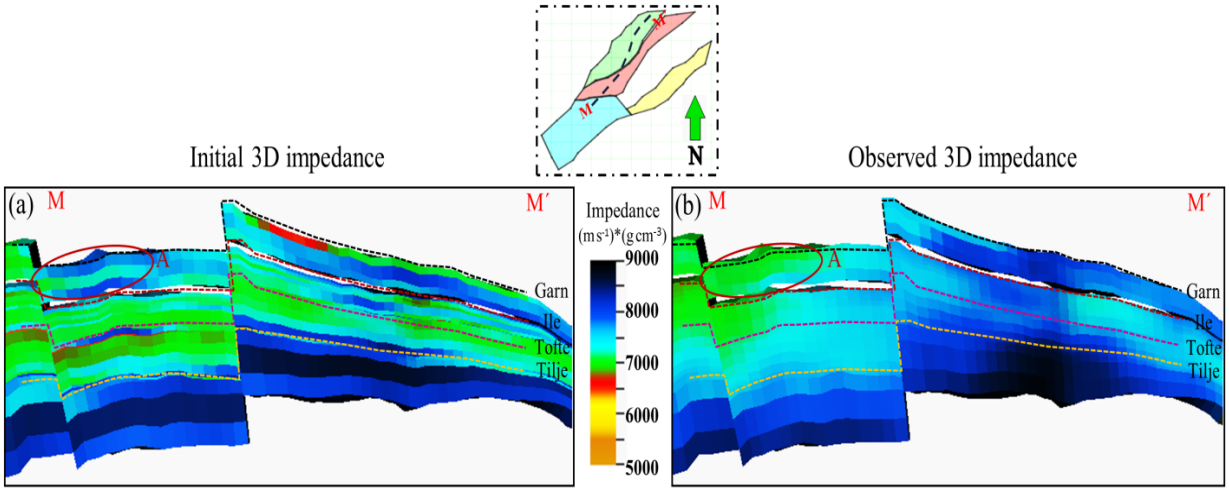

Figure 5.5. Profile of the preliminary comparison between (a) synthetic 3D impedance (derived by initial simulation model) and (b) observed 3D impedance (derived by inversion results). Location of the profile in segments E and D is given by the broken line in the thumbnail plot. The cross-section of observed impedance model showing higher impedance around the dipper layers of Ile, Tofte and Tilje formations compared to initial model. The ellipse A delineates the regions around the southern part of segment D, where the initial model shows higher impedance compared to observed model for some zones of Garn Formation.

After the necessary porosity modifications have been made, we run the new simulation model and generated the updated synthetic 3D impedance model considering the first step of quantitative integration. For instance, Figure 5.6 illustrates the results of modified porosity for deeper layers of Ile-2 (layer K-08), Tofte-2 (layer K-14) and Tofte-1 (layer K-18) formations. Close examination reveals that the first step updated model (Figure 5.6b) is more consistent with the observed 3D impedance model (Figure 5.6c) rather than the initial model (Figure 5.6a). The reason can be explained by adding new realistic heterogeneities into the model in updated model. In fact, the predictions from new simulation model and inverted 3D impedance indicated fair similar behaviors (especially

for layer K-18). The marked areas in Figure 5.6 highlighted the improvement of matching regarding the modified porosity values in the first step of updating.

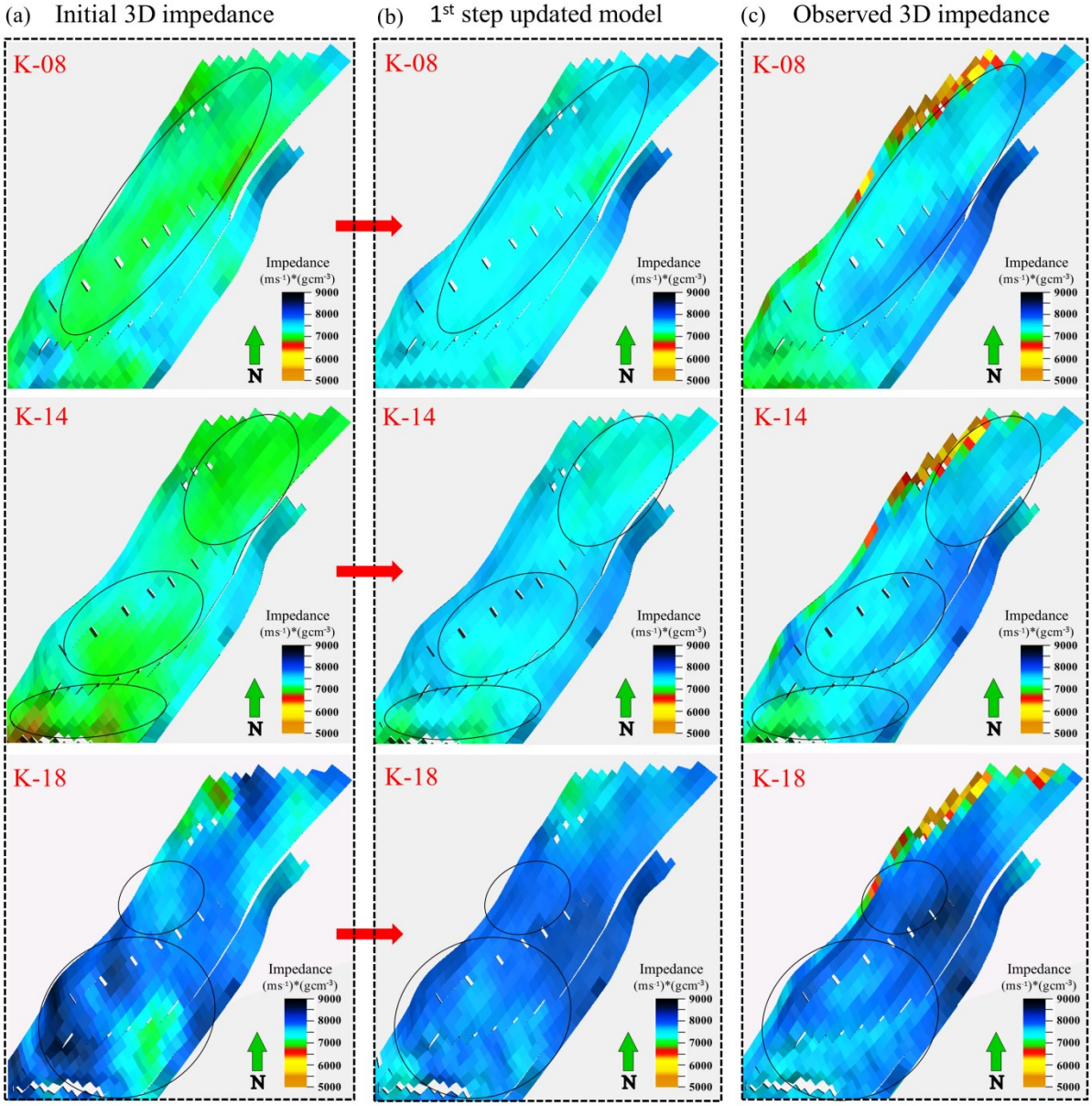

Figure 5.6. Maps of the evolution of matching between the observed and synthetic 3D impedance models throughout our workflow in step 1. Maps of (a) initial synthetic 3D impedance, (b) updated synthetic 3D impedance and (c) observed 3D impedance for the deeper layers of Ile-2 (layer K-08), Tofte-2 (layer K-14) and Tofte-1 (layer K-18) formations (from top to bottom). The ellipses represent the regions of matching improvements with observed 3D model during the porosity adjustments in the first stage of updating methodology.

In the second step of updating, different maps were analyzed for the 4D comparison of synthetic and observed impedance changes from 2001 to 2006, looking for inconsistencies. Primary, we compared the 4D impedance response of initial simulation

model and 4D inversion results to understand the behavior of production activity and certainty of the model adjustments in the first step of updating. We identified several mismatches due to the continuous and consistent decreases in impedance below the sealing Not-1 Formation on the 4D impedance response of initial simulation model, which was less strongly seen on the 4D inversion results. For instance, Figures 5.7a and 5.7d illustrate the 4D impedance response of initial simulation model and seismic inversion results in the deeper zone of Tofte-2 Formation (layer K-14), respectively. Northern regions of segments E and D indicated softening anomaly for both models (Figures 5.7a and 5.7d), where the decreases in impedance were much higher in the initial simulation model compared to seismic inversion results. In contrast, the southern regions of both segments highlighted the contrary 4D anomalies (softening for the initial simulation model and hardening for the 4D inversion results). The possible explanation is that the pore pressure from the initial simulation model might be overestimated and the reservoir model predicted features such as high impedance decreases for the entire regions of segments (Figure 5.7a). This is in agreement with the bottom-hole pressure historical data, where the simulated BHP of initial model for the producers in which perforated below the sealing Not-1 Formation (all the producer wells except E-3AH), indicated higher BHP pressure values regarding the production-historical data (production graphs in Figure 5.9).

Additionally, the observed softening and hardening effects in the 4D inversion results (blue and red anomalies in Figure 5.7d) were previously interpreted by Maleki et al., 2017. The softening anomalies were related to the pore pressure increases from the neighbor water injectors (F-1H, F-2H and F-3H) and hardening anomalies were caused by OWC movement from 2001 to 2006 (water saturation increases) due to the partially water flooded areas between the Ile and Tofte formations. It seems that overestimated pore pressure in the initial simulation model causes softening effects for the 4D impedance responses in the entire regions of segments E and D (Figure 5.7a). In fact, these areas experienced a higher reduction in velocity (consequently in impedance) compared to 4D inversion results and extended throughout southern of segments and dominated the water saturation increases. Thereby, the porosity modifications in the first stage of updating, including various decreases in porosity below the Not-1 Formation, appears consistent with

the production-history graphs of BHP (red dots and dashed black lines in Figure 5.9) and time-lapse seismic interpretation.

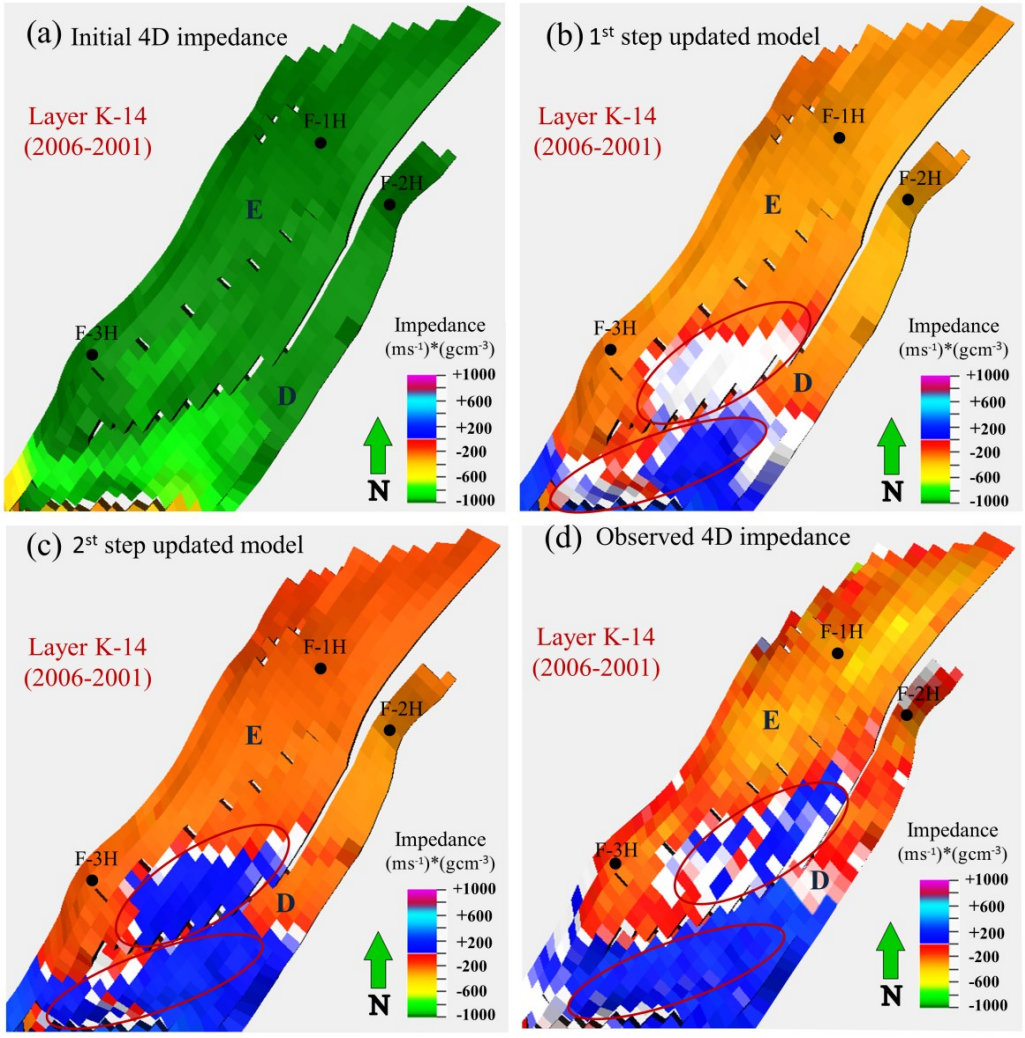

Figure 5.7. Maps of the evolution of matching between the synthetic and observed 4D impedance models (2006 minus 2001) throughout our workflow in steps 1 and 2. Black dots denote well-head position of injectors. (a) Map of initial synthetic impedance variations for the deeper zone of Tofte-2 Formation (layer K-14). (b) Map of updated synthetic impedance variations in the first step of updating for the deeper zone of Tofte-2 Formation (layer K-14). (c) Map of updated synthetic impedance variations in the second step of updating for the deeper zone of Tofte-2 Formation (layer K-14). (d) Map of observed impedance variations for the deeper zone of Tofte-2 Formation (layer K-14). The red ellipses show the regions of matching improvements with observed 4D impedance model during the modifications of permeability in the second stage of updating methodology.

Nevertheless, the porosity adjustments improved the matching of softening anomalies from initial simulation model (northern flank of segments E and D) with the inversion results, some discrepancies were found at the southern flanks of segments between the first step updated model (Figure 5.7b) and the observed 4D inversion results

(Figure 5.7d). The updated simulation model predicted gentle increases in impedance compared to the significant observed increases in impedance (indicated by red ellipses). These inconsistencies suggest re-examination of the reservoir model assumptions. For instance, the blue division along the southern areas of segment E (Figure 5.7d) is not detected in first step of updating (Figure 5.7b), which might be an indication to review the permeability in these areas to improve fluid movements in the simulation model. Thus, following the guidance of 4D comparisons, we modified the fluid flow predictions of the first step updated simulation model (including the multipliers of horizontal and vertical permeability) to resolve the fluid movement. We adjusted the permeability for Tofte and Tilje formations in the southern regions of segments E and D. Figure 5.7c illustrates the synthetic 4D impedance model considering the applied permeability modifications in the second step of updating. It is clear that the synthetic 4D impedance response of new simulation model (Figure 5.7c) and observed impedance variations (Figure 5.7d) implied a fair similar behavior, rather than the first step updated model (Figure 5.7b).

Meanwhile, upper layer of Garn Formation (layer K-01) indicated strong hardening effect on the 4D impedance response of initial simulation model (Figure 5.8a) compared to 4D seismic inversion results (Figure 5.8d). This strong hardening effect was caused by significant decreases in pore pressure of initial simulation model, which is in agreement with the initial simulated BHP data of well E-3AH (blue line in Figure 5.9). Additionally, the softening anomalies in the Garn Formation could be attributed to the gas coming out of solution as pressure decreased in the entire segments E and D and the presence of gas saturation increased (Figure 5.8a). Notably, the softening anomaly of initial simulation model in the segment E appeared more detectable compared to the softening effect in the segment D (Figure 5.8a). Moreover, the initial simulated BHP was lower than the production-history data in well E-3AH after beginning of 2002 (Figure 5.9). It seems that the predicted pressure of initial simulation model might be underestimated for the Garn Formation, which it is in agreement with the porosity adjustments in the first step of updating procedure (various increases in porosity for some regions of Garn Formation). However, we observed gentle decreases in impedance after the first step of updating (blue signals in Figure 5.8b) compared to observed impedance variations (Figure 5.8d), where indicating that simulation model should be revisited for the Garn Formation. Thereby, we

modified the horizontal permeability for the Garn Formation in the segments E and D. The predictions from the second step updating model appeared more consistent with observed 4D inversion results, as shown in Figures 5.8c and 5.8d. In fact, the permeability adjustments improved the values of gas saturation increases in the segment E (Figure 5.8c). Moreover, the strong softening anomaly at the edge of north-western region of segment E (observed 4D impedance results in Figure 5.8d) was interpreted due to the poor imaging as there is no production activity near this area that could cause decreases in impedance and the anomaly was located in the edge region of segment E.

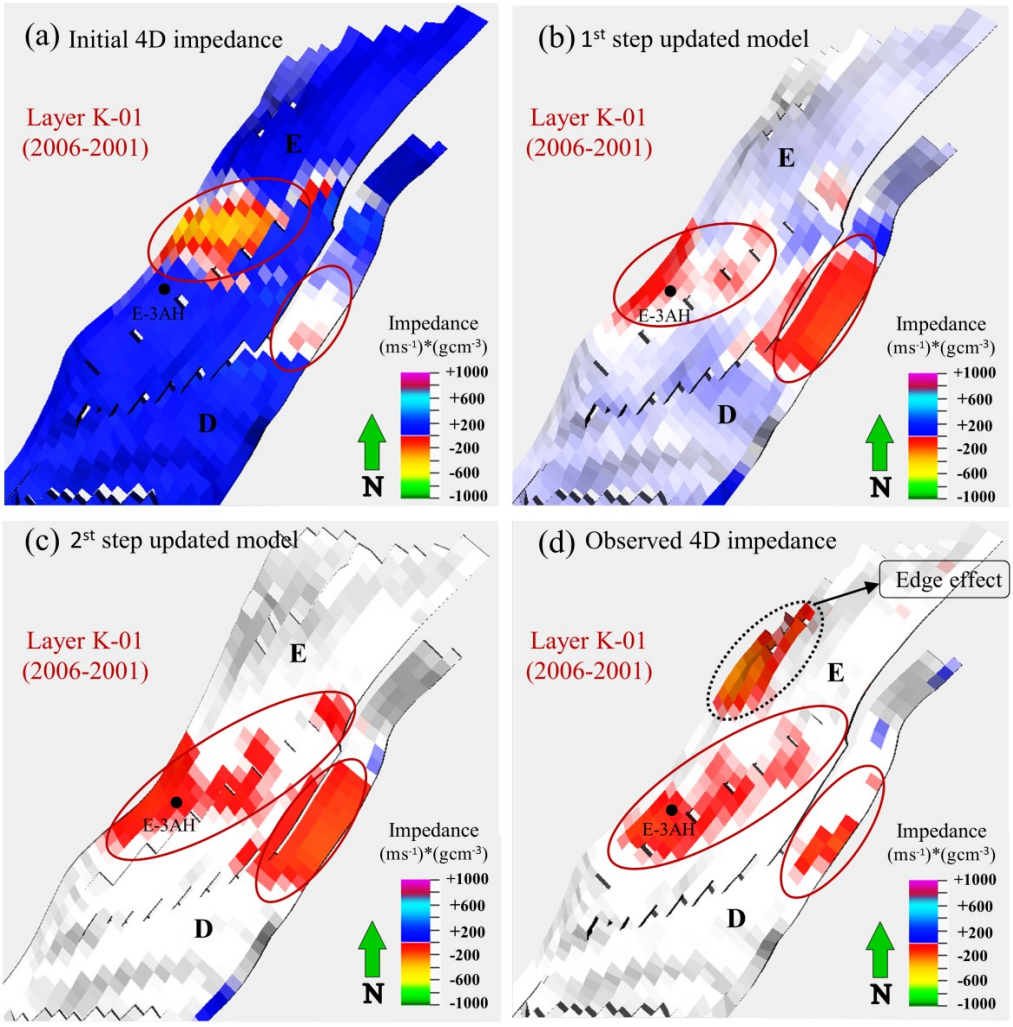

Figure 5.8. Maps of the evolution of matching between the synthetic and observed 4D impedance models (2006 minus 2001) throughout our workflow in steps 1 and 2. Back dot denote well-head position of producer E-3AH. (a) Map of initial synthetic impedance variations for the upper zone of Garn Formation (layer K-01). (b) Map of updated synthetic impedance variations in the first step of updating for the upper zone of Garn Formation (layer K-01). (c) Map of updated synthetic impedance variations in the second step of updating for the upper zone of Garn Formation (layer K-01). (d) Map of observed impedance for the upper zone of Garn Formation (layer K-01). The red ellipses highlight the effect of increases in gas saturation for segments E and D.

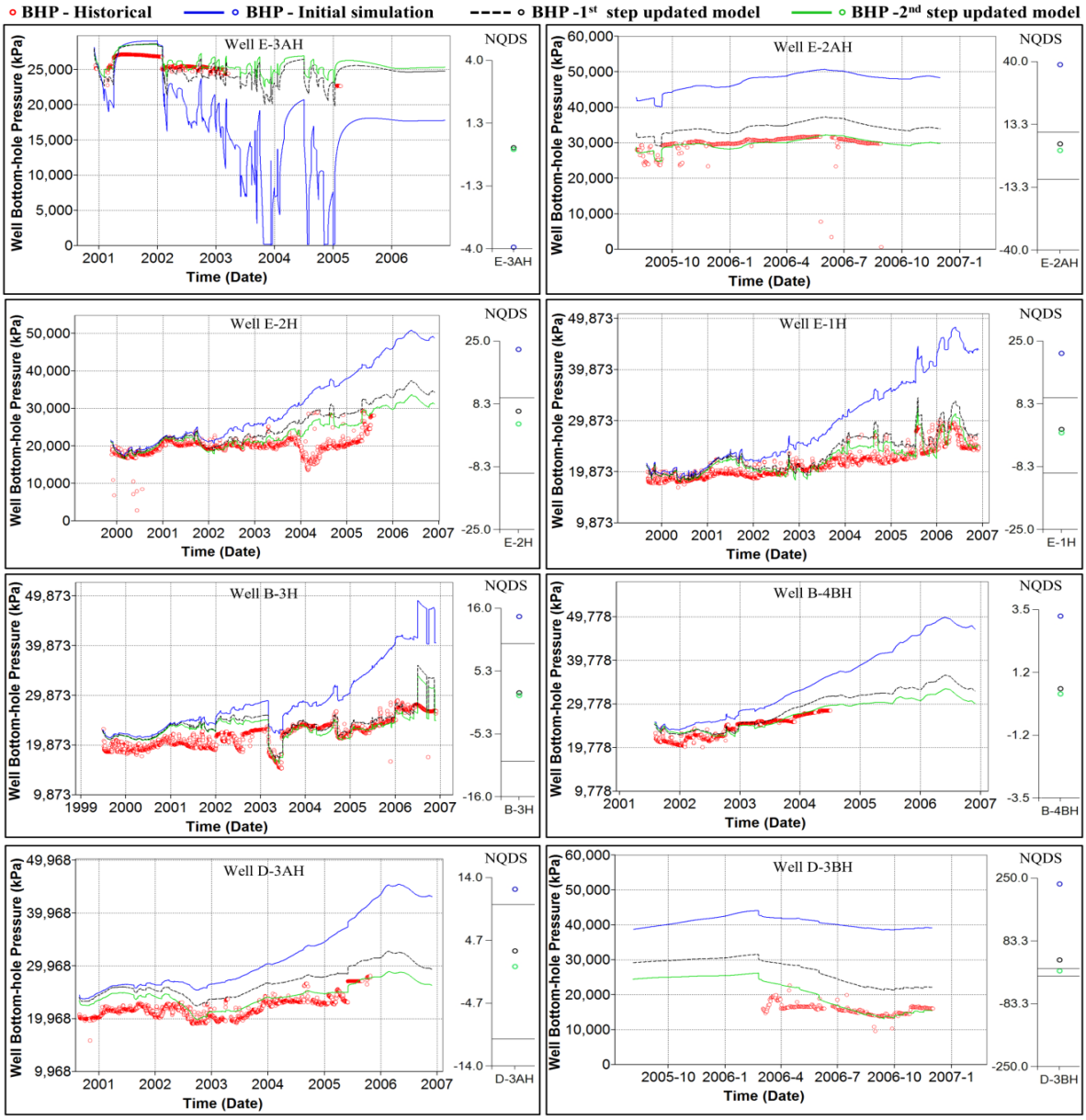

Figure 5.9. The BHP rates through the different updating steps. Red points represent the BHP history data, while blue lines, black dotted and green lines show the BHP of initial, first step updated and second step updated simulation models, respectively. The blue, black and green dots represent the value of NQDS for the initial, first step updated and second step updated simulation models, respectively. Notably, all producers are perforated below the Not-1 formation except well E-3AH.

Alternatively, comparison of the BHP production curves and the quadratic deviations (NQDS) within the updated simulation models indicated enhancement of BHP history matching during the different steps of updating process (Figure 5.10). The NQDS values of the initial simulation model were distributed above and below the acceptance range [-10 10]. Nevertheless, high deviations towards the BHP history-data of initial

simulation model were resolved with the modifications arising from the 3D and 4D impedance observations. Notably, it must be highlighted that the observed initial good match of oil production rate, water production rate, gas production rate and gas-oil ratio were preserved after the updating steps.

Furthermore, we noticed some mismatches between the synthetic 4D impedance response (after the second step of updating) and the observed 4D impedance model throughout the formations below the sealing Not-1 Formation. Figures 5.10a and 5.10c map the observed 4D impedance model and the synthetic 4D impedance response regarding second step of updating strategy in the deeper layers of Ile-1 formation (layer K-11), respectively. The hardening anomalies of observed impedance extended continuously in the southern regions of segments E and D, while the updated synthetic impedance model implied the anomaly to be confined and less strong, especially in the southern region of segment E. Moreover, the updated simulation model estimated significant increases in pore pressure for the southern region of map compared to northern part (Figure 5.10e). Also, there were strong increases in water saturation for the southern flanks of both segments (Figure 5.10d). These discrepancies suggest that the hardening signal appears to be very compartmentalized and less strong in the updated simulation model (Figure 5.10d), as it is overlaid by the high pressure zone. Furthermore, producers E-2H and B-4BH were perforated in the southern regions of segment E and D, in the deeper layers of Ile Formation (Ile-1). These producers started producing more water after October 2001 (B-4BH) and April 2001 (E-2H). Nevertheless good matched of BHP were obtained for these wells considering the second step of updating strategy (green lines in Figure 5.9), the matching of fluid rates (Oil rate (Qo), water rate (Qw) and gas-oil-ratio) with production history-data significantly improved toward the acceptance range of NQDS (between -10 and +10) as shown in Figure 5.11. Subsequently, inconsistencies between the observed and synthetic 4D impedance models and the knowledge of acceptable matched of well production data, suggest that the sensitivity of PEM to pressure should be reconsidered (particularly below the sealing Not-1 Formation).

We therefore calibrated the rock stress sensitivity parameters for three sub-zones of A (Garn Formation), B (Ile and Tofte formations) and C (Tilje Formation) as described in Table 5.5. This separation agrees with geology knowledge of Norne Field, as Tilje

Formation is composed of interbedded sandstones, shales and siltstones, often heterolithic, and an unconformity separates it from the overlying Tofte Formation due to tectonic uplift and subsequent erosion (Swiecicki et al., 1998). The Ile and Tofte formations are contained with fine to medium sandstones interbedded with thinly laminated siltstones, shales and some carbonate-cemented which are separated from Garn Formation (with coarser sandstones) due to the effective Not-1 sealing layer, which breaking the communication between the reservoirs above and below it.

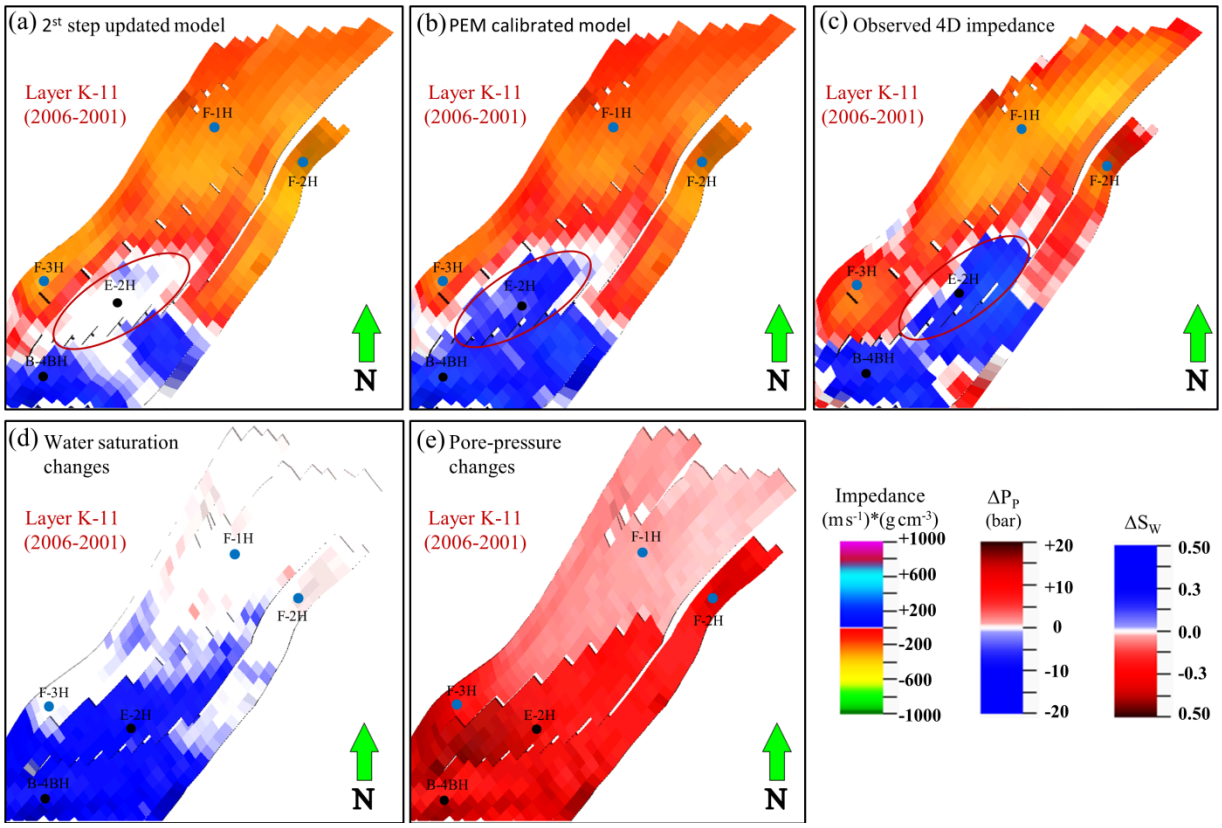

Figure 5.10. Maps of the evolution of matching between the synthetic and observed 4D impedance models (2006 minus 2001) throughout our workflow in step 3. Blue dots denote well-head position of injectors, while black dots represent well-head positions of producers. (a) Map of updated synthetic impedance variations in the second step of updating for the deeper zone of Tofte-2 Formation (layer K-14). (b) Map of updated synthetic impedance variations in the pressure dependency modification for the deeper zone of Ile-1 Formation (layer K-11). (c) Map of observed impedance for the deeper zone of Ile-1 Formation (layer K-11). (d) Map of water saturation changes considering updated simulation model for the deeper zone of Ile-1 Formation (layer K-11). (e) Map of pore-pressure changes considering updated simulation model for the deeper zone of Ile-1 Formation (layer K-11). The ellipses show the regions of matching improvements with observed 4D impedance model during the modifications of pressure sensitivity of PEM in the third stage of updating methodology.

Thus, we calibrated the pressure dependency of PEM for zones B and C (formations below the Not-1 Formation) to capture the approximate same values for both observed and

updated synthetic 4D impedance anomalies. However, the rock stress sensitivity of PEM was not modified for the Garn Formation, as the updated synthetic impedance was consistent with the observed 4D impedance (Figures 5.8c and 5.8d). Moreover, the NQDS of BHP and fluid rates of producer E-3AH (was perforated in the Garn Formation) were in the acceptable range after second step of updating (Figures 5.9 and 5.11). As a matter of fact, the synthetic 4D impedance results derived by calibrated PEM (Figure 5.10b) matched nicely with the observed 4D impedance model (Figure 5.10c), since the actual values of hardening signals in the updated simulation model (caused by water saturation increases) increased more in the southern regions of segments E and D.

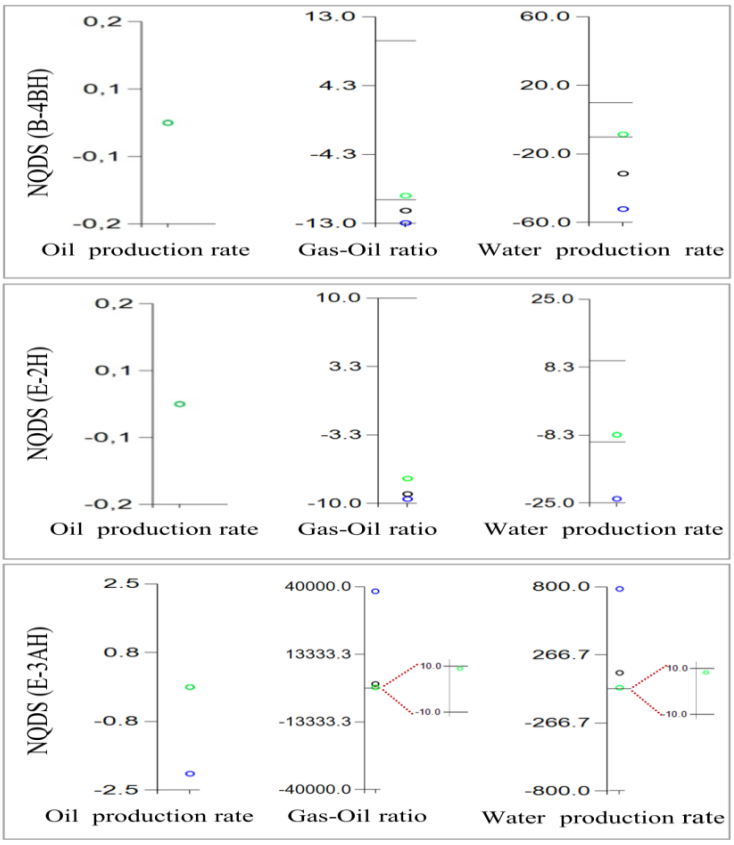

Figure 5.11. NQDS of fluid rates for producers B-4BH, E-2H and E-3AH through the different updating steps. The blue, black and green dots represent the value of NQDS for the initial, first step updated and second step updated simulation models, respectively. Notably, E-3AH is perforated in the Garn Formation, while B-4Bh and E-2H are perforated below the Not-1 Formation. The NQDS of second steps updated model are in the acceptable ranges of -10 to +10.

Table 5.4. Modified pressure dependency of PEM in the Norne reservoir segments of E and D.

Zone	Formation	Layer	P_k	P_μ	E_k	E_μ
A	Garn	K-01 to K-03	5.62	7.97	3	2
B	Ile - Tofte	K-04 to K-18	5.62	7.97	2.50	1.50
C	Tilje	K-19 to K-22	5.62	7.97	3.40	2.40

Figure 5.12 demonstrates the evolution of updating steps in the last step of methodology throughout a profile along segments E and D. The hardening signal in the 4D impedance response of updated simulation model seems to be less compartmentalized and detectable across the eastern region of Fault-1 (Figure 5.12a), as opposed to the observed 4D impedance model (Figure 5.12c). The possible explanation is that the high pressure zone (Figure 5.12d) dominated the water saturation increases in the updated simulation model (Figure 5.12e). Furthermore, the magnitude of decreases in the impedance (softening anomaly in Figure 12a) for the deeper layers (below the top of Tilje Formation) were observed lesser compared to observed 4D impedance model (Figure 5.12c). Subsequently, after the calibration of PEM pressure dependency, the hardening anomaly from the simulation model (caused by water saturation increases) extended more between Ile and Tilje formations and reached to the formations across the eastern region of Fault-1 (Figure 5.12b). Additionally, the calibrated pressure dependency in PEM highlighted more decreases in impedance below the top of Tilje Formation (Figure 5.12b) rather than the updated simulation model (Figure 5.12a), which correlated agreeably with the observed 4D impedance (Figure 5.12c).

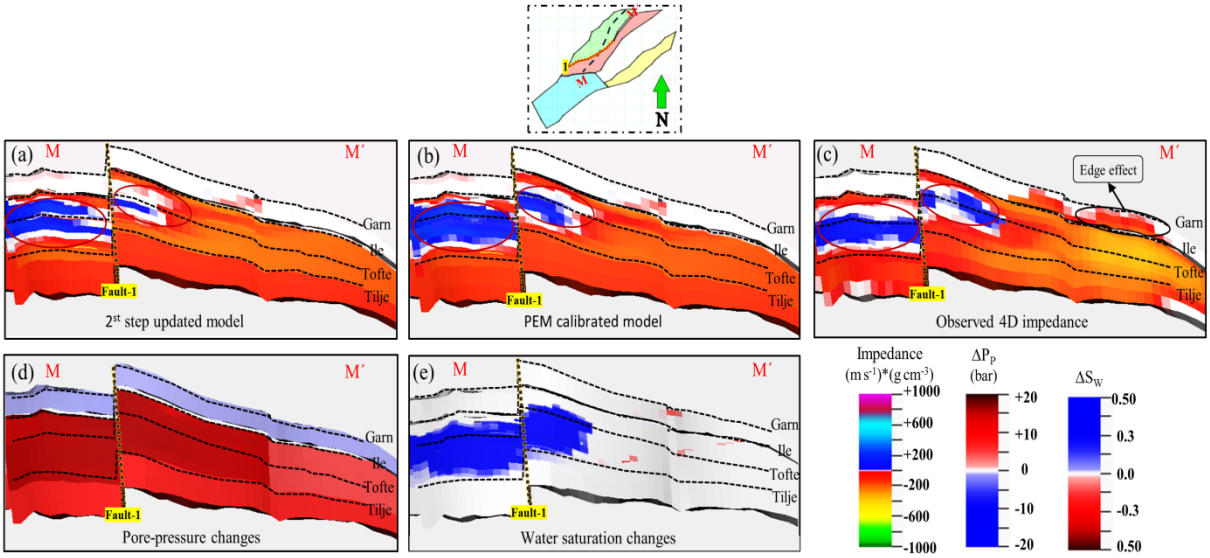

Figure 5.12. A profile of the evolution of matching between the synthetic and observed 4D impedance models throughout our workflow in step 3. Location of the profile in segments E and D is given by the broken line in the thumbnail plot. (a) 4D impedance response of simulation model during the second step of updating. (b) 4D impedance response of simulation model during the calibration of PEM pressure dependency. (c) observed 4D impedance model (derived by inversion results). (d) pore-pressure changes considering second step updated simulation model. (e) water saturation changes considering second step updated simulation model. The ellipses show the regions of matching improvements with observed 4D impedance model during the modifications of pressure sensitivity of PEM in the third stage of updating methodology.

5.6. Conclusions

An updating methodology for reservoir modelling that incorporates data from multiple and diverse sources have been designed. The workflow provides a systematic and quantitative integration to reconcile 3D and 4D seismic impedances, together with the simulation model and historical production-data in order to adjust reservoir simulation response and enhance the interpretive capability of reservoir properties. It also proposes an innovative procedure to calibrate the pressure dependency of petro-elastic model, referring to observed 4D model and matched well production data, to ensure realistic values for changes in in-situ elastic parameters. The proposed procedure is successfully applied to a real case, the benchmark model of the Norne Field.

To thoroughly investigate, we converted the inversion results of base (2001) and monitor (2006) seismic surveys to the simulation scale using time to depth conversion and re-scaling to access the observed impedance models (3D and 4D). Furthermore, the initial synthetic impedance models were generated throughout the rock-physics modeling and initial reservoir flow simulation to convert the extracted dynamic and static properties to elastic properties. The initial estimations of synthetic impedance models (3D and 4D) highlighted significant pressure mismatches which were confirmed by the well pressure data (BHP). Thereby, in the first stage of updating, we compared the observed and initial synthetic 3D impedance models to add realistic heterogeneities into the model. The evaluated inconsistencies from the different sections and maps suggested various decreases in porosity for the formations below the sealing Not-1 and increases in some regions of Garn Formation. These modifications improved the pressure estimation and the matching of softening 4D effects that were caused by pore pressure increases. Subsequently, the second stage of comparison evaluated the consistency between the observed and synthetic 4D seismic impedance models considering the updated model from previous step, looking for discrepancies. Alternatively, we observed some softening anomalies resulting from gas coming out of solution (due to the pore-pressure decreases) in the Garn Formation. Despite these softening effects, the fluid-gradient changes caused the increases in impedance (mainly in the southern regions of segments E and D), where the water contact rise in these segments is a consequence of the production activity up to 2006. Accordingly, we updated the permeability (horizontal and vertical) for the simulation model considering observed 4D

discrepancies. Consequently, the remained incompatible pore-pressure estimation and fluid movement were resolved during the second step of updating.

Meanwhile, we considered the reliability of the updated parameters, referring to production-history data. The history matching results indicated that the applied adjustments were able to update reservoir properties and, thus, produced a simulation model that better followed the observed 3D and 4D seismic impedance data with the capability to overcome the challenges of pressure estimations. In fact, this procedure leaded to significant improvements in NQDS deviations towards the production-history data of BHP and fluid rates within the acceptance range of -10 to +10. Eventually, we calibrated the pressure sensitivity of petro-elastic model, using calibrated simulation model from the previous step (that provides good estimates of pressure) and observed 4D impedance model for the formations below the Not-1 Formation. As a final result of the proposed workflow, we have an updated simulation model consistent with observed seismic and well production data, as well as, a calibrated petro-elastic model.

We have shown that joint integration of 3D and 4D seismic impedance models with the flow-simulation model results (in an iterative loop) builds confidence in identifying the properties and specific regions of the field where updates to the simulation model might be appropriate. Indeed, the proposed quantitative integration is key to close the loop between seismic and engineering domains, providing valuable input for reservoir characterization and monitoring in the Norne Field. Additionally, as Norne Field is a benchmark case, these results can be considered to enrich the discussions over deterministic and probabilistic seismic history-matching studies.

6. CONCLUSIONS

The current thesis proposed four sequence of procedures in the realistic case of Norne Filed: (1) various 3D model-based inversion to analyze the influence of well constraint, in which is fundamental to improve the reservoir characterization and provide more robust understanding of reservoir framework, (2) a procedure to highlight the advantages of time-lapse seismic interpretation in terms of seismic impedance variations compared to standard seismic amplitude differences, (3) a qualitative time-lapse seismic interpretation scheme that uses 4D seismic inversion results, well-history and engineering data to identify anomalies caused by production-related changes and the injected fluids and (4) a reservoir simulation model updating workflow that quantitatively integrates 3D and 4D seismic impedance data, in a feedback loop, to evaluate the consistency between the reservoir simulation model and seismic data considering the uncertainty of the pressure sensitivity in the rock physics model. In addition to the methodologies, which can be seen as the main results of this work, especially the third and the fourth, there are some important results specific to each of the four of them, which should be highlighted.

From the various 3D seismic inversion (including different number and position of wells), it can be concluded that:

- We highlight the importance of the varied number and position of wells to estimate the initial impedance model, particularly in structurally complex geological area of Norne Field.
- Despite the challenging seismic to well calibration of the deviated wells, the seismic modeling outcome of the 9-well constrained inversion is implied reliable and more robust interpretation than 2-well constrained in which may affect the accuracy of reservoir characterization and geological modelling of Norne Field.
- The derived impedance results from nine wells indicate that the Garn, Ile and Tofte formations are the possible main reservoirs due to their low impedance zones, which is in agreement with previous studies.

The results obtained from the comparison in Article-2 presented the advantage of time-lapse seismic interpretation in terms of seismic impedance variations compared to the standard seismic amplitude differences. Some of the results to be highlighted are:

- Opposed to seismic amplitude, which are sensitive to layer interface properties, inversion replaces the seismic signal by a blocky impedance response, and also improves interdisciplinary communication.
- The amplitude and impedance changes are compared in the segment C of Norne Field to evaluate the impact of different seismic attributes in time-lapse seismic interpretation and shed light on the 4D seismic anomalies. It seems that both estimated acoustic impedance changes (softening and hardening signals) improved significantly the vertical resolution compared to standard amplitude differences where there are associated production-induced effects within reservoir; including a better delineation of the water movements and pressure variations are achieved.
- Meanwhile, the impedance variations of model-based inversion procedure present clearer images of the reliable 4D anomalies compared to coloured inversion.

The combined interpretation methodology presented in Article-3 (joint interpretation of time-lapse seismic inversion with the production-history data and flow-simulation model results) is key to understanding production/injection effects within the reservoir segments of the Norne benchmark case. Some of the results to be highlighted are:

- This type of time-lapse seismic interpretation technique enables to qualify the 4D seismic effects in terms of P-impedance variations and identifies the production effects in the Norne benchmark case which is valuable input for the reservoir characterization.
- The inverted 4D impedance anomalies are resulted from competing production effects, such as pore-pressure and saturation changes, associated with the injection of water and gas and the production of oil. Furthermore, we consider the reliability of the observed anomalies, referring to production/injection history data.
- Most softening anomalies are located in areas surrounding injector wells, strongly indicating that increased pore-pressure overshadowed the saturation replacement effects.
- Despite these softening effects, the fluid-gradient change (zones with rising water levels replacing hydrocarbon) causes the increases in impedance that can be seen mainly in segments E, D and C, where the water contact rise in these segments is a consequence of the production activity up to 2006.

- The comparison of the 4D impedance anomalies with the available simulation model of Norne benchmark case (non-history-matched) indicates the regions of the flow model to be further updated.

The methodology presented in Article-4 provides a systematic and quantitative integration of inverted seismic data (3D and 4D) and engineering studies to develop an updating procedure for adjusting reservoir simulation response and enhance the interpretive capability of reservoir properties. It also proposes an innovative procedure to calibrate the pressure dependency of petro-elastic model, referring to observed 4D impedance data and matched production-history data, to ensure realistic values for changes in in-situ elastic parameters. Some points to highlight for the fourth and last article of this thesis are:

- The proposed procedure applies on the segment E and D of Norne Field. The observed 3D and 4D impedance results become more useful when integrated quantitatively with reservoir flow simulation model, and with production-history data.
- The methodology allows checking the reservoir behavior (geological framework and flow), taking into account the reservoir static and dynamic properties uncertainties, to verify that it is in agreement with the 3D and 4D seismic impedance data. Thus, it can be useful to identify possible adjustments in the initial reservoir simulation model.
- The 3D comparison of observed and initial impedance models adds a significant control to the porosity modifications and resulting in model with more reliable pressure estimations.
- The 4D comparison of observed and initial impedance models provides the permeability adjustments to resolve the remained discrepancies and improves the estimation of water saturation changes below the Not-1 Formation and gas saturation increases in the Garn Formation.
- The history matching results indicate that the applied methodology produces a simulation model able to better follow the 3D and 4D seismic impedance data, as well as well-history data. In fact, initial estimations of synthetic impedance models (3D and 4D) highlight improper estimation of reservoir flow simulation model and considerable initial well pressures mismatches which are confirmed by BHP data.

- This procedure leads also to significant improvements in NQDS deviations towards the production-history data of BHP and fluid rates within the acceptance range.
- There is a risk when automatically implementing updates to the simulation model using observed seismic and simulation comparison techniques (due to the uncertain PEM setting). Therefore, we propose to first ensure that the simulation model provides reasonable pressures estimates, which in our case was supported by BHP measurements and then revisit the petro-elastic modeling evaluating the calibration of the pressure sensitivity. The results allow reduction of errors in some regions of the estimated impedance changes, where, according to the updated simulation model, hardening signals are not observed.
- The presented methodology provides a geologically consistent reservoir model that matches the production data, the static data, and the available geological knowledge, improving the reservoir characterization of Norne benchmark database.

6.1. Future research directions

The procedures presented in this work could be extended and improved in future research studies:

- Extension of the quantitative integration methodology to other regions of the Norne Field.
- The 4D and 3D seismic inversion were carried out in the post-stack amplitude data by calculating the P-wave impedance (3D and variations). However, a second seismic attribute with a different response to the changes in dynamic properties is S-wave impedance. Thus, further quantitative integration support might be achieved from time-lapse amplitude v. offset (AVO) analysis or pre-stack inversion procedure to provide both compressional and shear impedance anomalies that could improve the interpretation of seismic data and reservoir characterization by separating fluid and pore pressure effects.
- In this study the history matching process was performed in a deterministic way which was substantial to calibrate the PEM. Further research should attempt for a probabilistic approach (or automatic history matching) using the provided PEM.

- The quantitative integration of reservoir simulation model and 4D seismic data could be extended to be performed in different domains (e.g. amplitude or pressure and saturation). For instance, in the case of pressure and saturation domain, the sequence would be: (1) estimate of the pressure and saturation changes from 4D seismic through a petro-elastic inversion procedure, (2) use multiple simulation models to constrain the estimation of pressure and saturation from 4D seismic, (3) performance of a history matching, (4) use of the new updated reservoir properties to go back to step 1 and repeat all the cycle until a satisfactory matching is reached.
- It is important to note that the dataset used was acquired and processed more than a decade ago. Modern acquisition techniques and processing algorithms are very likely to provide more reliable data. For instance, repeated well logging with wireline re-entry into wells can be useful to build the precise monitor initial model (for 4D seismic inversion) or more recent seismic acquisition tools such as broadband, ocean bottom seismic (OBS), ocean bottom nodes (OBN) and permanent reservoir monitoring system (PRM) could improve the resolution and repeatability of the time-lapse seismic data.

REFERENCES

AARRE, V. Estimating 4D velocity changes and contact movement on the Norne Field. In: **SEG Technical Program Expanded Abstracts 2006**. Society of Exploration Geophysicists, 2006. p.3115–3119.

ABUBAKAR, A.; VAN DEN BERG, P.; FOKKEMA, J. A feasibility study on nonlinear inversion of time-lapse seismic data. In: **SEG Technical Program Expanded Abstracts 2001**. Society of Exploration Geophysicists, 2001.

AMINI, H. **A pragmatic approach to simulator-to-seismic modelling for 4D seismic interpretation.** 2014. 270p. Thesis (PhD) - Heriot-Watt University.

ASCHJEM, G. **Mapping reservoir changes using 4D seismic on the Norne G-segment, Norwegian Sea**. 2013. 75p. MSc dissertation - Norwegian University of Science and Technology, Norway.

AVANSI, G.D.; MASCHIO, C.; SCHIOZER, D.J. Simultaneous history-matching approach by use of reservoir-characterization and reservoir-simulation studies. **SPE Reservoir Evaluation & Engineering**, v.19, p.694–712, 2016.

AYZENBERG, M.; HUSTOFT, L.; SKJEI, N.; FENG, T. Seismic 4D Inversion for Quantitative Use in Automated History Matching. In: 75th **EAGE Conference and Exhibition incorporating SPE EUROPEC**. 2013

BECQUEY, M.; LAVERGNE, M.; WILLEM, C. Acoustic impedance logs computed from seismic traces. **Geophysics**, v.44, p.1485–1501, 1979.

BERTEUSSEN, K.A.; URSINL, B. Approximate computation of the acoustic impedance from seismic data. **Geophysics**, v.48, p.1351–1358, 1983.

BOUTTE, D. Through the continuous life cycle of reservoir, geophysics makes its mark. **The Leading Edge**, v.26, n.11, p.1376–1379, 2007. Society of Exploration Geophysicists.

BRICENO, A.; MACBETH, C.; MANGRIOTIS, M. D. Towards an Effective Petroelastic Model for Simulator to Seismic Studies. In: **78th EAGE Conference and Exhibition**. 2016.

BULAND, A.; El OUAIR, Y. Bayesian time-lapse inversion. **Geophysics**, v.71, p.R43–R48, 2006.

BYERLEY, G.; SINGER, L.; ROSE, P. Resaturated pay: A new infill target type identified through the application and continuous improvement of 4D seismic at the Forties Field. **The Leading Edge**, v.35, n.10, p.831-838, 2016. Society of Exploration Geophysicists.

CALVERT, R. Insights and Methods for 4D Reservoir Monitoring and Characterization. **SEG/EAGE Distinguished Instructor Short Course**, 2005.

CHENG, N.; OSDAL, B. Updating the Norne Reservoir Model Using 4D Seismic Data. In: **IO Workshop, Center for Integrated Operations in the Petroleum Industry at NTNU,** Trondheim, Norway. 2008.

COOKE, D.A.; SCHNEIDER, W.A. Generalized inversion of reflection seismic data. **Geophysics**, v.48, p.665–676, 1983.

CORREIA, G. G.; SCHIOZER, D. J. Reservoir characterization using electrofacies analysis in the sandstone reservoir of the Norne Field (offshore Norway). **Petroleum Geoscience**, v.22, p.165–176, 2016.

CORREIA, G. G. Integration of reservoir characterization with history matching guided by pilot wells: application to the Norne Field. 2017. 218p. Thesis (PhD) – University of Campinas (UNICAMP), Brazil.

DADASHPOUR, M.; CIAURRI, D.E.; KLEPPE, J.; LANDRØ, M. Porosity and permeability estimation by integration of production and time-lapse near and far offset seismic data**. Journal of Geophysics And Engineering**, v.6, n.4, p.325–344, 2009.

DALLAND, A.; WORSLEY, D.; OFSTAD, K. A lithostratigraphic scheme for the Mesozoic and Cenozoic succession offshore mid- and northern Norway. **Norwegian Petroleum Directorate Bulletin***,* v.4, p.1–65, 1988.

DE MARSILY, G.; LAVEDAN, G.; BOUCHER, M.; FASANINO, G. **Interpretation of interference tests in a well field using geostatistical techniques to fit the permeability distribution in a reservoir model**. In: Geostatistics natural resources characterization, Part 2, p.831–849, 1984.

ELLISON, A. Modeling, philosophy and limitation. **Computing & Control Engineering Journal**, v.4, n.4, p.190–192, 1993.

EL OUAIR, Y.; LYGREN, M.; OSDAL, B.; HUSBY, O.; SPRINGER, M. Integrated reservoir management approach: From time-lapse acquisition to reservoir model update at the Norne Field. In: **International Petroleum Technology Conference**, Doha, Qatar, 21–23 November, 2005. Doi: 10.2523/10894-MS

FANCHI, J. R. **Principles of Applied Reservoir Simulation (2nd Edition)**. Gulf Professional Publishing. 2001, 356p.

FRANCIS, A. Acoustic impedance inversion pitfalls and some fuzzy analysis. **The Leading Edge,** v.26, n.3, p.275–280, 1997.

GASSMANN, F. Elastic waves through a packing of spheres. **Geophysics,** v.16, n.4, p.673-685, 1951. Society of Exploration Geophysicists.

GLUCK, S.; DESCHIZEAUX, B.; MIGNOT, A.; PINSON, C.; HUGUET, F. Time-lapse impedance inversion of post-stack seismic data. In: **SEG Technical Program Expanded Abstracts 2000**. Society of Exploration Geophysicists, 2000. p.1509–1512.

GOODWAY, B.; CHEN, T.; DOWNTON, J. Improved AVO fluid detection and lithology discrimination using Lamé petrophysical parameters; "λρ", "μρ", & "λρ/μρ" fluid stack, from P and S inversions. In: **SEG Technical Program Expanded Abstracts 1997**. Society of Exploration Geophysicists, 1997. p.183–186.

GOSSELIN, O.; AANONSEN, S.I.; AAVATSMARK, I.; COMINELLI, A.; GONARD, R.; KOLASINSKI, M.; FERDINANDI, F.; KOVACIC, L.; NEYLON, K. History Matching Using Time-lapse Seismic (HUTS). In: **SPE Annual Technical Conference and Exhibition**, **SPE 84464-MS**. Colorado, USA, 5–8 October, 2003.

GREAVES, R.J.; FULP, T.J. Three-dimensional seismic monitoring of an enhanced oil recovery process. **Geophysics**, v.52, n.9, p.1175–1187, 1987.

GUDERIAN, K.; KLEEMEYER, M.; KJELDSTAAD A.; PETTERSSON S.E.; REHLING, J. Draugen field: Successful reservoir management using 4D seismic. In: **65th EAGE Conference and Exhibition**. 2003.

HAMMER, E.; MØRK, M.B.E.; NÆSS, A. Facies controls on the distribution of diagenesis and compaction in fluvial-deltaic deposits. **Marine and Petroleum Geology**. v.27, n.8, p.1737–1751, 2010.

HE, W.; MACBETH, C. 4D seismic inversion designed for direct simulation model comparison. In: **Beijing International Geophysical Conference and Exposition**, Beijing, China, 24–27 April, 2009. https://doi.org/10.1190/1.3603776

HOFFMAN, B.T. **Geologically consistent history matching while perturbing facies**. 2005. 300p. Thesis (PhD) - Stanford University.

HOFFMAN, B.T.; CAERS, J. History matching by jointly perturbing local facies proportions and their spatial distribution: Application to a Norne Sea reservoir. **Journal of Petroleum Science and Engineering**. v.57, p.257–272, 2007**.**

HUANG, Y.; MACBETH, C.; BARKVED, O.; GESTEL, J.P.; DYBVIK, O.P. Enhanced dynamic interpretation from correlating well activity to frequently acquired 4D seismic signatures. **The Leading Edge**, v.30, n.9, p.1042–1050, 2011. Society of Exploration Geophysicists.

HUANG, Y.; ALSOS, T.; SØRENSEN, H.M.; TIAN, S. Proving the value of 4D seismic data in the late-life field–Case study of the Norne main field. **First Break**, v.31, n.9, p.57–67, 2013.

HUANG, X.; KELKAR, M.; CHOPRA, A.; YANG, C. T. Wavelet sensitivity study on inversion using heuristic combinatorial algorithms. In: **SEG Technical Program Expanded Abstracts 1995**. Society of Exploration Geophysicists, 1995. p.1088–1090.

JOHNSTON, D. H. **Practical Applications of Time-lapse Seismic Data.** Society of Exploration Geophysicists. Tulsa, OK, USA, 2013, 270p.

KOSTER, K.; GABRIELS, P.; HORVEI, A. Reservoir monitoring of the Draugen Field through time-lapse Seismic and it's business impact. In: Abu Dhabi International Petroleum Exhibition and Conference, **SPE 87300-MS**. Abu Dhabi, United Arab Emirates, 13–15 October, 2000. https://doi.org/10.2118/87300-MS

LAFET, Y.; DUBOZ, P.; DESCHIZEAUX, B.; LEFEUVRE, F.; HUBANS, C. 4-D Stratigraphic Inversion of the Girassol Field–Towards a More Quantitative Approach. In: **67th EAGE Conference & Exhibition**. 2005.

LANCASTER, S.; WHITCOMBE, D. Fast-track 'coloured' inversion. In: **SEG Technical Program Expanded Abstracts 2000**. Society of Exploration Geophysicists, 2000. p.1572–1575.

LANDRØ, M.; SOLHEIM, O. A.; HIDLE, E.; EKREN, B. O.; STRØNEN, L. K. The Gullfaks 4D seismic study. **Petroleum Geoscience**, v.5, p.213–226, 1999.

LANDRØ, M. Discrimination between pressure and fluid saturation changes from time-lapse seismic data. **Geophysics**, v.66, p.836–844, 2001.

LANDRØ, M. 4D seismic. In: Bjorlykke, K. (ed.) Petroleum Geoscience: **From Sedimentary Environments to Rock Physics**. Springer, Berlin, p.427–444, 2010.

LEVY S.; FULLAGAR, P. K. Reconstruction of a sparse spike train from a portion of its spectrum and application to high resolution deconvolution. **Geophysics**, v.46, p.1235–1243, 1981.

LINDSETH, R. O. Synthetic sonic logs: a process for stratigraphic interpretation. **Geophysics**, v.44, p.3–26, 1979.

LORENZEN, R. J. L. **Inversion of multicomponent time-lapse seismic data for reservoir characterization of Vacuum field, New Mexico**. 2000. 378p. Thesis (PhD) - Colorado School of Mines, USA.

LUCIA, F. J. **Carbonate Reservoir Characterization. An Integrated Approach**. Austin: Springer, 2007. 336p.

LYGREN, M.; HUSBY, O.; OSDAL, B.; EL OUAIR, Y.; SPRINGER, M. History matching using 4D seismic and pressure data on the Norne field. In: **67th EAGE Conference & Exhibition.** 2005.

MACBETH, C. A classification for the pressure-sensitivity properties of a sandstone rock frame. **Geophysics**, v.69, n.2, p.497-510, 2004.

MALEKI, M.; DAVOLIO, A.; SCHIOZER, D.J. Reservoir characterization using model based post-stack inversion: a case study in Norne field to show the impact of the number of wells in inversion. In: **Rio Oil & Gas Expo and Conference**, **IPB1957_16**, Rio de Janeiro, Brazil, 24–27 October, 2016.

MALEKI, M.; DAVOLIO, A.; SCHIOZER, D.J. Using simulation and production data to resolve ambiguity in interpreting 4D seismic inverted impedance in the Norne Field. **Petroleum Geoscience**, 2017. https://doi.org/10.1144/petgeo2017-032

OSDAL, B.; ALSOS, T.; Seismic modelling of eclipse simulations and comparison with real 4D data at the Norne Field. In: **64th EAGE Conference & Exhibition**. 2002.

OSDAL, B. Using high quality and repeatable q-marine data in reservoir monitoring on the Norne Field. In: **66th EAGE Conference and Exhibition**, 2004.

OSDAL, B.; HUSBY, O.; ARONSEN, H.A.; CHEN, N.; ALSOS, T. Mapping the fluid front and pressure buildup using 4D data on Norne Field. **The Leading Edge**, v.25, n.9, p.1134–1141, 2006. Society of Exploration Geophysicists.

OSDAL, B.; ALSOS, T. Norne 4D and reservoir management – the keys to success. In: **72th EAGE Conference and Exhibition incorporating SPE EUROPEC**. 2010.

PETERS, L.; ARTS, R.; BROUWER, G.; GEEL, C.; CULLICK, S.; LORENTZEN, R.J.; CHEN, Y.; DUNLOP, N.; VOSSEPOEL, F.C.; XU, R.; SARMA, P.; ALHUTHALI, A.H.H.; REYNOLDS, A. Results of the Brugge benchmark study for flooding optimization and history matching. **SPE Reservoir Evaluation & Engineering**, v.13, p.391–405, 2010.

PETERSON, R. A.; FILLIPONE, W. R.; COKER, F. B. The synthesis of seismograms from well log data. **Geophysics**, v.20, p.516– 538, 1955.

ROGGERO, F.; DING, D.Y.; BERTHET, P.; LERAT, O.; CAP, J.; SCHREIBER, P.E. Matching of production history and 4D seismic data: Application to the Girassol Field, offshore Angola. In: **SPE Annual Technical Conference and Exhibition**, **SPE-109929-MS**, California, USA, 11–14 November, 2007.

ROGGERO, F.; LERAT, O.; DING, D.Y.; BERTHET, P.; BORDENAVE, C.; LEFEUVRE, F.; PERFETTI, P. History matching of production and 4D seismic data: Application to the Girassol Field, offshore Angola. **Oil & Gas Science and Technology**, v.67, n.2, p. 237–262, 2012.

RUSSELL, B. H.; HAMPSON, D.P. A comparison of post-stack seismic inversion methods. In: **SEG Technical Program Expanded Abstracts 1991**. Society of Exploration Geophysicists, 1991. p.876–878.

RUSSELL, B. H. **Introduction to Seismic Inversion Methods**. Society of Exploration Geophysicists. Tulsa, OK, USA, 1998, 178p.

RWECHUNGURA, R.W.; SUWARTADI, E.; DADASHPOUR, M.; KLEPPE, J.; FOSS, B. The Norne Field Case – A unique comparative case study. In: **SPE Intelligent Energy Conference and Exhibition**, **SP-127538**, Utrecht, Netherlands, 23–25 March, 2010.

SANTOS, J. M. C.; DAVOLIO, A.; SCHIOZER, D.J. 4D seismic interpretation of the Norne Field – A semi-quantitative approach. In: **78th EAGE Conference and Exhibition**. 2016.

SANTOS, J. M. C. **Semi-quantitative 4D seismic interpretation integrated with reservoir simulation: application to the Norne Field**. 2017. 108p. MSc dissertation – University of Campinas (UNICAMP), Brazil.

SARKAR, S.; GOUVEIA, W.; JOHNSTON, D. On the inversion of time-lapse seismic data. In: **SEG Technical Program Expanded Abstracts** 2003. Society of Exploration Geophysicists, 2003. p.1489–1492.

SENGBUSH, R. L.; LAWRENCE, P. L.; MCDONALD, F. J. Interpretation of synthetic seismograms. **Geophysics**, v.26, p.138–157, 1961.

SHAMSA, A.; LINES, L. A case study in the application of inversion methods to a Persian Gulf reservoir. In: **SEG Technical Program Expanded Abstracts** 2010. Society of Exploration Geophysicists, 2010. p.2896–2900.

SIX, B.; COLNARD, O. ; AZIEZ, Y. ; COULON, J.; CAILLY, F. 4-D seismic inversion – A case study offshore Congo. In: **75th EAGE Conference and Exhibition incorporating SPE EUROPEC**. 2013

SKJERVHEIM, J.A.; EVENSEN, G.; AANONSEN, S.I.; RUUD, B.O.; JOHANSEN, T.A. Incorporating 4D seismic data in reservoir simulation models using ensemble kalman filter. **SPE Journal**, v.12, p.282–292, 2007. https://doi.org/10.2118/95789-PA

STATOIL. **Annual reservoir development plan/Norne Field**, Support Documentation, 2004.

STEFFENSEN, I.; KARSTADT, P.I. Norne field development – fast track from discovery to production. **Journal of Petroleum Technology**, v.48, p.296–339, 1996.

STEPHEN, K.D.; SOLDO, J.; MACBETH, C.; CHRISTIE, M.A. Multiple model seismic and production history matching: a case study. **SPE Journal**, v.11, p.418–430, 2006.

STEPHEN, K.D.; MACBETH, C. Reducing reservoir prediction uncertainty by updating a stochastic model using seismic history matching. **SPE Reservoir Evaluation & Engineering**, v.11, p.991–999, 2008. https://doi.org/10.2118/100295-PA

STOVAS, A.; LANDRØ, M. Fluid-pressure discrimination in anisotropic reservoir rocks – A sensitivity study. **Geophysics**, v.70, p.O1–O11, 2005.

STRONEN, K.L.; DIGRANES, P. The Gullfaks Field - 4D seismic enhances oil recovery and improves the reservoir description. In: **62th EAGE Conference and Exhibition**. 2000.

SUMAN, A. **Joint Inversion of production and time-lapse seismic data: Application to Norne Field**. 2013. 173p. Thesis (PhD) - Stanford University.

SWIECICKI, T.; GIBBS, P.; FARROW, G.; COWARD, M.P. A tectonostratigraphic framework for the Mid-Norway region. **Marine and Petroleum Geology**. v.15, n.3, p.245–276, 1998.

TIAN, S.; MACBETH, C.; SHAMS, A.; Updating the reservoir model using engineering-consistent 4D seismic inversion. In: **76th EAGE Conference and Exhibition**, 2014.

TIAN, S. **Closing the loop by engineering consistent 4D seismic to simulator inversion.** 2014. 216p. Thesis (PhD), Heriot-Watt University, Edinburgh.

TURA, A.; LUMEY, D. Estimating pressure and saturation changes time-lapse AVO data. In: **SEG Technical Program Expanded Abstracts 1999**. Society of Exploration Geophysicists, 1999. p. 1655–1658.

TURA, A.; BARKER, T.; CATTERMOLE, P.; COLLINS, C.; DAVIS, J.; HATCHELL, P., KOSTER, K.; SCHUTJENS, P.; WILLS, P. Monitoring primary depletion reservoirs using amplitudes and time shifts from high-repeat seismic surveys. **The Leading Edge**, v.24, no.12, p.1214–1221, 2005.

TURA, A.; ETUK, U.; UDO, S. Using time-lapse seismic for field development at Nembe Creek, Nigeria. **The Leading Edge**, v.25, no.9, p.1142–1149, 2006.

TURA, A.; DOBBS, S.; DAVIES, K.; HERMANN, O.; ZHANG, J. Remaining oil thickness and well positioning using 4D at Alba Field, North Sea. In: **SEG Technical Program Expanded Abstracts 2009**. Society of Exploration Geophysicists, 2009. p.3944–3948.

VEDANTI, N.; and SEN, M. K. Seismic inversion tracks in situ combustion: A case study from Balol oil field, India. **Geophysics**, v.74, p.B103–B112, 2009.

VEEKEN, P. C. H.; DA SILVA, M. Seismic inversion methods and some of their constraints. **First break**, v.22, p.47–70, 2004.

VERLO, S. B.; HETLAND, Mari. **Development of a field case with real production and 4D data from the Norne Field as a benchmark case for future reservoir simulation model testing.** 2008. 123p. MSc dissertation - Norwegian University of Science and Technology, Norway.

WALKER, C.; ULRYCH, T. J. Autoregressive recovery of the acoustic impedance. **Geophysics**, v.1548, p.1338–1350, 1983.

WILLIAMSON, P.; CHERRETT, A.; SEXTON, P. A new approach to warping for quantitative time–lapse characterisation. In: **69th EAGE Conference and Exhibition incorporating SPE EUROPEC**. 2007.

YAN, T. **History matching of production and 4D seismic data: Application to the Norne Field.** 2014. 104p. MSc dissertation - Norwegian University of Science and Technology, Norway.

APPENDIX A - Complementary results of Article-1

Article-1 presents some discussions concerning the various model-based 3D seismic inversions, including different number and position of wells. However, the challenges facing inversion analysis of the 9-well constrained are significant due to the difficulty of proceeding inversion with an appropriate estimated wavelet and set of inversion parameters that provide high correlation for the all nine wells. During the well to seismic calibration step, we extracted different statistical wavelets for each well, in which indicated high correlation between seismic data and synthetic seismogram at the well location. Meanwhile, defining the best set of inversion parameters for all the nine wells could be challenging as it is linked to the type of constraint, average block sizes, prewhitening percent and number of iteration. The constraint defines the initial guess as a starting point for the inversion and sets boundaries on how far impedance may deviate from the initial guess. Hard constraint is related to the maximum allowable deviations in absolute impedance as a percentage of the average impedance of the constraint log. However, the soft constraint does not set any absolute bounds on how far the impedance can move from the initial guess. In fact, this process balances the seismic trace and the initial guess impedance, using the relative weights. For instance, the value 0 for soft constraint represents that initial guess is ignored; while the value 1 indicates that seismic trace is ignored. Thus, the values between 0 and 1 donates that both initial guess and seismic trace are weighted. Meanwhile, the average block size sets the thickness in milliseconds for the initial equal travel-time layers of the model. The prewhitening is basically a noise level that is added to the amplitude spectrum of the data before analysis which is needed to stabilize the operation of inversion. Moreover, high number of iterations improves the convergence, while increasing the run time.

Thereby, we divided the analysis of inversion parameters in the 9-well constrained case into two main steps: 1) estimate an appropriate wavelet for the inversion, supported by constant inversion parameters; 2) choose the best set of inversion parameters considering the chosen wavelet from previous step. For instance, Figure A.1 illustrates the inversion analysis plot for the well B-4H including three different statistical wavelets (M-1, M-2 and M-3). P-wave impedance error represents the RMS deviation between the actual P-wave

impedance log and predicted one (derived by seismic trace at the well location), while the seismic error donates the deviation between the original seismic and synthetic inverted trace at the well location. It seems that wavelet M-3 provides less error compared to wavelets M-1 and M-2 as shown in Figure A-1. Following exhaustive quality control for the nine wells, we choose the wavelet M-3 (Figure A.2) to apply 3D model-based inversion for the 9-well constrained case.

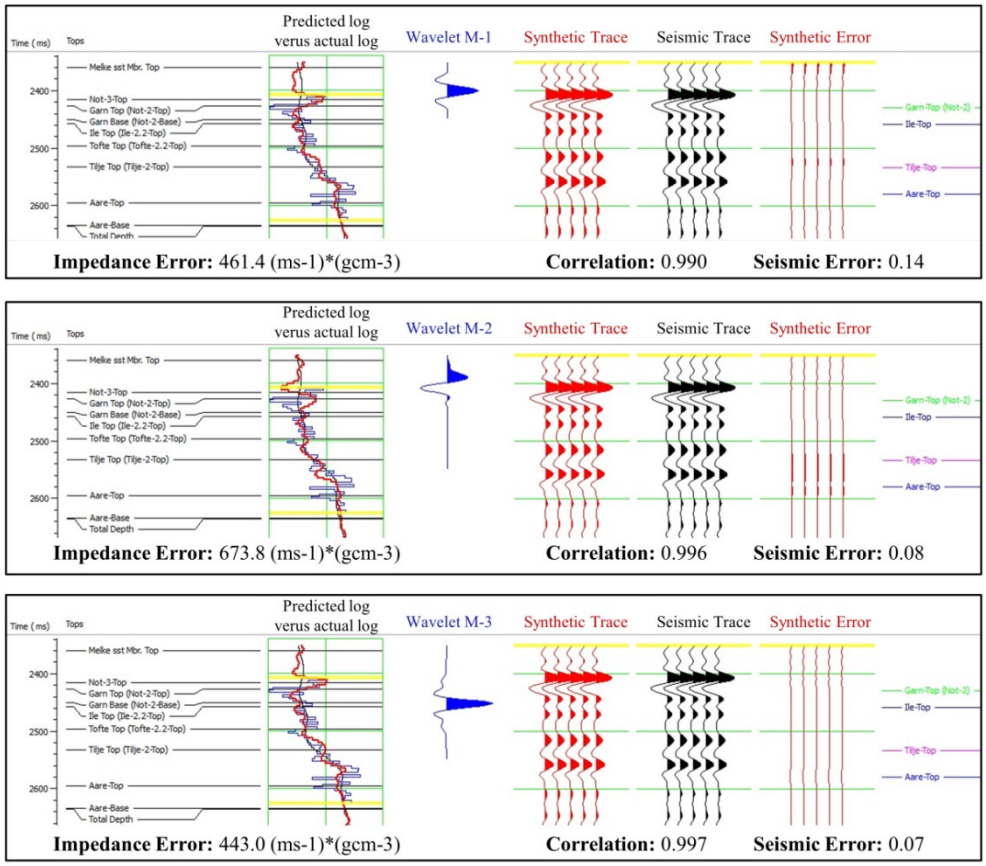

Figure A.1. Inversion analysis plot for the well B-4H including different statistical wavelets. Red traces denote synthetic inverted seismic trace, while black traces represent actual seismic trace. Note the reduction of impedance and seismic errors using wavelet M-3.

Furthermore, we defined three various scenarios for the inversion parameters using the wavelet M-3 (Table A.1). The main differences between these scenarios are the type of constraint and number of iterations. We catalogued the scenarios in Table A.1 in terms of the varied inversion parameters. For instance, Figure A.3 indicates the quality control for well B-4H with the wavelet M-3 and various inversion parameters. It is clear that errors are substantially diminished (particularly the seismic error) using the scenario-3. Eventually, we evaluated all scenarios for the mentioned nine wells and choose parameters of scenario-

3 as inversion parameters for the 9-well constrained case to run the 3D inversion in the Norne seismic survey of 2001.

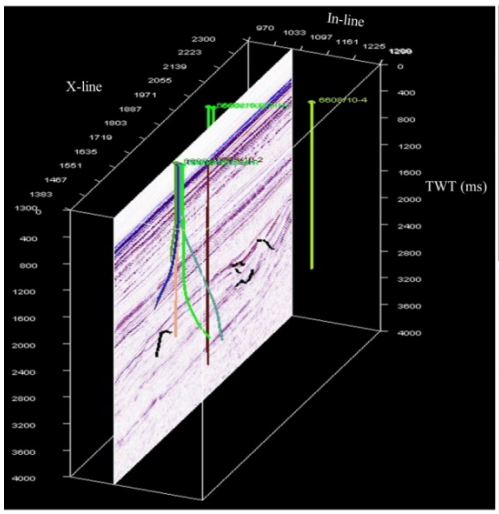

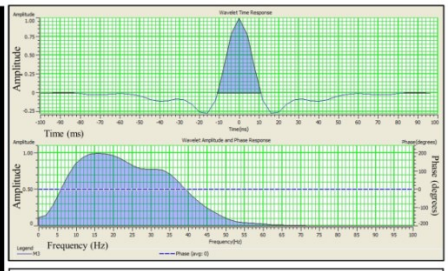

Wavelet M-3 Information	
In-line range	1076
X-line range	1320 - 2700
Time range	2390 - 2700
Wavelet length	200 ms
Phase rotation	0
Taper length	25 msec

Figure A.2. Detailed information of the statistical wavelet M-3; including location of the in-line 1076 and nine wells (left), and phase and amplitude spectrums of the extracted wavelet (right).

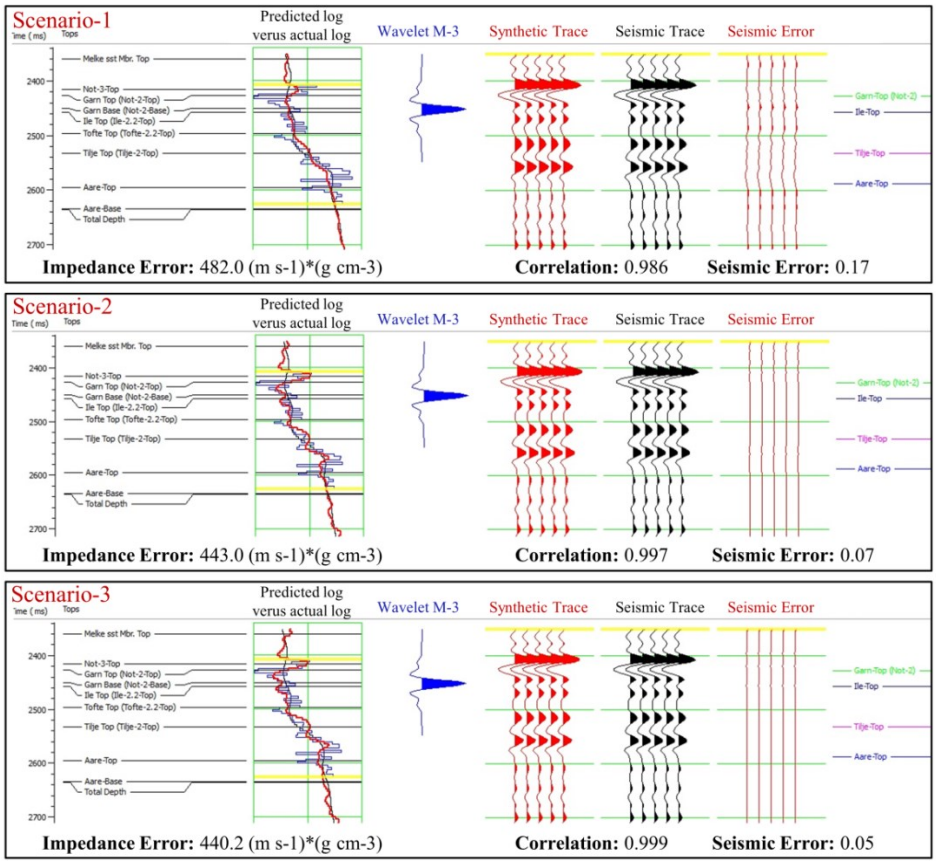

Figure A.3. Inversion analysis plot for the well B-4H including different scenarios of inversion parameters. Red traces denote synthetic inverted seismic trace, while black traces represent actual seismic trace. Note the reduction of impedance and seismic errors using scenario-3.

Table A.1. Description of each scenario of inversion parameters.

scenario	constraint	Maximum impedance change	Average block size	Prewhitening	Number of iterations
1	Soft	0.5	2	1 %	10
2	Hard	100 %	2	1 %	10
3	Hard	80 %	2	1 %	60

APPENDIX B - Complementary results of Article-3

The joint interpretation of time-lapse seismic inversion with the flow-simulation model results proposed in Article-3 relays on the well production/injection history data to build confidence in identifying the production effects in the Norne benchmark case. For instance, these information provide additional support that the fluid-gradient change (zones with rising water levels replacing hydrocarbon) caused the increases in impedance that can be seen mainly in segments E, D and C, where the water contact rise in these segments is a consequence of the production activity up to 2006. The well-history data of principal producer (water rate) and injector (water and gas rates) wells for interpreting the anomalies derived by 4D seismic inversion in the Norne Field are illustrated in Figures B-1, B-2, B-3, B-4, B-5 and B-6. Well E-1H had produced water since 2005 (Figure B-1). Well E-1H had produced a substantial amount of water since mid-2002 (Figure B-2). Well B-3H 1H had produced considerable amount of water since mid-2001 (Figure B-3). Well C-2H injected water into Tofte and Tilje formations until mid-2006 (Figure B-4). Well B-2H had produced water since 2004 (Figure B-5). Eventually, well C-4AH injected water into the Ile Formation until January 2005, which is a water-saturated layer in this region, and gas injection started in 2005, lasting 6 months (Figure B-5).

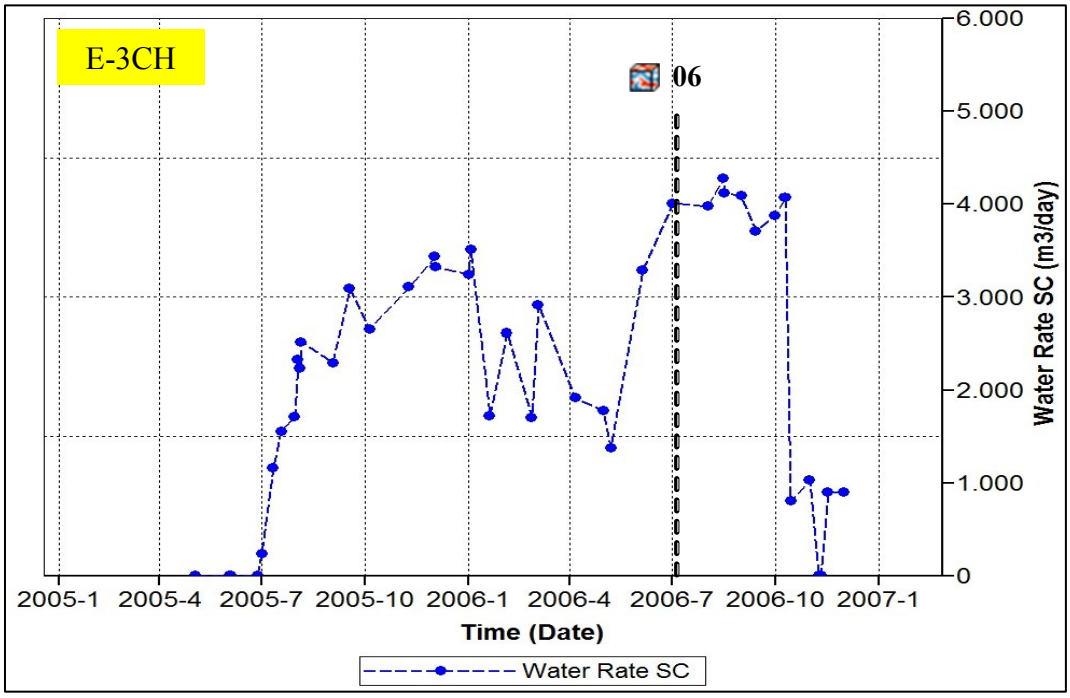

Figure B.1. Produced water rate of well E-3CH

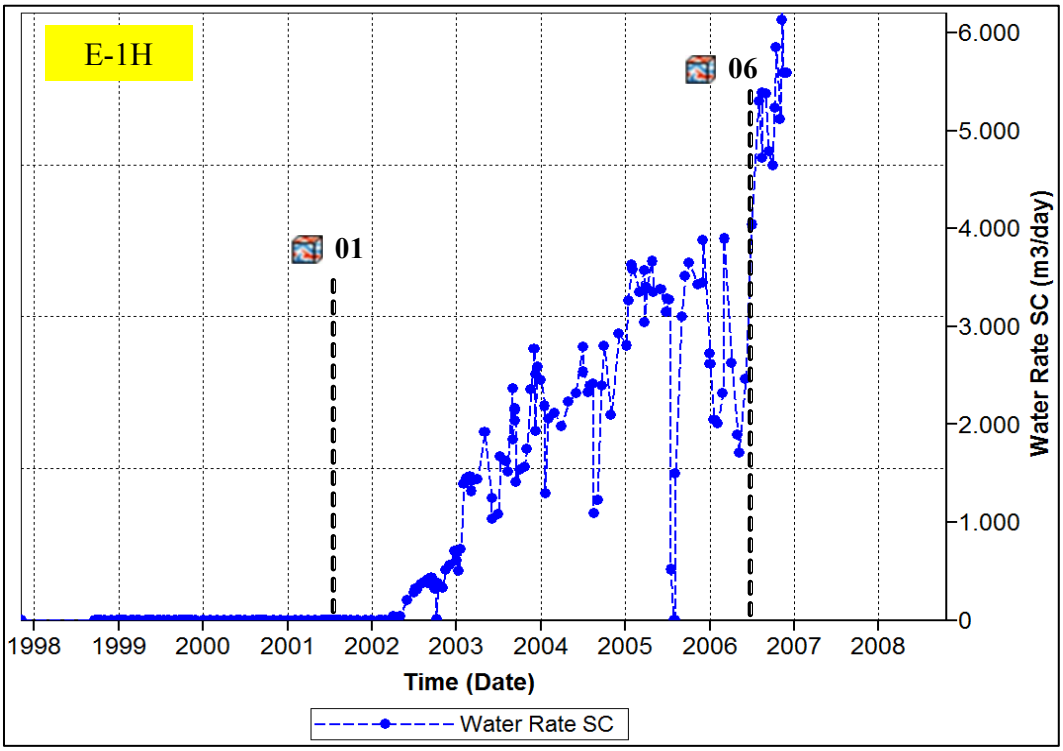

Figure B.2. Produced water rate of well E-1H.

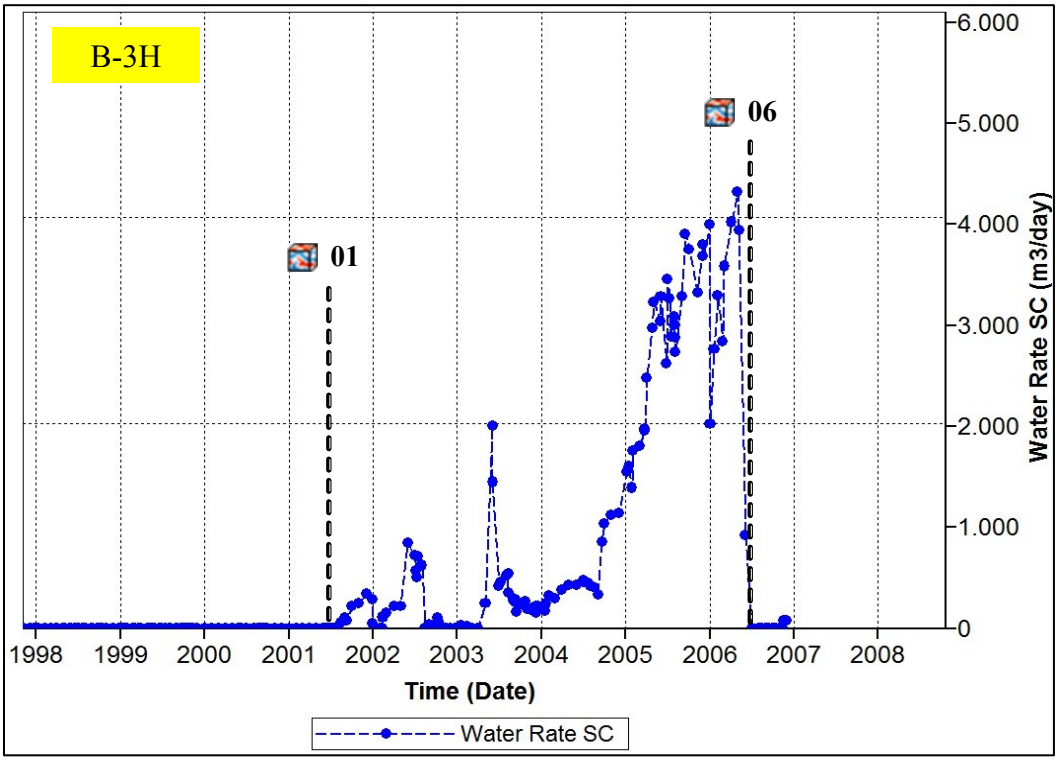

Figure B.3. Produced water rate of well B-3H.

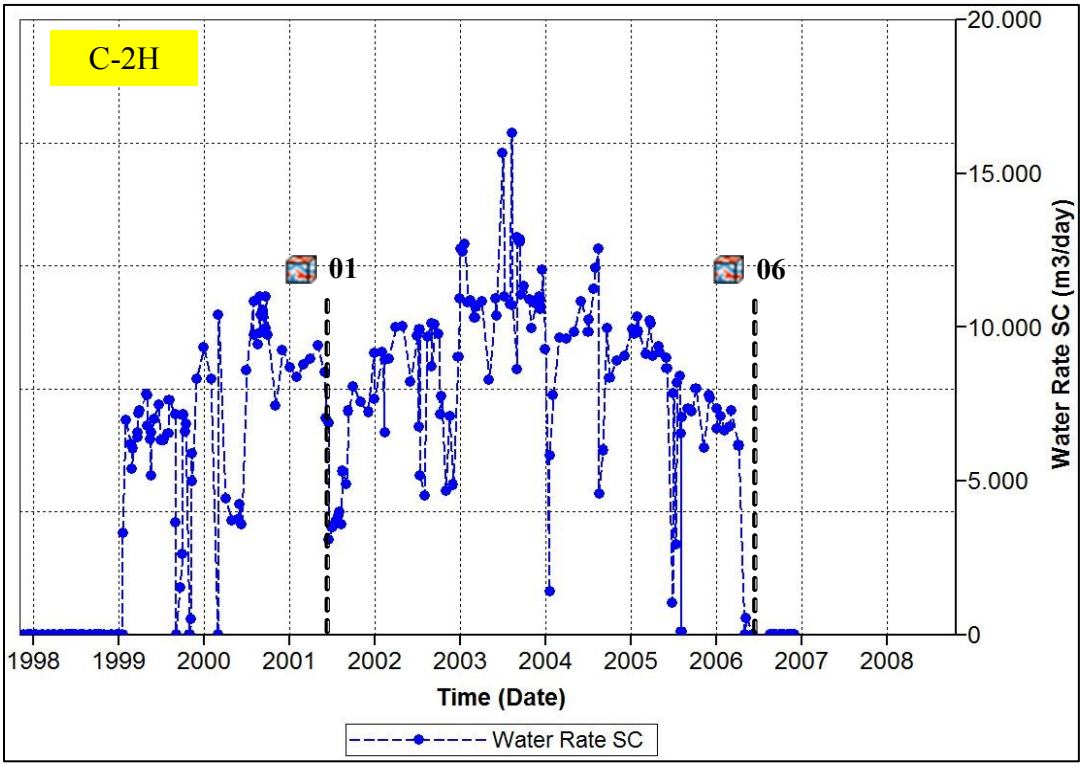

Figure B.4. Injected water rate of well C-2H.

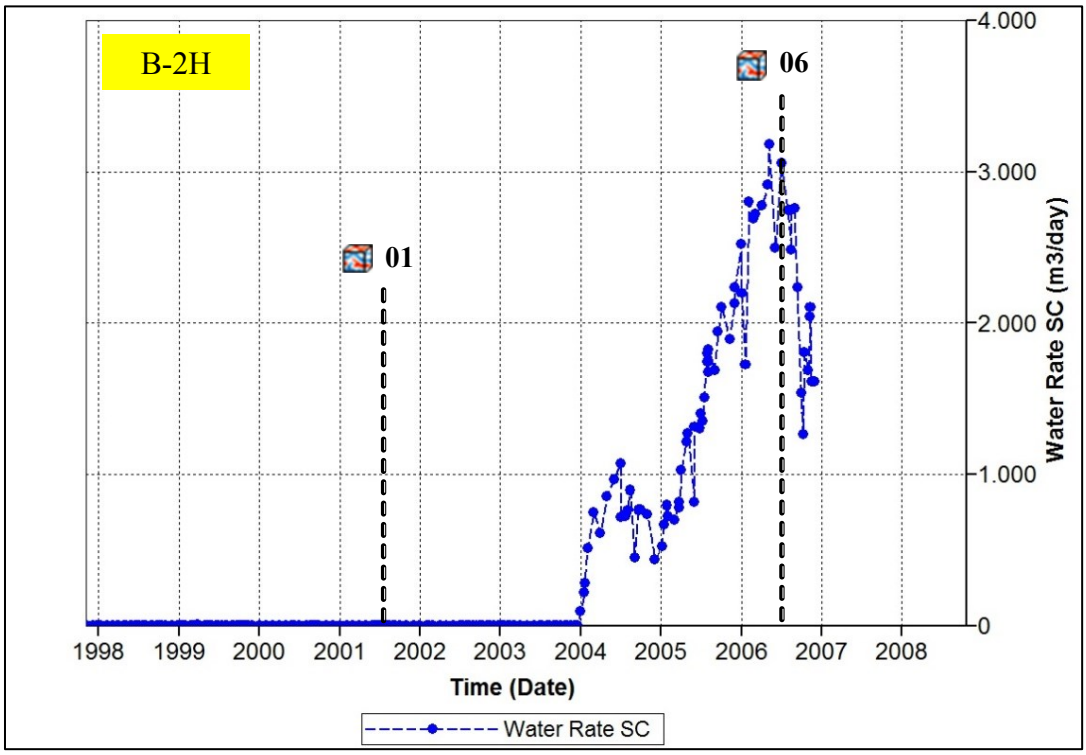

Figure B.5. Produced water rate of well B-2H.

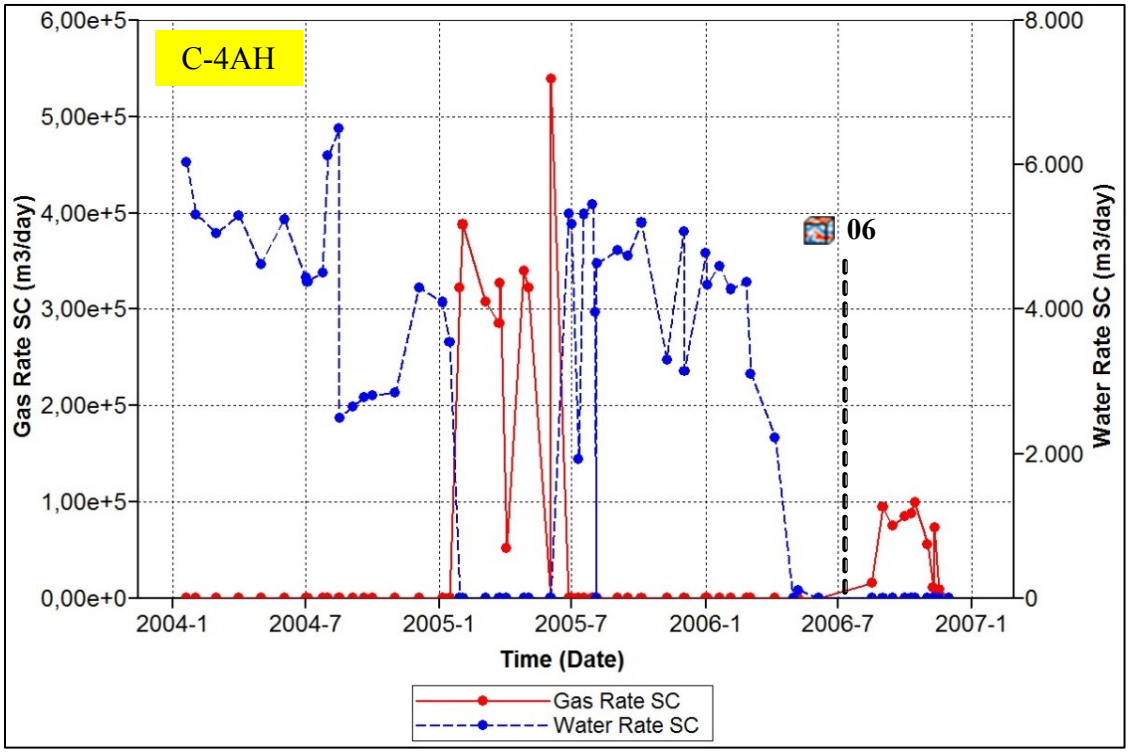

Figure B.6. Injected water and gas rates of well C-4AH.